The Stability of Hotspots for a Reaction-Diffusion Model of Urban Crime with Focused Police Patrol

Wang Hung Tse* , Michael J. Ward†

December 5, 2017

Abstract

1 Introduction

In this chapter, we consider the simple interaction case for the police-criminal dynamics ($I(\rho, U) = U$) in the three-component reaction-diffusion model. The following model is included as a special case of a general form proposed in [26]. In particular, the simple interaction term $-U$ in the ρ-equation (criminal density) represents a criminal removal rate proportional to the number of police present at the same spatial location. The nonlinear police movement term corresponds to a choice of the function $v(A)$ not explicitly studied in [26], given by

$$v(A) = qD\nabla \log A\,.$$

Our simple police interaction model on the one-dimensional domain $0 \le x \le S$ is formulated as

$$A_t = \epsilon^2 A_{xx} - A + \rho A^3 + \alpha\,, \tag{1.1a}$$

$$\rho_t = D\left(\rho_x - 2\rho A_x/A\right)_x - \rho A^3 + \gamma - \alpha - U\,, \tag{1.1b}$$

$$\tau_u U_t = D\left(U_x - qUA_x/A\right)_x\,, \tag{1.1c}$$

where $A_x = \rho_x = U_x = 0$ at $x = 0, S$. By integrating (1.1c) over the domain, we obtain that the total level U_0 of police deployment is conserved in time, so that

$$U_0 \equiv \int_0^S U(x,t)\,dx\,. \tag{1.2}$$

In (1.1c), the parameter $q > 0$ measures the degree of focus in the police patrol toward maxima of the attractiveness field A. We will assume in our analysis below that $q > 1$. The choice $q = 2$ models a "cops-on-the-dots" strategy (cf. [12], [26], [38]) whereby the police have the same degree of focus as do the criminals towards maxima of A. When q is above or below 2, the police force drift in a less or more focused manner, respectively, as compared to the movement of the criminals. In (1.1c), the "diffusivity" of the police is $D_p \equiv D/\tau_u$, so that when $\tau_u < 1$, the police are more mobile than the criminals. Conversely, $\tau_u > 1$ corresponds to the police being comparatively more "sluggish" in their movements.

*Dept. of Mathematics, UBC, Vancouver, Canada
†Dept. of Mathematics, UBC, Vancouver, Canada. (corresponding author ward@math.ubc.ca)

For the analysis, it is convenient to introduce the new variables V (cf. [14]) and u by

$$\rho = VA^2\,, \qquad U = uA^q\,. \tag{1.3}$$

When $\epsilon \ll 1$ the attractiveness field A is spatially localized. For the diffusivity D, we consider the regime $D = \mathcal{O}(\epsilon^{-2})$ where steady-state hotspot patterns were found to have a stability threshold for the basic crime model (cf. [14]). For this regime in D, we take $V = \mathcal{O}(\epsilon^2)$ to obtain a distinguished balance (cf. [14]). This motivates the rescaling

$$V = \epsilon^2 v\,, \qquad D = \epsilon^{-2}\mathcal{D}_0\,, \tag{1.4}$$

so that in terms of v, u, and $\mathcal{D}_0 = \mathcal{O}(1)$, (1.1) becomes

$$A_t = \epsilon^2 A_{xx} - A + \epsilon^2 vA^3 + \alpha\,, \tag{1.5a}$$

$$\epsilon^2\left(A^2 v\right)_t = \mathcal{D}_0\left(A^2 v_x\right)_x - \epsilon^2 vA^3 + \gamma - \alpha - uA^q\,, \tag{1.5b}$$

$$\tau_u\epsilon^2\left(A^q u\right)_t = \mathcal{D}_0\left(A^q u_x\right)_x\,. \tag{1.5c}$$

One key issue that we will study for (1.5) is to determine whether there is an optimum degree of focus in the patrolling so as to reduce the number of possible crime hotspots in a given 1-D spatial region. More specifically, we will investigate whether there are optimal values of q and τ_u so as to obtain the fewest number of stable steady-state hotspots on a given domain length. In mathematical terms, we will determine how the stability threshold in the diffusivity D, with $D = \epsilon^{-2}\mathcal{D}_0$, for steady-state hotspot patterns depends on q, the police diffusivity D/τ_u, and the total level U_0 of police deployment.

To analyze the linear stability of a K-hotspot steady-state solution, in §3 we use asymptotic analysis to derive the nonlocal eigenvalue problem (NLEP), characterizing $\mathcal{O}(1)$ time-scale instabilities of the pattern. The methodology to derive this NLEP involves using a reference domain $|x| \le \ell$ containing a single hotspot centered at $x = 0$, and then imposing Floquet-type boundary conditions at $x = \pm\ell$. In terms of this reference problem, the NLEP for the finite-domain problem $0 < x < S$ with Neumann conditions at $x = 0, S$ can then readily be extracted, as similar to that done in [14] for the basic two-component crime model. Such a Floquet-based approach to study the linear stability of multi-spike steady-states was first introduced in [22] in the context of 1-D spatially-periodic spike patterns for a class of two-component reaction-diffusion systems. It has subsequently been extended to study the linear stability of 1-D mesa patterns [15], of 1-D spikes for a competition model with cross-diffusion effects [17], and 1-D hotspot patterns for the basic crime model [14]. There are two novel features in the derivation of the NLEP for our three-component RD system with police. Firstly, in our asymptotic analysis, we must carefully derive rather intricate jump conditions across the hotspot region. Secondly, the resulting NLEP that we obtain has two nonlocal terms, instead of one. As a result, its analysis is seemingly beyond the general NLEP stability theory with a single nonlocal term, as surveyed in [36]. However, by using some key identities that are particular to our three-component RD crime model, we show how to reformulate the NLEP more conveniently in terms of a single nonlocal term, which can then be more readily analyzed.

In §5 we show for the special case where $q = 3$ that the spectrum of the NLEP can be reduced to the study of a simple algebraic equation for the eigenvalue parameter. More specifically, we show that the problem of determining unstable eigenvalues of the NLEP reduces to determining roots λ in $\mathrm{Re}(\lambda) > 0$ to a quadratic equation. By analyzing this simple spectral problem for $q = 3$, we show explicitly that, when D is below a certain competition instability threshold, a spatial pattern of two hotspots can be destabilized by an asynchronous, or anti-phase, temporal oscillation in the hotspot amplitudes when the police diffusivity D/τ_u falls below a Hopf bifurcation value. This Hopf bifurcation threshold can be determined

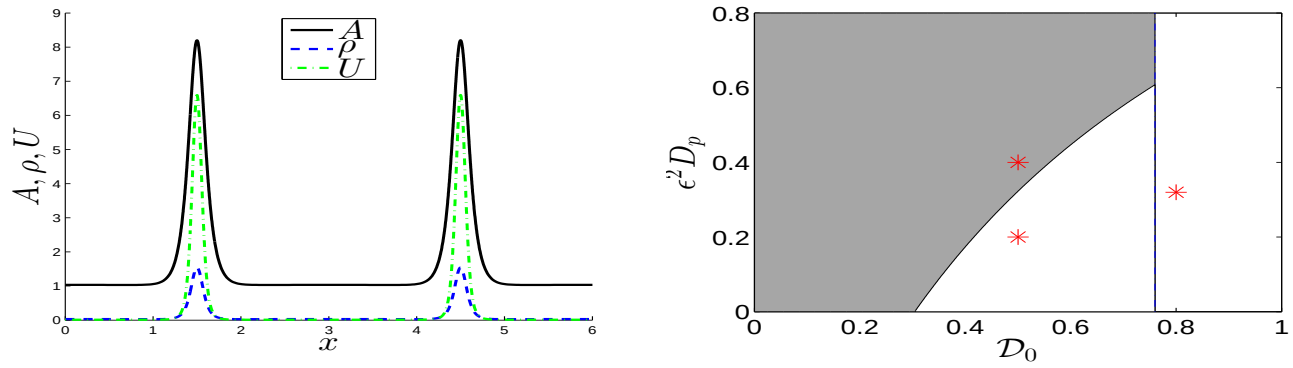

Figure 1: Left panel: The steady-state two-hotspot solution for $S = 6$, $\gamma = 2$, $\alpha = 1$, $U_0 = 2$, $\mathcal{D}_0 = 0.5$, $\epsilon = 0.075$, and $q = 3$. Right panel: the shaded region of linear stability in the (scaled) police diffusivity $\epsilon^2 D_p \equiv \mathcal{D}_0/\tau_u$ versus $\mathcal{D}_0$ parameter plane. The thin vertical line is the competition stability threshold $\mathcal{D}_{0,c}$ given in Proposition 5.2, while the leftmost edge of the instability region (at $D_p = 0$) is $\mathcal{D}_{0,c}/(1 + 3U_0/\omega)$ where $\omega = S(\gamma - \alpha) - U_0$. For $\mathcal{D}_0 > \mathcal{D}_{0c}$ the hotspot solution is unstable due to a competition instability, while in the unshaded region for $\mathcal{D}_0 < \mathcal{D}_{0c}$, the hotspot steady-state is unstable to an asynchronous oscillatory instability of the hotspot amplitudes. The full PDE simulations in Fig. 2 are done at the marked points.

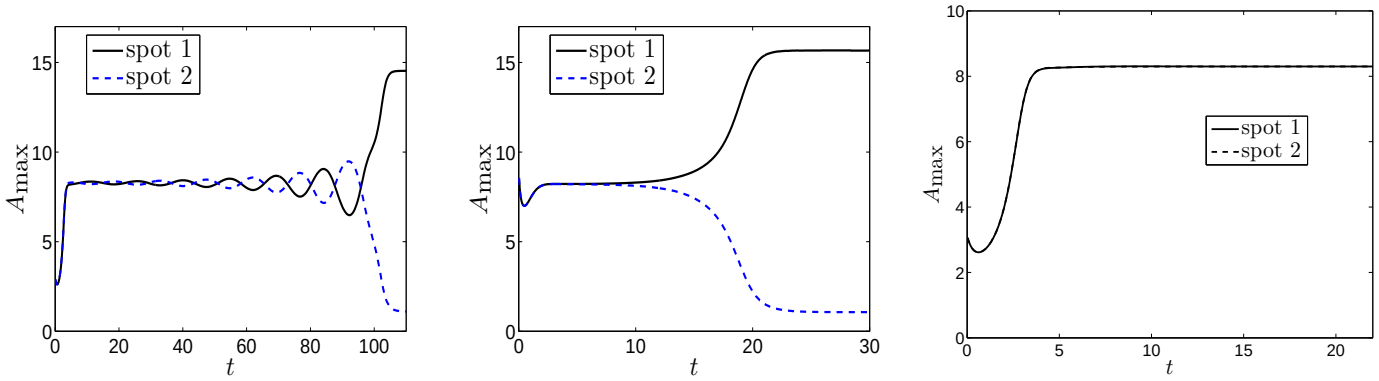

Figure 2: Plot of the spot amplitudes computed numerically from the full PDE system (1.5) for a two-spot pattern with $S = 6$, $\gamma = 2$, $\alpha = 1$, $U_0 = 2$, $\epsilon = 0.075$, and $q = 3$, at the marked points in the right panel of Fig. 1. Left panel: $\hat{\tau}_u = 2.5$ and $\mathcal{D}_0 = 0.5$, so that $\epsilon^2 D_p = 0.2$. Spot amplitudes are unstable to asynchronous oscillations, which leads to the collapse of one hotspot. Middle panel: $\hat{\tau}_u = 2.5$ and $\mathcal{D}_0 = 0.8$, so that $\epsilon^2 D_p = 0.32$. Spot amplitudes are unstable to a competition instability. Right panel: $\hat{\tau}_u = 1.25$ and $\mathcal{D}_0 = 0.5$, so that $\epsilon^2 D_p = 0.4$. Spot amplitudes are stable to asynchronous oscillations and there is no competition instability. These results are consistent with the linear stability predictions in the right panel of Fig. 1 (see also the left panel of Fig. 7 below).

analytically. The existence of such robust asynchronous temporal oscillations in the hotspot amplitudes is a qualitatively new phenomena, which does not occur in the study of spike stability for other RD systems such as the Gierer-Meinhardt and Gray-Scott models. For these two-component models, previous NLEP stability analyzes have shown that the dominant oscillatory instability of the spike amplitudes is always a synchronous instability.

2 Asymptotic Construction of a Multiple Hotspot Steady-State

In this section we construct a steady-state solution to (1.5) on $0 \le x \le S$ with $K \ge 1$ interior hotspots.

To construct a steady-state with K interior hotspots to (1.5) on $0 < x < S$, where the hotspots have a common amplitude, we will first construct a one-hotspot solution to (1.5) on $|x| \le l$ centered at $x = 0$. Then, by using the translation-invariance property of (1.5), we obtain a K interior hotspot steady-state solution on the original domain of length $S = (2\ell)K$. In terms of this reference domain $|x| \le \ell$, (1.2) yields that

$$U_0 = K \int_{-\ell}^{\ell} U \, dx \,. \tag{2.1}$$

In this way, we need only construct a one-hotspot steady-state solution to (1.5) centered at $x = 0$ and impose $A_x = v_x = u_x = 0$ at $x = \pm\ell$. We refer to this as the *canonical* hotspot problem.

From the steady-state of (1.5c), together with $U = uA^q$ and (2.1), it follows that u is spatially constant and given by

$$u = \frac{U_0}{K \int_{-\ell}^{\ell} A^q \, dx} \,. \tag{2.2}$$

By using (2.2) in (1.5), the steady-state problem for the three-component system reduces to the following two-component problem with a nonlocal term:

$$\epsilon^2 A_{xx} - A + \epsilon^2 v A^3 + \alpha = 0 \,, \qquad |x| \le \ell \,; \qquad A_x = 0 \quad x = \pm\ell \,, \tag{2.3a}$$

$$\mathcal{D}_0 \left(A^2 v_x \right)_x - \epsilon^2 v A^3 + \gamma - \alpha - \frac{U_0}{K} \frac{A^q}{\int_{-\ell}^{\ell} A^q \, dx} = 0 \,, \qquad |x| \le \ell \,; \qquad v_x = 0 \quad x = \pm\ell \,. \tag{2.3b}$$

We now construct the solution to (2.3) with a single hotspot centered at $x = 0$. In the outer region we have $A \sim \alpha + \mathcal{O}(\epsilon^2)$, while in the inner region we put $y = \epsilon^{-1} x$ and $A \sim A_0/\epsilon$ to obtain on $-\infty < y < \infty$ that

$$A_{0yy} - A_0 + v A_0^3 + \epsilon\alpha = 0 \,, \qquad \mathcal{D}_0 \epsilon^{-4} \left(A_0^2 v_y \right)_y + \mathcal{O}(\epsilon^{-1}) = 0 \,.$$

Therefore, to leading order it follows that $v \sim v_0$ is a constant, and that

$$A_0 \sim \frac{w(y)}{\sqrt{v_0}} \,, \tag{2.4}$$

where $w(y) = \sqrt{2}\,\mathrm{sech}\, y$ is the homoclinic solution of

$$w'' - w + w^3 = 0 \,, \qquad -\infty < y < \infty \,; \qquad w(0) > 0 \,, \quad w'(0) = 0 \,, \quad w \to 0 \quad \text{as} \quad y \to \pm\infty \,. \tag{2.5}$$

The integrals of $w(y)$ that are needed below are

$$\int_{-\infty}^{\infty} w \, dy = \int_{-\infty}^{\infty} w^3 \, dy = \sqrt{2}\pi \,, \quad \int_{-\infty}^{\infty} w^2 \, dy = 4 \,, \quad \int_{-\infty}^{\infty} w^4 \, dy = \frac{16}{3} \,, \quad \frac{\int_{-\infty}^{\infty} w^5 \, dy}{\int_{-\infty}^{\infty} w^3 \, dy} = \frac{3}{2} \,. \tag{2.6}$$

More generally, we can readily calculate in terms of the usual Gamma function $\Gamma(z)$ that

$$I_q \equiv \int_{-\infty}^{\infty} w^q \, dy = 2^{3q/2-1} \frac{[\Gamma(q/2)]^2}{\Gamma(q)} \,. \tag{2.7}$$

We return to (2.2), and for $q > 1$ we estimate the key integral

$$\int_{-\ell}^{\ell} A^q \, dx \sim 2\ell\alpha + \epsilon^{1-q} v_0^{-q/2} \int_{-\infty}^{\infty} w^q \, dy = \mathcal{O}(\epsilon^{1-q}) \gg 1 \,.$$

From (2.2), it follows that $u = \mathcal{O}(\epsilon^{q-1}) \ll 1$ since $q > 1$. With our assumption $q > 1$, the integral $\int_{-\ell}^{\ell} A^q \, dx$, and thus u, depend to leading-order only on the inner region contribution from A^q. For $q > 1$, we obtain to leading-order from (2.2) that

$$u \sim \epsilon^{q-1} \tilde{u}_e \,, \qquad \text{where} \qquad \tilde{u}_e \equiv \frac{U_0 v_0^{q/2}}{K I_q} \,. \tag{2.8}$$

Next, we determine v_0 by integrating (2.3b) on $-\ell < x < \ell$ and then imposing $v_x(\pm\ell) = 0$. This yields that

$$\epsilon^2 \int_{-\ell}^{\ell} v A^3 \, dx = 2\ell \, (\gamma - \alpha) - U_0/K \,.$$

Therefore, since $A \sim \alpha = \mathcal{O}(1)$ in the outer region, while $A = \mathcal{O}(\epsilon^{-1})$ in the inner region, it follows that, when $q > 1$, the dominant contribution to the integral arises from the inner region where $v \sim v_0$. In this way, we estimate

$$\frac{\int_{-\infty}^{\infty} w^3 \, dy}{\sqrt{v_0}} = 2\ell \, (\gamma - \alpha) - U_0/K \,. \tag{2.9}$$

From (2.9), a steady-state hotspot solution exists only when the total level U_0 of police deployment is below a threshold given by

$$U_0 < U_{0,max} \equiv 2\ell K \, (\gamma - \alpha) = S(\gamma - \alpha) \,. \tag{2.10}$$

Here $S = 2\ell K$ is the original domain length. We will assume that (2.10) holds, so that a K-hotspot steady-state exists.

Upon solving (2.9) for v_0, and using (2.6) for $\int_{-\infty}^{\infty} w^3 \, dy$, we get

$$v_0 = 2\pi^2 \left[2\ell \, (\gamma - \alpha) - U_0/K \right]^{-2} = 2\pi^2 K^2 \left[S(\gamma - \alpha) - U_0 \right]^{-2} \,. \tag{2.11}$$

Since v_0 increases when either K increases or the total level U_0 of police increases, it follows from (2.4) that the maximum $A_{\max} \equiv A(0) \gg 1$ of the attractiveness field, given by

$$A_{\max} \equiv A(0) \sim \epsilon^{-1} A_0(0) = \frac{\epsilon^{-1}}{\pi K} \left[S(\gamma - \alpha) - U_0 \right] \,, \tag{2.12}$$

decreases with increasing K or increasing police deployment U_0. However, this maximum value of A is independent of the police patrol focus parameter q.

To complete the asymptotic construction of the hotspot, we must determine v. In the outer region, we expand $v \sim v_e(x) + \dots$ and recall that $A \sim \alpha + \mathcal{O}(\epsilon^2)$ so that $A^q / \int_{-\ell}^{\ell} A^q \, dx = \mathcal{O}(\varepsilon^{q-1}) \ll 1$ since $q > 1$. In this way, from (2.3b), we obtain to leading order that $v_e(x)$ satisfies

$$\mathcal{D}_0 v_{exx} = -\frac{(\gamma - \alpha)}{\alpha^2} \,, \quad -\ell < x < \ell \,; \qquad v_e(0) = v_0 \,, \qquad v_{ex}(\pm\ell) = 0 \,. \tag{2.13}$$

The solution to (2.13) is

$$v_e(x) = \frac{\zeta}{2} \left[(\ell - |x|)^2 - \ell^2 \right] + v_0 \,, \qquad 0 < |x| \le \ell \,; \qquad \zeta \equiv -\frac{(\gamma - \alpha)}{\mathcal{D}_0 \alpha^2} \,, \tag{2.14}$$

where v_0 is given in (2.11). This expression is a uniformly valid leading order solution for v on $|x| \le \ell$.

We summarize the results for our leading-order construction of a steady-state K-hotspot pattern as follows:

Proposition 2.1 *Let $\epsilon \to 0$, $q > 1$, and $0 < U_0 < U_{0,max}$, as in (2.10). Then, (1.5) admits a steady-state solution on $(0, S)$ with K interior hotspots of a common amplitude. On each sub-domain of length $2\ell = S/K$, and translated to $(-\ell, \ell)$ to contain exactly one hotspot at $x = 0$, the steady-state solution, to leading order, is given by*

$$A \sim \frac{w(x/\epsilon)}{\epsilon\sqrt{v_0}}\,, \quad \text{if} \quad x = \mathcal{O}(\epsilon)\,; \qquad A \sim \alpha\,, \quad \text{if} \quad x = \mathcal{O}(1)\,, \tag{2.15a}$$

$$v \sim v_e = \frac{\zeta}{2}\left[(\ell - |x|)^2 - \ell^2\right] + v_0\,, \qquad \text{where} \quad v_0 = 2\pi^2 K^2 \left[S(\gamma - \alpha) - U_0\right]^{-2}\,, \tag{2.15b}$$

$$u \sim \epsilon^{q-1}\tilde{u}_e\,, \qquad \text{where} \quad \tilde{u}_e \equiv \frac{U_0 v_0^{q/2}}{K I_q}\,, \qquad I_q \equiv \int_{-\infty}^{\infty} w^q\, dy = 2^{3q/2-1}\frac{[\Gamma(q/2)]^2}{\Gamma(q)}\,. \tag{2.15c}$$

Here $w(y) = \sqrt{2}\,\mathrm{sech}\, y$ is the homoclinic of (2.5).

In terms of the criminal and police densities, given respectively by $\rho = \epsilon^2 v A^2$ and $U = uA^q$ (see (1.3) and (1.4)), we can write (2.15) as follows:

Corollary 2.2 *Under the same conditions as in Proposition 2.1, (2.15) yields to leading-order that*

$$A \sim \frac{w(x/\epsilon)}{\epsilon\sqrt{v_0}}\,, \quad \text{if} \quad x = \mathcal{O}(\epsilon)\,; \qquad A \sim \alpha\,, \quad \text{if} \quad \mathcal{O}(\epsilon) \ll |x| < \ell\,, \tag{2.16a}$$

$$\rho \sim [w(x/\epsilon)]^2\,, \quad \text{if} \quad x = \mathcal{O}(\epsilon)\,; \qquad \rho \sim \epsilon^2 v_e \alpha^2\,, \quad \text{if} \quad \mathcal{O}(\epsilon) \ll |x| < \ell\,, \tag{2.16b}$$

$$U \sim \frac{U_0}{\epsilon K I_q}[w(x/\epsilon)]^q\,, \quad \text{if} \quad x = \mathcal{O}(\epsilon)\,; \qquad U \sim \epsilon^{q-1}\alpha^q \frac{U_0 v_0^{q/2}}{K I_q}\,, \quad \text{if} \quad \mathcal{O}(\epsilon) \ll |x| < \ell\,, \tag{2.16c}$$

where v_e and v_0 are given in (2.15) and $w(y) = \sqrt{2}\,\mathrm{sech}\, y$.

From (2.16), we observe that the criminal density near a hotspot is independent of the police deployment U_0 and patrol focus q. However, the maximum of the attractiveness field is decreased by increasing U_0.

3 Derivation of the NLEP for a K-Hotspot Steady-State Pattern

To analyze the linear stability of a K-hotspot steady-state solution, we must use asymptotic analysis to derive the corresponding nonlocal eigenvalue problem (NLEP). To do so, we first follow the methodology in [14] by deriving the NLEP for a one-hotspot solution on the reference domain $|x| \le \ell$, with Floquet-type boundary conditions imposed at $x = \pm\ell$. In terms of this reference problem, the NLEP for the finite-domain problem $0 < x < S$ with Neumann conditions at $x = 0, S$ is then readily recovered, as similar to that done in [14] for the basic crime model.

3.1 Linearization with Floquet Boundary Conditions

To study the linear stability of a K-hotspot steady-state we introduce the perturbation

$$A = A_e + e^{\lambda t}\phi\,, \qquad v = v_e + e^{\lambda t}\epsilon\psi\,, \qquad u = u_e + e^{\lambda t}\epsilon^q\eta\,, \tag{3.1}$$

where (A_e, v_e, u_e) is the steady-state with a single hotspot centered at the origin in $|x| \le \ell$. The orders of the perturbations ($\mathcal{O}(1)$, $\mathcal{O}(\epsilon)$ and $\mathcal{O}(\epsilon^q)$ for the A, v and u components, respectively) are chosen so that ϕ, ψ, and η are all $\mathcal{O}(1)$ in the inner region. Upon substituting (3.1) into (1.5) and linearizing, we obtain that

$$\epsilon^2\phi_{xx} - \phi + 3\epsilon^2 v_e A_e^2\phi + \epsilon^3 A_e^3\psi = \lambda\phi\,, \tag{3.2a}$$

$$\mathcal{D}_0\left(2A_e v_{ex}\phi + \epsilon A_e^2\psi_x\right)_x - 3\epsilon^2 A_e^2 v_e\phi - \epsilon^3 A_e^3\psi - q u_e A_e^{q-1}\phi - \epsilon^q\eta A_e^q = \lambda\epsilon^2\left(2A_e v_e\phi + \epsilon A_e^2\psi\right)\,, \tag{3.2b}$$

$$\mathcal{D}_0\left(qA_e^{q-1}\phi u_{ex} + \epsilon^q A_e^q\eta_x\right)_x = \epsilon^2\tau_u\lambda\left(qA_e^{q-1}u_e\phi + \epsilon^q A_e^q\eta\right)\,. \tag{3.2c}$$

For $K \geq 2$, we will impose for the long-range components ψ and η in (3.2b) and (3.2c) the following Floquet-type boundary conditions at $x = \pm\ell$:

$$\begin{pmatrix} \eta(\ell) \\ \psi(\ell) \end{pmatrix} = z \begin{pmatrix} \eta(-\ell) \\ \psi(-\ell) \end{pmatrix}, \qquad \begin{pmatrix} \eta(\ell) \\ \psi(\ell) \end{pmatrix} = z \begin{pmatrix} \eta_x(-\ell) \\ \psi_x(-\ell) \end{pmatrix}, \tag{3.3}$$

where z is a complex-valued parameter. For the $K = 1$ case, considered separately in §3.3 below, we need only impose Neumann conditions at $x = \pm l$ for the perturbations. Here we treat the $K \geq 2$ case.

For $K \geq 2$, the NLEP associated with a K-hotspot pattern on $[-l, (2K-1)l]$ with *periodic boundary conditions*, on a domain of length $2Kl$, is obtained by setting $z^K = 1$, which yields

$$z_j = e^{2\pi i j/K}, \qquad j = 0, \ldots, K-1\,. \tag{3.4}$$

By using these values of z_j in (3.3) we obtain the spectral problem for the linear stability of a K-hotspot solution on a domain of length $2Kl$ subject to periodic boundary conditions. The next step is then to relate the spectra of the periodic problem to the Neumann problem in such a way that the Neumann problem is still posed on a domain of length S (cf. [14]). As discussed in §3 of [14] for $K \geq 2$, this involves simply replacing $2K$ with K in (3.4). As such, our Floquet parameter in (3.3) for a hotspot steady-state on a domain of length $S = 2lK$, having $K \geq 2$ interior hotspots and Neumann boundary conditions at $x = 0$ and $x = S$ is $z = e^{\pi i j/K}$. With this value of z, we calculate the identity

$$\frac{(z-1)^2}{2z} = \mathrm{Re}(z) - 1 = \cos\left(\frac{\pi j}{K}\right) - 1\,, \quad j = 0, \ldots, K-1\,, \tag{3.5}$$

which is needed in our analysis below.

We now begin our derivation of the NLEP. For (3.2a), in the inner region where $A_e \sim \epsilon^{-1} w/\sqrt{v_0}$, $v_e \sim v_0$, and $\psi \sim \psi(0) \equiv \psi_0$, we obtain to leading-order that

$$\Phi'' - \Phi + 3w^2\Phi + \frac{\psi(0)}{v_0^{3/2}} w^3 = \lambda\Phi\,. \tag{3.6}$$

Here $\Phi(y) = \phi(\epsilon y)$ is the leading order term for the inner expansion of ϕ. In contrast, in the outer region, we obtain to leading order from (3.2) that

$$\phi \sim \epsilon^3\alpha^3\psi/[\lambda + 1 - 3\epsilon^2\alpha^2 v_e] = \mathcal{O}(\epsilon^3), \qquad \psi_{xx} \approx 0\,, \qquad \eta_{xx} \approx 0\,. \tag{3.7}$$

To determine $\psi(0)$, which from (3.6) will yield the NLEP, we must first carefully derive appropriate jump conditions for ψ_x and η_x across the hotspot region centered at $x = 0$. This is done in the next sub-section.

3.2 Jump Conditions and the Derivation of the NLEP for $K \geq 2$

To derive the appropriate jump condition for ψ_x across the hotspot region, we integrate (3.2b) over an intermediate domain $-\delta < x < \delta$ with $\epsilon \ll \delta \ll 1$. We use the facts that $A_e \sim \epsilon^{-1} w/\sqrt{v_0}$, $\phi \sim \Phi(y)$, $A_e(\pm\delta) \sim \alpha$, and $u_e = \epsilon^{q-1}\tilde{u}_e$ as given in (2.15), to obtain, upon letting $\delta/\epsilon \to +\infty$, that

$$\begin{aligned} \epsilon\mathcal{D}_0\alpha^2\left[\psi_x\right]_0 + 2\mathcal{D}_0\alpha\left[v_{ex}\phi\right]_0 \;&=\; 3\epsilon\int_{-\infty}^{\infty} w^2\Phi\,dy + \frac{\epsilon\psi(0)}{v_0^{3/2}}\int_{-\infty}^{\infty} w^3\,dy \\ &\quad + \frac{\epsilon q\tilde{u}_e}{v_0^{(q-1)/2}}\int_{-\infty}^{\infty} w^{q-1}\Phi\,dy + \frac{\epsilon\eta(0)}{v_0^{q/2}}\int_{-\infty}^{\infty} w^q\,dy + \mathcal{O}(\epsilon^2\lambda)\,, \end{aligned}$$

where we have introduced the notation $[a]_0 \equiv a(0^+) - a(0^-)$ to indicate that the evaluation is to be done with the outer solution. In addition, below we will use the convenient shorthand notation that $\int(\ldots) \equiv \int_{-\infty}^{\infty}(\ldots)\,dy$. Since $\phi = \mathcal{O}(\epsilon^3)$ in

the outer region from (3.7), we can neglect the second term on the left-hand side of the expression above. For eigenvalues for which $\lambda \ll \mathcal{O}(\epsilon^{-1})$, we obtain that

$$\mathcal{D}_0\alpha^2[\psi_x]_0 = 3\int w^2\Phi + \frac{\psi(0)}{v_0^{3/2}}\int w^3 + \frac{q\tilde{u}_e}{v_0^{(q-1)/2}}\int w^{q-1}\Phi + \frac{\eta(0)}{v_0^{q/2}}\int w^q\,. \tag{3.8}$$

Now from (3.2b), we use $\phi = \mathcal{O}(\epsilon^3)$ in the outer region, together the fact $\epsilon^q\eta A_e^q \ll \mathcal{O}(\epsilon)$ since $q > 1$. In this way, from (3.2b) and (3.8), we obtain the following leading-order BVP problem for ψ with a jump condition for ψ_x across $x = 0$:

$$\psi_{xx} = 0\,, \quad |x| \le \ell\,; \qquad e_0\,[\psi_x]_0 = e_1\psi(0) + e_2\eta(0) + e_3\,, \quad \psi(\ell) = z\psi(-\ell)\,, \quad \psi_x(\ell) = z\psi_x(-\ell)\,, \tag{3.9a}$$

where we have defined e_j, for $j = 0, \ldots, 3$, by

$$e_0 \equiv \mathcal{D}_0\alpha^2\,, \qquad e_1 \equiv \frac{1}{v_0^{3/2}}\int w^3\,, \qquad e_2 \equiv \frac{1}{v_0^{q/2}}\int w^q\,, \qquad e_3 \equiv 3\int w^2\Phi + \frac{q\tilde{u}_e}{v_0^{(q-1)/2}}\int w^{q-1}\Phi\,. \tag{3.9b}$$

This BVP is defined in terms of $\eta(0)$, which itself must be calculated from a separate BVP. To formulate this additional BVP, we integrate (3.2c) over $-\delta < x < \delta$, with $\epsilon \ll \delta \ll 1$, and let $\delta/\epsilon \to \infty$ to obtain

$$\mathcal{D}_0\epsilon^q\alpha^q\,[\eta_x]_0 + \mathcal{D}_0 q\alpha^{q-1}\mathcal{O}(\epsilon^{q+2}) = \epsilon^3\tau_u\lambda\left[\frac{q\tilde{u}_\epsilon}{v_0^{(q-1)/2}}\int w^{q-1}\Phi + \frac{\eta(0)}{v_0^{q/2}}\int w^q\right]. \tag{3.10}$$

To achieve a distinguished balance in (3.10), we introduce $\hat{\tau}_u$ defined by

$$\hat{\tau}_u \equiv \epsilon^{3-q}\tau_u\,. \tag{3.11}$$

With this scaling, the police diffusivity $D_p \equiv \epsilon^{-2}\mathcal{D}_0/\tau_u$, is simply

$$D_p \equiv \epsilon^{1-q}\mathcal{D}_0/\hat{\tau}_u\,. \tag{3.12}$$

In this way, (3.10) yields the following jump condition for the outer solution:

$$\mathcal{D}_0\alpha^q\,[\eta_x]_0 = \hat{\tau}_u\lambda\left[\frac{q\tilde{u}_e}{v_0^{(q-1)/2}}\int w^{q-1}\Phi + \frac{\eta(0)}{v_0^{q/2}}\int w^q\right]. \tag{3.13}$$

Now in the outer region we obtain from (3.2c) that

$$\mathcal{D}_0\epsilon^q\alpha^q\eta_{xx} + \mathcal{O}(\epsilon^{q+2}) = \epsilon^2\tau_u\lambda\left[\mathcal{O}(\epsilon^{q+2}) + \mathcal{O}(\epsilon^q)\right]. \tag{3.14}$$

We will consider the range of τ_u, and consequently $\hat{\tau}_u$, where

$$\tau_u \ll \mathcal{O}(\epsilon^{-2})\,, \qquad \text{for which} \qquad \hat{\tau}_u \ll \mathcal{O}(\epsilon^{1-q})\,. \tag{3.15}$$

We will assume in our theory below that $\hat{\tau}_u = \mathcal{O}(1)$, so that (3.15) holds for all $q > 1$.

For this range, (3.14) reduces to $\eta_{xx} \approx 0$ to leading order. In this way, we obtain using (3.13), the following BVP for the leading-order outer solution for η with a jump condition for η_x across $x = 0$:

$$\eta_{xx} = 0\,, \quad |x| \le \ell\,; \qquad d_0\,[\eta_x]_0 = d_1\eta(0) + d_2\,, \quad \eta(\ell) = z\eta(-\ell)\,, \quad \eta_x(\ell) = z\eta_x(-\ell)\,. \tag{3.16a}$$

Here the constants d_0, d_1, and d_2, are defined by

$$d_0 \equiv \mathcal{D}_0\alpha^q, \qquad d_1 \equiv \frac{\hat{\tau}_u\lambda}{v_0^{q/2}}\int w^q, \qquad d_2 \equiv \frac{\hat{\tau}_u\lambda q\tilde{u}_e}{v_0^{(q-1)/2}}\int w^{q-1}\Phi\,. \tag{3.16b}$$

To solve the BVPs (3.16) and (3.9), and in this way determine $\psi(0)$ and $\eta(0)$, we need to establish a simple lemma.

Lemma 3.1 *Consider the BVP for $y = y(x)$ on $-\ell < x < \ell$ given by*

$$y_{xx} = 0\,, \quad -\ell < x < \ell\,; \qquad f_0\,[y_x]_0 = f_1 y(0) + f_2\,; \qquad y(\ell) = z y(-\ell)\,, \quad y_x(\ell) = z y_x(-\ell)\,, \tag{3.17}$$

where f_0, f_1 and f_2, are nonzero constants, and let z satisfy (3.5). Then, $y(0)$ is given by

$$y(0) = f_2 \left[\frac{f_0}{\ell} \frac{(z-1)^2}{2z} - f_1 \right]^{-1} = -\frac{f_2}{f_0(1-\cos(\pi j/K))/\ell + f_1}\,. \tag{3.18}$$

Proof: Let $y_0 = y(0)$. The solution of this BVP is continuous but not differentiable at $x = 0$, and has the form

$$y(x) = \begin{cases} y_0 + A_+ x & \text{if } 0 < x < \ell\,, \\ y_0 + A_- x & \text{if } -\ell < x < 0\,, \end{cases}$$

where $y_0 \equiv y(0)$. Upon imposing the Floquet boundary conditions we obtain $A_+ = zA_-$ and $y_0 + A_+\ell = z\,(y_0 - A_-\ell) = zy_0 - A_+\ell$, which yields that $A_+ = (z-1)y_0/(2\ell)$. Then, upon imposing the jump condition across $x = 0$ we get

$$f_1 y_0 + f_2 = f_0\,[y_x]_0 = f_0\,(A_+ - A_-) = \frac{f_0 y_0}{2\ell}\,(z-1)\left(1 - \frac{1}{z}\right)\,.$$

Upon solving for $y(0)$, and recalling the identify (3.5), we obtain (3.18) for $y(0)$. ■

Upon using Lemma 3.1 with $f_0 = e_0$, $f_1 = e_1$, and $f_2 = e_2\eta(0) + e_3$, we calculate from (3.9) that

$$\psi(0) = -\frac{e_2\eta(0) + e_3}{e_0(1-\cos(\pi j/K))/\ell + e_1}\,. \tag{3.19}$$

Then, by applying Lemma 3.1 with $f_0 = d_0$, $f_1 = d_1$, and $f_2 = d_2$, we calculate from (3.16) that

$$\eta(0) = -\frac{d_2}{d_0(1-\cos(\pi j/K))/\ell + d_1}\,. \tag{3.20}$$

The final step in the derivation of the NLEP is to substitute (3.20) into (3.19) and simplify the resulting expression for $\psi(0)$ so as to express it explicitly in terms of the original parameters. This will identify the key coefficient $\psi(0)/v_0^{3/2}$ in (3.6).

We first define D_j by

$$D_j \equiv \frac{\mathcal{D}_0}{\ell}\left(1 - \cos\left(\frac{\pi j}{K}\right)\right)\,, \qquad j = 0, \ldots, K-1\,, \quad \text{where} \quad l = S/(2K)\,, \tag{3.21}$$

so that $D_j < D_{j+1}$ for any $j = 0, 1, 2, \ldots, K-2$. Then, by calculating e_0 and d_0 from (3.9b) and (3.16b), and substituting (3.20) into (3.19), we obtain

$$\psi(0) = -\frac{1}{D_j\alpha^2 + e_1}\left[e_3 - \frac{e_2 d_2}{D_j\alpha^q + d_1}\right]\,. \tag{3.22}$$

Then, by using the expression for $\tilde{u}_e$, as given in (2.8), we rewrite the expressions for e_1, e_2, e_3, d_1, and d_2 in (3.9b) and (3.16b), as

$$e_1 = \frac{\int w^3}{v_0^{3/2}}\,, \qquad e_2 = \frac{\int w^q}{v_0^{q/2}}\,, \qquad e_3 = 3\int w^2\Phi + \frac{U_0\sqrt{v_0}}{K}\frac{q\int w^{q-1}\Phi}{\int w^q}\,, \tag{3.23a}$$

$$d_1 = \hat{\tau}_u\lambda\frac{\int w^q}{v_0^{q/2}}, \qquad d_2 = \hat{\tau}_u\lambda\left(\frac{U_0\sqrt{v_0}}{K}\frac{q\int w^{q-1}\Phi}{\int w^q}\right)\,. \tag{3.23b}$$

Upon substituting (3.23) into (3.22), we obtain, after some algebra, that

$$\mathcal{B}(\lambda) \equiv -\frac{\psi(0)}{v_0^{3/2}} = \frac{1}{\left(1 + v_0^{3/2}D_j\alpha^2/\int w^3\right)}\left[\frac{3\int w^2\Phi}{\int w^3} + \frac{v_0^{q/2}D_j\alpha^q}{v_0^{q/2}D_j\alpha^q + \hat{\tau}_u\lambda\int w^q}\left(\frac{U_0\sqrt{v_0}}{K\int w^3}\right)\left(\frac{q\int w^{q-1}\Phi}{\int w^q}\right)\right]\,. \tag{3.24}$$

We first consider the synchronous mode for which $j=0$, and $\mathcal{D}_0=0$ from (3.21). In this case, upon substituting (3.24) into (3.6) we obtain the following NLEP for the synchronous mode $j=0$:

$$L_0\Phi - 3w^3\frac{\int w^2\Phi}{\int w^3} = \lambda\Phi\,, \qquad \Phi\to 0 \quad \text{as} \quad |y|\to\infty\,. \tag{3.25}$$

From Lemma 3.2 of [14] it follows that any nonzero eigenvalue of (3.25) must satisfy $\mathrm{Re}(\lambda)<0$. We summarize this result as follows:

Proposition 3.2 *For $\epsilon\to 0$, $K\geq 2$, $q>1$, $0<U_0<U_{0,max}$, $\mathcal{D}_0=\epsilon^2 D=\mathcal{O}(1)$, and $\tau_u\ll\mathcal{O}(\varepsilon^{-2})$, a K-hotspot steady-state solution for (1.5) is always linearly stable on an $\mathcal{O}(1)$ time-scale to synchronous perturbations of the hotspot amplitudes.*

Remark 3.3 *In the large diffusivity ratio limit, for the two-component Gierer-Meinhardt and Gray-Scott RD systems in 1-D, the dominant oscillatory temporal instability in the spike amplitudes is always due to the synchronous mode (cf. [34], [16]). In contrast, for our three-component RD system (1.5), Proposition 3.2 shows that synchronous mode is always linearly stable.*

Therefore, in our linear stability analysis we need only consider the asynchronous modes $j=1,\ldots,K-1$, for which $D_j\neq 0$. For these modes, (3.24) motivates the introduction of new quantities $\chi_{0,j}$, $\chi_{1,j}$ and $\mathcal{C}_q(\lambda)$, defined by

$$\chi_{0,j}\equiv\frac{1}{1+v_0^{3/2}D_j\alpha^2/\int w^3}\,, \qquad \chi_{1,j}\equiv\left(\frac{U_0\sqrt{v_0}}{K\int w^3}\right)\frac{\chi_{0,j}}{\mathcal{C}_q(\lambda)}\,, \qquad \mathcal{C}_q(\lambda)\equiv 1+\frac{\hat{\tau}_u\lambda\int w^q}{v_0^{q/2}D_j\alpha^q}\,. \tag{3.26}$$

Then $\mathcal{B}(\lambda)$ in (3.24) can be written compactly as

$$\mathcal{B}(\lambda)\equiv -\frac{\psi(0)}{v_0^{3/2}} = \chi_{0,j}\frac{3\int w^2\Phi}{\int w^3} + \chi_{1,j}\frac{q\int w^{q-1}\Phi}{\int w^q}\,. \tag{3.27}$$

In this way, from (3.6) and (3.27), we obtain an NLEP with two nonlocal terms. The result is summarized as follows:

Proposition 3.4 *For $\epsilon\to 0$, $K\geq 2$, $q>1$, $0<U_0<U_{0,max}$, $\mathcal{D}_0=\epsilon^2 D=\mathcal{O}(1)$, and $\tau_u\ll\mathcal{O}(\varepsilon^{-2})$, the linear stability on an $\mathcal{O}(1)$ time-scale of a K-hotspot steady-state solution for (1.5), for the asynchronous modes $j=1,\ldots,K-1$, is characterized by the spectrum of the following NLEP for $\Phi(y)$ with two nonlocal terms:*

$$L_0\Phi - \chi_{0,j}w^3\frac{3\int w^2\Phi}{\int w^3} - \chi_{1,j}w^3\frac{q\int w^{q-1}\Phi}{\int w^q} = \lambda\Phi\,, \qquad \textit{where} \qquad L_0\Phi\equiv\Phi''-\Phi+3w^2\Phi\,. \tag{3.28}$$

Here $\chi_{0,j}$ and $\chi_{1,j}$ are defined in (3.26), and $w(y)=\sqrt{2}\,\mathrm{sech}\,y$.

Next, we express $\chi_{0,j}$ and $\chi_{1,j}$ in the NLEP (3.28) in terms of the original parameters. To do so, we first substitute (2.11) for v_0 into the expression (3.26) for $\chi_{0,j}$ and $\chi_{1,j}$. This suggests that it is convenient to introduce two new quantities κ_q and ω defined by

$$\kappa_q\equiv\left(\int w^q\right)^{-1}\left(\frac{\sqrt{2}\pi\alpha K}{\omega}\right)^q\,, \qquad \text{where} \qquad \omega\equiv S(\gamma-\alpha)-U_0\,. \tag{3.29}$$

In terms of these new variables, (3.26) becomes

$$\chi_{0,j}=\left(1+\frac{\kappa_3 D_j}{\alpha}\right)^{-1}\,, \qquad \chi_{1,j}=\frac{U_0}{\omega\mathcal{C}_q(\lambda)}\chi_{0,j}\,, \qquad \mathcal{C}_q(\lambda)\equiv 1+\frac{\hat{\tau}_u\lambda}{D_j\kappa_q}\,. \tag{3.30}$$

Next, we proceed to reformulate (3.28) as an NLEP with a single nonlocal term. To do so, we use the special property of the local operator L_0 that $L_0 w^2 = 3w^2$ (cf. [14]). Owing to the decay of Φ and w as $|y| \to \infty$, and since L_0 is self-adjoint, we obtain from Green's identity that $\int \left(w^2 L_0 \Phi - \Phi L_0 w^2 \right) = 0$. By using (3.28) for $L_0\Phi$, together with $L_0 w^2 = 3w^2$ and the integral ratio $\int w^5 / \int w^3 = 3/2$ from (2.6), we conclude from this Green's identity that

$$\left(\frac{\int w^2 \Phi}{\int w^3} \right) \left[\frac{9\chi_{0,j}}{2} + (\lambda - 3) \right] = -\frac{3q\chi_{1,j}}{2} \left(\frac{\int w^{q-1} \Phi}{\int w^q} \right) . \tag{3.31}$$

There are several interesting limiting cases of the key identity (3.31) for any eigenpair of the NLEP (3.28) with two nonlocal terms. Since $\chi_{1,j}$ is proportional to U_0 from (3.30), we first observe from (3.31) that for any eigenpair for which $\int w^m \Phi \neq 0$ for any $m > 0$, we must have $\lambda = 3 - 9\chi_{0,j}/2$ if and only if $U_0 = 0$. We remark that this recovers the result in equation (3.17) of [14] that the unique discrete eigenvalue of the linearization of a K-hotspot steady-state of the two-component "basic" crime model with no police is

$$\lambda = 3 - \frac{9\chi_{0,j}}{2} , \tag{3.32}$$

where $\chi_{0,j}$ is defined in (3.30). By setting $\lambda = 0$ in this expression, the stability threshold in equation (3.19) of [14] is recovered. This is discussed in more detail in §4.3 below.

A second special case of (3.31), which is examined in detail in §5, is when $q = 3$, for which (3.31) becomes

$$\left(\frac{\int w^2 \Phi}{\int w^3} \right) \left[\frac{9}{2} \left(\chi_{0,j} + \chi_{1,j} \right) + \lambda - 3 \right] = 0 . \tag{3.33}$$

Therefore, when $q = 3$, and for any eigenpair Φ and λ of (3.28) with $\int w^2 \Phi \neq 0$, we have that λ must satisfy

$$\frac{9}{2} \left(\chi_{0,j} + \chi_{1,j} \right) + \lambda - 3 = 0 . \tag{3.34}$$

By using (3.30) for $\chi_{1,j}$, we obtain that (3.34) reduces to a family of quadratic equations for λ of the form

$$c_2 \lambda^2 + c_1 \lambda + c_0 = 0 , \tag{3.35a}$$

where c_0, c_1, and c_2, are defined for $j = 1, \ldots, K-1$ by

$$c_2 = \frac{\hat{\tau}_u}{3\chi_{0,j} D_j \kappa_3} , \qquad c_1 = \frac{\hat{\tau}_u}{D_j \kappa_3} \left(\frac{3}{2} - \frac{1}{\chi_{0,j}} \right) + \frac{1}{3\chi_{0,j}} , \qquad c_0 = \frac{3U_0}{2\omega} + \frac{3}{2} - \frac{1}{\chi_{0,j}} . \tag{3.35b}$$

In §5 we will analyze the implications of (3.35) for the possibility of Hopf bifurcations.

Since $U_0 > 0$, and since we only consider eigenfunctions for which $\int w^m \Phi \neq 0$ for any $m > 0$, we have $\lambda \neq 3 - 9\chi_{0,j}/2$. Therefore, in (3.31) we can isolate $\int w^2 \Phi$ as

$$\frac{3 \int w^2 \Phi}{\int w^3} = \frac{-9}{9\chi_{0,j} + 2(\lambda - 3)} \left(\chi_{1,j} \frac{q \int w^{q-1} \Phi}{\int w^q} \right) .$$

Upon substituting this expression back into (3.27) for $\beta(\lambda)$ we eliminate the nonlocal term $\int w^2 \Phi$, and obtain that

$$\beta(\lambda) = \chi(\lambda) \frac{\int w^{q-1} \Phi}{\int w^q} , \qquad \text{where} \qquad \chi(\lambda) \equiv q\chi_{1,j} \left(\frac{2(\lambda - 3)}{9\chi_{0,j} + 2(\lambda - 3)} \right) . \tag{3.36}$$

Finally, by substituting (3.30) for $\chi_{0,j}$ and $\chi_{1,j}$ into (3.36) we obtain an NLEP with one nonlocal term:

Proposition 3.5 *For $\epsilon \to 0$, $K \geq 2$, $q > 1$, $0 < U_0 < U_{0,max}$, $\mathcal{D}_0 = \epsilon^2 D = \mathcal{O}(1)$, and $\tau_u \ll \mathcal{O}(\varepsilon^{-2})$, the linear stability on an $\mathcal{O}(1)$ time-scale of a K-hotspot steady-state solution for (1.5), for the asynchronous modes $j = 1, \ldots, K-1$, is characterized by the spectrum of the NLEP for $\Phi(y)$ given by*

$$L_0\Phi - \chi(\lambda) w^3 \frac{\int w^{q-1}\Phi}{\int w^q} = \lambda \Phi\,, \qquad \Phi \to 0 \quad as \quad |y| \to \infty\,, \tag{3.37a}$$

where $L_0\Phi \equiv \Phi'' - \Phi + 3w^2\Phi$. Here the multiplier $\chi(\lambda)$ of the NLEP is defined by

$$\chi(\lambda) \equiv \frac{qU_0}{\omega \mathcal{C}_q(\lambda)} \left(\frac{(\lambda-3)\chi_{0,j}}{(\lambda-3) + 9\chi_{0,j}/2} \right), \qquad where \quad \frac{1}{\chi_{0,j}} = 1 + \frac{\kappa_3 D_j}{\alpha}\,, \quad and \quad \mathcal{C}_q(\lambda) = 1 + \frac{\hat{\tau}_u \lambda}{D_j \kappa_q}\,. \tag{3.37b}$$

Here κ_q and ω are defined in (3.29), D_j is defined in (3.21), and $\hat{\tau}_u$ is related to τ_u by (3.11).

Remark 3.6 *We observe that our NLEP (3.37) has the general form*

$$L_0\Phi - \left(\frac{a_0 + a_1\lambda}{b_0 + b_1\lambda + b_2\lambda^2} \right) w^3 \frac{\int w^{q-1}\Phi}{\int w^q} = \lambda \Phi\,,$$

where the coefficients a_0, a_1, b_0, b_1 and b_2 are independent of λ. To our knowledge there have been no previous studies of NLEPs in 1-D where the multiplier χ of the NLEP is a proper rational function of degree two. Some results of this type are given in [28] for the linear stability analysis of spot patterns on the sphere for the Brusselator RD system.

The key model parameters we will use to analyze the NLEP are $\hat{\tau}_u$, q, U_0, $\mathcal{D}_0$, and ω. We remark that $\omega = U_{0,\max} - U_0$ where $U_{0,\max} = S(\gamma - \alpha)$ is the maximum police deployment for which a hotspot steady-state can exist.

3.3 Derivation of the NLEP for a Single Hotspot: $K = 1$ case

For $K \geq 2$, the NLEP (3.37) was derived by imposing Floquet boundary conditions at $x = \pm\ell$. For the case of a single hotspot, we can impose the Neumann boundary conditions directly at $x = \pm\ell$, as the Floquet analysis is not needed. With the same procedure as that leading to (3.9) and (3.16) above, we now obtain

$$\psi_{xx} = 0\,, \quad |x| \leq \ell\,; \qquad e_0 \left[\psi_x\right]_0 = e_1\psi(0) + e_2\eta(0) + e_3\,, \qquad \psi_x(\pm\ell) = 0\,, \tag{3.38}$$

together with the BVP for $\eta(x)$, given by

$$\eta_{xx} = 0\,, \quad |x| \leq \ell\,; \qquad d_0 \left[\eta_x\right]_0 = d_1\eta(0) + d_2\,, \qquad \eta_x(\pm\ell) = 0\,. \tag{3.39}$$

Here the coefficients e_0, e_1, e_2, e_3 and d_0, d_1 and d_2, are as defined in (3.9b) and (3.16b), respectively.

From these two problems it immediately follows that $\eta(x) = \eta(0)$ on $|x| \leq \ell$ and that $\eta(0) = -d_2/d_1$. In addition, we find that $\psi(x) = \psi(0)$ on $|x| \leq \ell$, with $\psi(0)$ given by

$$\psi(0) = -\frac{1}{e_1}\left(e_2\eta(0) + e_3\right) = -\frac{1}{e_1}\left(e_3 - \frac{e_2 d_2}{d_1}\right).$$

This is precisely the formula given in (3.22) with D_j set to zero.

Therefore, by proceeding in the same way as was done in the Floquet analysis performed earlier for the $K \geq 2$ case, we simply set D_j to zero in the expression (3.24), and in this way determine $\beta(\lambda)$ as

$$\beta \equiv -\frac{\psi(0)}{v_0^{3/2}} = \frac{3\int w^2\Phi}{\int w^3}\,. \tag{3.40}$$

By substituting (3.40) into (3.6) we obtain that the NLEP for a single hotspot solution is given by (3.25). For this NLEP, Lemma 3.2 of [14] proves that $\mathrm{Re}(\lambda) < 0$ for eigenfunctions for which $\int w^2\Phi \neq 0$. Therefore, we conclude that a single hotspot steady-state solution is unconditionally stable for any $\mathcal{D}_0$ when $\tau_u \ll \mathcal{O}(\epsilon^{-2})$.

3.4 Reformulation of the NLEP as Zeros of a Meromorphic Function

We now reformulate our NLEP (3.37) for a $K \geq 2$ hotspot steady-state so that its unstable discrete eigenvalues are the zeros of a meromorphic function $\zeta(\lambda)$ in the right-half $\mathrm{Re}(\lambda) \geq 0$ of the complex plane. To do so, we first write (3.37) as

$$(L_0 - \lambda)\,\Phi = \chi(\lambda) w^3 \frac{\int w^{q-1}\Phi}{\int w^q}\,, \qquad \text{so that} \qquad \Phi = \chi(\lambda)\frac{\int w^{q-1}\Phi}{\int w^q}\,(L_0-\lambda)^{-1}\,w^3\,.$$

We then multiply both sides of this expression by w^{q-1} and integrate to get

$$\left(\int w^{q-1}\Phi\right)\left[1 - \chi(\lambda)\frac{\int w^{q-1}\,(L_0-\lambda)^{-1}\,w^3}{\int w^q}\right] = 0\,. \tag{3.41}$$

Provided that the eigenfunction satisfies $\int w^{q-1}\Phi \neq 0$, we conclude that an eigenvalue λ of the NLEP (3.37) must be a root of

$$\zeta(\lambda) \equiv \mathcal{C}(\lambda) - \mathcal{F}(\lambda) = 0\,, \qquad \text{where} \qquad \mathcal{F}(\lambda) \equiv \frac{\int w^{q-1}\,(L_0-\lambda)^{-1}\,w^3}{\int w^q}\,. \tag{3.42a}$$

Here $\mathcal{C}(\lambda) \equiv [\chi(\lambda)]^{-1}$, and in terms of $\chi_{0,j}$ and $\mathcal{C}_q(\lambda)$, as defined in (3.37b), we have

$$\mathcal{C}(\lambda) = \frac{\omega \mathcal{C}_q(\lambda)}{qU_0}\left(\frac{1}{\chi_{0,j}} + \frac{9}{2(\lambda-3)}\right)\,. \tag{3.42b}$$

We will proceed to analyze the zeros of the meromorphic function $\zeta(\lambda) \equiv \mathcal{C}(\lambda) - \mathcal{F}(\lambda)$ in two cases: $q = 3$ and $q > 1$, with the former being explicitly solvable, and the latter requiring the Nyquist criterion to count the number of zeros in the unstable right half-plane $\mathrm{Re}(\lambda) > 0$. Moreover, we will also investigate the possibility of a Hopf bifurcation, by seeking a pure imaginary root of the form $\lambda = \pm i\lambda_I$ to (3.42) with $\lambda_I > 0$. Since $j = 1, \ldots, K-1$, such a Hopf bifurcation will correspond to an asynchronous temporal oscillation of the hotspot amplitudes.

Remark 3.7 *When $\int w^{q-1}\Phi = 0$, the NLEP (3.37) reduces to the local eigenvalue problem $L_0\Phi = \lambda\Phi$ with the extra condition $\int w^{q-1}\Phi = 0$. From Proposition 5.6 of [6], L_0 has exactly two discrete eigenvalues. One is $\Phi = w^2$ with $\lambda = 3$, arising from the identity $L_0 w^2 = 3w^2$, for which $\int w^{q-1}\Phi \neq 0$, while the other is the odd eigenfunction $\Phi = w'$ for which $\lambda = 0$ and $\int w^{q-1}\Phi = 0$. Therefore, since there are no instabilities associated with modes for which $\int w^{q-1}\Phi = 0$, the zeroes of $\zeta(\lambda)$, as defined in (3.42), in $Re(\lambda) > 0$ will determine any instability of the K-hotspot steady-state with $K \geq 2$.*

4 Analysis of the NLEP: Competition Instability

In order to analyze zero-eigenvalue crossings for the NLEP (3.37), as well as the possibility of Hopf bifurcations, in §4.1 we need to provide some global properties of $\mathcal{F}(\lambda)$, as defined in (3.42a), on both the non-negative real axis $\lambda \geq 0$ and on the non-negative imaginary axis $\lambda = i\lambda_I$ with $\lambda_I \geq 0$. In §4.2 we apply the winding number criterion of complex analysis to count the number of zeroes of $\zeta(\lambda)$, defined in (3.42), in the unstable right half-plane $\mathrm{Re}(\lambda) > 0$. With these properties, in §4.3 we study the competition stability threshold characterized by zero-eigenvalue crossings of the NLEP (3.37). Oscillatory instabilities for $q = 3$ and for general $q > 1$ due to a Hopf bifurcation are studied in detail in §5 and §6, respectively.

Before summarizing the global properties of $\mathcal{F}(\lambda)$, we first show that $\mathcal{F}(\lambda)$ can be found explicitly when $q = 3$ by using the identity $L_0 w^2 = 3w^2$. When $q = 3$, we calculate the integral I in the numerator for $\mathcal{F}(\lambda)$, given in (3.42a), as

$$I \equiv \int w^2\,(L_0-\lambda)^{-1}\,w^3 = \frac{1}{3}\int \left(L_0 w^2\right)(L_0-\lambda)^{-1}\,w^3 = \int \left[(L_0-\lambda)w^2 + \lambda w^2\right](L_0-\lambda)^{-1}\,w^3\,.$$

Upon integrating this last expression by parts, we get the algebraic equation $I = \left(\int w^5 + \lambda I\right)/3$, so that $I = \int w^5/(3-\lambda)$. Then, since $\mathcal{F} = I/\int w^3$ and $\int w^5/\int w^3 = 3/2$ from (2.6), we conclude that

$$\mathcal{F}(\lambda) = \frac{3}{2(3-\lambda)}\,, \qquad \text{when} \quad q = 3\,. \tag{4.1}$$

4.1 Key Global and Asymptotic Properties of $\mathcal{F}(\lambda)$

We first recall some key properties of $\mathcal{F}(\lambda)$, defined in (3.42a), on the non-negative real axis $\lambda \geq 0$.

Proposition 4.1 *On the non-negative real axis $\lambda \geq 0$, $\mathcal{F}(\lambda)$ given in (3.42a) satisfies*

(i) $\mathcal{F}(\lambda) \sim \frac{1}{2} + \frac{\lambda}{4}\left(1 - \frac{1}{q}\right) + \mathcal{O}(\lambda^2)$ *as* $\lambda \to 0\,.$

(ii) $\mathcal{F}(\lambda) \to +\infty$ *as* $\lambda \to 3^-\,.$

(iii) $\mathcal{F}'(\lambda) > 0\,,$ *for* $0 < \lambda < 3,$ *when* $q = 2, 3, 4\,.$

(iv) $\mathcal{F}(\lambda) < 0\,,$ *for* $\lambda > 3\,.$

Proof: The statements in (i), (ii), and (iv), as well as in (iii) for $q = 2$ and $q = 4$, were proved in Proposition 3.5 of [34]. For $q = 3$, the monotonicity result in (iii) is seen to hold by using the explicit form for $\mathcal{F}(\lambda)$ given in (4.1). ■

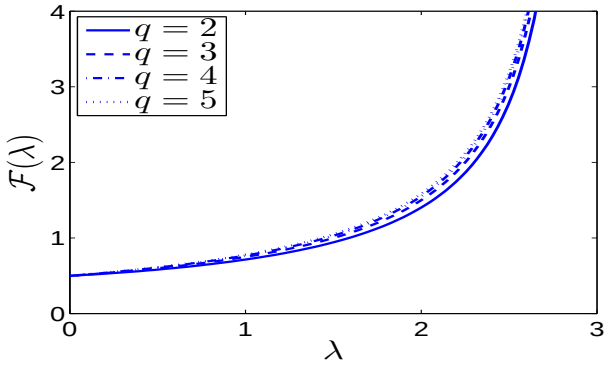

Figure 3: Plot of $\mathcal{F}(\lambda)$ on $0 < \lambda < 3$ for $q = 2, 3, 4, 5$. Note that $\mathcal{F}(0) = 1/2$ and that $\mathcal{F}(\lambda) \to +\infty$ as $\lambda \to 3$ from below. We observe that $\mathcal{F}(\lambda)$ is rather insensitive to changes in q.

In addition to the results (i), (ii), and (iv), which hold for all $q > 1$, we conjecture that the monotonicity result in (iii) holds not just for $q = 2, 3, 4$ but for all $q > 1$. As additional support of this conjecture, in Fig. 3 we plot the numerically computed function $\mathcal{F}(\lambda)$ on $0 < \lambda < 3$ for $q = 2, 3, 4, 5$.

Conjecture 4.2 *The monotonocity property (iii) of Proposition 4.1 that $\mathcal{F}'(\lambda) > 0$ on $0 < \lambda < 3$ holds for all $q > 1$.*

Next, in order to count the number of eigenvalues of the NLEP (3.37) in $\mathrm{Re}(\lambda) > 0$ below, we need some properties of $\mathcal{F}(\lambda)$, as defined in (3.42a), as restricted to the non-negative imaginary axis. By rewriting the operator as

$$(L_0 - i\lambda_I)^{-1} = (L_0 + i\lambda_I)\left[(L_0 + i\lambda_I)^{-1}(L_0 - i\lambda_I)^{-1}\right] = L_0\left[L_0^2 + \lambda_I^2\right]^{-1} + i\lambda_I\left[L_0^2 + \lambda_I^2\right]^{-1}\,,$$

we readily obtain upon upon separating $\mathcal{F}(i\lambda_I) = \int w^{q-1}(L_0 - i\lambda_I)^{-1}w^3/\int w^q$ into real and imaginary parts that

$$\mathcal{F}(i\lambda_I) = \mathcal{F}_R(\lambda_I) + i\mathcal{F}_I(\lambda_I)\,; \qquad \mathcal{F}_R(\lambda_I) = \frac{\int w^{q-1}L_0\left[L_0^2 + \lambda_I^2\right]^{-1}w^3}{\int w^q}\,, \qquad \mathcal{F}_I(\lambda_I) = \frac{\lambda_I\int w^{q-1}\left[L_0^2 + \lambda_I^2\right]^{-1}w^3}{\int w^q}\,. \tag{4.2}$$

We then recall some rigorous results of [34] for $\mathcal{F}_R(\lambda_I)$ and $\mathcal{F}_I(\lambda_I)$ on $\lambda_I \geq 0$.

Proposition 4.3 *For $\lambda = i\lambda_I$ with $\lambda_I > 0$, we have that $\mathcal{F}_R(\lambda_I)$ and $\mathcal{F}_I(\lambda_I)$ satisfy*

(i) $\mathcal{F}_R(\lambda_I) = \mathcal{O}(\lambda_I^{-2}) \quad as \quad \lambda_I \to +\infty\,, \quad \mathcal{F}_R(0) = 1/2.$

(ii) $\mathcal{F}_R'(\lambda_I) < 0\,, \quad when \quad q = 2, 3\,.$

(iii) $\mathcal{F}_I(\lambda_I) = \mathcal{O}(\lambda_I^{-1}) \quad as \quad \lambda_I \to +\infty.$

(iv) $\mathcal{F}_I(\lambda_I) \sim \frac{\lambda_I}{4}\left(1 - \frac{1}{q}\right) > 0 \quad as \quad \lambda_I \to 0^+\,.$

(v) $\mathcal{F}_I(\lambda_I) > 0\,, \quad when \quad q = 2, 3, 4.$

Proof: The statement in (i), and in (ii) for $q = 2$, were proved in Proposition 3.1 of [34]; Statements (iii), (iv), and (v) for $q = 2, 4$, were proved in Proposition 3.2 of [34]. The results in (ii) and (v) for $q = 3$ follow by using the explicit formula in (4.1). For $q = 3$, we have $\mathcal{F}(i\lambda_I) = 3/\left[2(3 - i\lambda_I)\right]$, so that

$$\mathcal{F}_R(\lambda_I) = \frac{9}{2(9+\lambda_I^2)}\,, \quad \mathcal{F}_R'(\lambda_I) = -\frac{9\lambda_I}{(9+\lambda_I^2)^2}\,, \quad \mathcal{F}_I(\lambda_I) = \frac{3\lambda_I}{2(9+\lambda_I^2)}\,, \quad \mathcal{F}_I'(\lambda_I) = \frac{3(9-\lambda_I^2)}{2(9+\lambda_I^2)^2}\,, \quad \text{for} \quad q = 3\,. \tag{4.3}$$

This clearly shows that properties (ii) and (v) also hold for $q = 3$. Moreover, it follows that $\mathcal{F}_I$ has a unique local maximum at the principal eigenvalue $\lambda_I = 3$ of L_0. ■

Although we only have a rigorous proof that $\mathcal{F}_R'(\lambda_I) < 0$ when $q = 2, 3$ and that $\mathcal{F}_I(\lambda_I) > 0$ when $q = 2, 3, 4$, we now conjecture that these key properties hold for all $q > 1$. In Fig. 4 we plot the numerically computed functions $\mathcal{F}_R(\lambda_I)$ and $\mathcal{F}_I(\lambda_I)$ for various values of q, which give numerical evidence for this conjecture. From this figure we observe that $\mathcal{F}_R(\lambda_I)$ is rather insensitive to changes in q.

Conjecture 4.4 *Properties (ii) and (v) in Proposition 4.3 that $\mathcal{F}_R'(\lambda_I) < 0$ and $\mathcal{F}_I(\lambda_I) > 0$ on $\lambda_I > 0$ hold for all $q > 1$.*

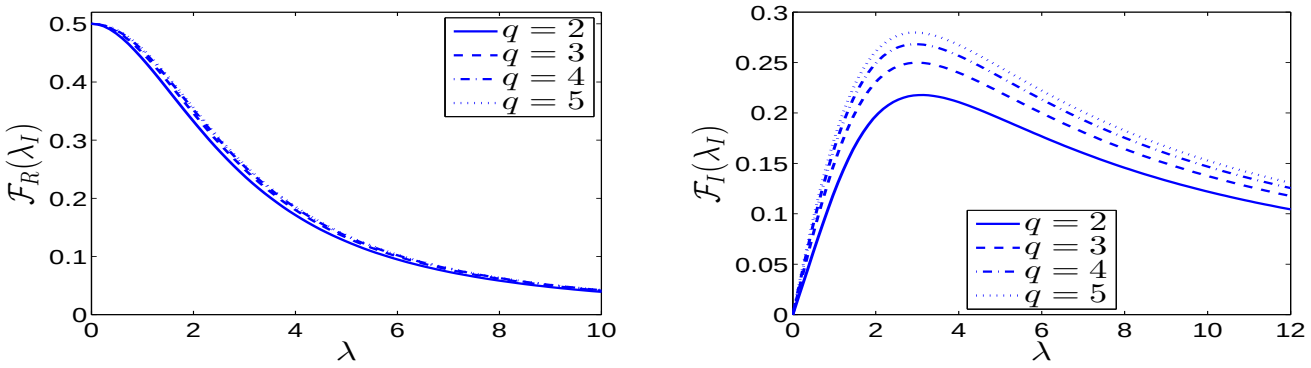

Figure 4: Plots of $\mathcal{F}_R(\lambda_I)$ (left panel) and $\mathcal{F}_I(\lambda_I)$ (right panel) for $q = 2, 3, 4, 5$. Note that $\mathcal{F}_R(0) = 1/2$ and $\mathcal{F}_I(0) = 0$, and that the maximum of $\mathcal{F}_I$ occurs near $\lambda_I = 3$. In fact, the maximum does occur exactly at $\lambda_I = 3$ when $q = 3$.

4.2 A Winding Number Criterion for the Number of Unstable Eigenvalues of the NLEP

We now use the argument principle of complex analysis to count the number N of eigenvalues of the NLEP (3.37) in $\mathrm{Re}(\lambda) > 0$. For each $j = 1, \ldots, K-1$, these discrete eigenvalues are the complex zeroes of the function $\zeta(\lambda) \equiv \mathcal{C}(\lambda) - \mathcal{F}(\lambda)$, as defined in (3.42). Here $\mathcal{F}(\lambda)$ is defined in (3.42a) and from (3.42b) we have that $\mathcal{C}(\lambda)$ has the explicit form

$$\mathcal{C}(\lambda) = a(1 + \tilde{\tau}_j \lambda)\left(1 - \frac{b}{3-\lambda}\right), \tag{4.4a}$$

where a, b, and $\tilde{\tau}_j$, are defined for $j = 1, \ldots, K-1$ by

$$a \equiv \frac{\omega}{qU_0\chi_{0,j}}, \qquad b \equiv \frac{9}{2}\chi_{0,j}, \qquad \tilde{\tau}_j \equiv \frac{\hat{\tau}_u}{D_j\kappa_q}, \qquad \frac{1}{\chi_{0,j}} = 1 + \frac{\kappa_3 D_j}{\alpha}. \tag{4.4b}$$

Here ω and κ_q are given in (3.29), while D_j and $\hat{\tau}_u$ are defined in (3.21) and 3.11, respectively.

From (4.4a), $\mathcal{C}(\lambda)$ is a meromorphic function with a simple pole at $\lambda = 3$. Moreover, $\mathcal{F}(\lambda)$ is analytic in $\mathrm{Re}(\lambda) \geq 0$ except at the simple pole at $\lambda = 3$. The simple poles of $\mathcal{C}(\lambda)$ and $\mathcal{F}(\lambda)$ do not cancel as $\lambda \to 3^-$, since when restricted to the real line we get $\mathcal{F}(\lambda) \to +\infty$ while $\mathcal{C}(\lambda) \to -\infty$ as $\lambda \to 3^-$. Thus, $\zeta(\lambda) = \mathcal{C}(\lambda) - \mathcal{F}(\lambda)$ has a simple pole at $\lambda = 3$.

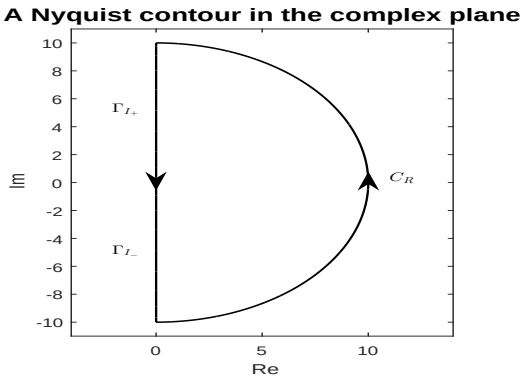

Figure 5: Schematic plot of the Nyquist contour Γ used for determining the number N of unstable eigenvalues of the NLEP (3.37).

To determine a formula for N, we calculate the winding of $\zeta(\lambda)$ over the Nyquist contour Γ traversed in the counterclockwise direction that consists of the following segments in the complex λ-plane (see the schematic in Fig. 5): Γ_I^+ ($0 < \mathrm{Im}(\lambda) < iR$, $\mathrm{Re}(\lambda) = 0$), Γ_I^- ($-iR < \mathrm{Im}(\lambda) < 0$, $\mathrm{Re}(\lambda) = 0$), and C_R defined by $|\lambda| = R > 0$ for $|\arg(\lambda)| < \pi/2$.

For each $j = 1, \ldots, K-1$, $\zeta(\lambda)$ is analytic in $\mathrm{Re}(\lambda) \geq 0$ except at the simple pole $\lambda = 3$ corresponding to the unique positive eigenvalue of the local operator L_0. Therefore, for each $j = 1, \ldots, N-1$, and assuming that $\zeta(\lambda)$ has no zeroes on the imaginary axis, we have by the argument principle that $N = 1 + (2\pi)^{-1}\lim_{R\to\infty}[\arg\zeta]_\Gamma$, where $[\arg\zeta]_\Gamma$ denotes the change in the argument of ζ over Γ. Since $\mathcal{F}(\lambda) = \mathcal{O}(|\lambda|^{-1})$ on the semi-circle C_R as $R = |\lambda| \to \infty$, we have that $\lim_{R\to\infty}[\arg\zeta]_{C_R} = \lim_{R\to\infty}[\arg\mathcal{C}]_{C_R}$. From (4.4a) we calculate that $\lim_{R\to\infty}[\arg\mathcal{C}]_{C_R} = \pi$ when $\hat{\tau}_u > 0$, and $\lim_{R\to\infty}[\arg\mathcal{C}]_{C_R} = 0$ when $\hat{\tau}_u = 0$. For the contour Γ_I^-, we use that $\zeta(\overline{\lambda}) = \overline{\zeta(\lambda)}$ so that $[\arg\zeta]_{\Gamma_I^-} = [\arg\zeta]_{\Gamma_I^+}$. In this way, for each $j = 1, \ldots, K-1$, we conclude that

$$N = \frac{3}{2} + \frac{1}{\pi}[\arg\zeta]_{\Gamma_I^+}, \quad \text{for} \quad \hat{\tau}_u > 0; \qquad N = 1 + \frac{1}{\pi}[\arg\zeta]_{\Gamma_I^+}, \quad \text{for} \quad \hat{\tau}_u = 0. \tag{4.5}$$

Here $[\arg\zeta]_{\Gamma_I^+}$ denotes the change in the argument of ζ as the imaginary axis $\lambda = i\lambda_I$ is traversed from $\lambda_I = +\infty$ to $\lambda_I = 0$.

We remark that (4.5) determines the number of unstable eigenvalues of the NLEP (3.37) for any *specific* asynchronous mode $j = 1, \ldots, K-1$. The total number of such unstable eigenvalues, for all asynchronous modes, is simply the union of

(4.5) over $j = 1, \ldots, K-1$. In this way, the problem of determining N for a particular mode j is reduced to calculating the change of argument of $\zeta(\lambda) = \mathcal{C}(\lambda) - \mathcal{F}(\lambda)$ as we traverse down the positive imaginary axis. To do so, we will need the properties of $\mathcal{F}(i\lambda_I)$ given in Proposition 4.3, together with results for $\mathcal{C}(i\lambda)$ to be obtained from (4.4).

4.3 The Competition Instability Threshold

We now determine the competition instability threshold value of the diffusivity $\mathcal{D}_0$, which is characterized by a zero-eigenvalue crossing of the NLEP (3.37). Since $\mathcal{F}(0) = 1/2$ (see (i) of Proposition 4.1), we conclude that $\zeta(0) = 0$ when $\mathcal{C}(0) = 1/2$. From using (3.42b), or equivalently (4.4), for $\mathcal{C}(\lambda)$ we conclude that $\lambda = 0$ when

$$\frac{\omega}{qU_0}\left(\frac{1}{\chi_{0,j}} - \frac{3}{2}\right) = \frac{1}{2}\,, \qquad j = 1, \ldots, K-1\,. \tag{4.6}$$

By using (4.4b) for $\chi_{0,j}$, together with (3.29) for κ_3, (4.6) yields that $\lambda = 0$ when

$$D_j = \frac{\omega^3}{4\pi^2 K^3 \alpha^2}\left(1 + \frac{qU_0}{\omega}\right)\,, \qquad j = 1, \ldots, K-1\,. \tag{4.7}$$

Finally, by using $D_j = 2K\mathcal{D}_0(1 - \cos(\pi j/K))/S$, as obtained from (3.21), we conclude that the NLEP has a zero-eigenvalue crossing at the $K-1$ distinct values $\mathcal{D}_{0,j}$ of $\mathcal{D}_0$ given by

$$\mathcal{D}_{0,j} = \frac{\omega^3 S}{8\pi^2\alpha^2 K^4\left(1 - \cos\left(\pi j/K\right)\right)}\left(1 + \frac{qU_0}{\omega}\right)\,, \qquad j = 1, \ldots, K-1\,. \tag{4.8}$$

As we show in Proposition 4.6 below, the competition instability threshold $\mathcal{D}_{0,c}$ corresponds to the smallest such $\mathcal{D}_{0,j}$, which occurs when $j = K-1$. This yields that

$$\mathcal{D}_{0,c} \equiv \mathcal{D}_{0,K-1} = \frac{\omega^3 S}{8\pi^2\alpha^2 K^4\left(1 + \cos\left(\pi/K\right)\right)}\left(1 + \frac{qU_0}{\omega}\right)\,. \tag{4.9}$$

In terms of the unscaled diffusivity $D = \epsilon^{-2}\mathcal{D}_0$, the competition stability threshold occurs at $D_c \equiv \epsilon^{-2}\mathcal{D}_{0,c}$.

Remark 4.5 *The zero-eigenvalue crossing condition (4.6) can also be obtained from the NLEP (3.28) with two nonlocal terms by setting $\Phi = w$ and $\lambda = 0$ in (3.28). By using the identity $L_0 w = 2w^3$, this substitution yields $2 - 3\chi_{0,j} - q\chi_{1,j} = 0$, where from (3.30) we have $\chi_{1,j} = U_0\chi_{0,j}/\omega$ at $\lambda = 0$. Some simple algebra then recovers (4.6).*

We now prove an instability result related to zero-eigenvalue crossings:

Proposition 4.6 *For $\epsilon \to 0$, $K \geq 2$, $q > 1$, $0 < U_0 < U_{0,max}$, $\mathcal{D}_0 = \epsilon^2 D = \mathcal{O}(1)$, a K-hotspot steady-state solution for (1.5) is unstable for all $\hat{\tau}_u \geq 0$ when $\mathcal{D}_0 > \mathcal{D}_{0,c}$, where $\mathcal{D}_{0,c}$ is the competition stability threshold defined in (4.9). For $\mathcal{D}_0 < \mathcal{D}_{0,c}$, a K-hotspot steady-state is linearly stable when $\hat{\tau}_u = 0$ and $q = 2, 3, 4$.*

Proof: We first prove that when $\mathcal{D}_0 > \mathcal{D}_{0,c}$, then $\zeta(\lambda) = 0$ in (3.42) has a positive real root in $0 < \lambda < 3$ for each $j = 1, \ldots, K-1$. This readily follows from the fact that $\mathcal{C}(0) > 1/2$ for each $j = 1, \ldots, K-1$, that $\mathcal{C}(\lambda) \to -\infty$ as $\lambda \to 3^-$, and from Proposition 4.1 where we have $\mathcal{F}(0) = 1/2$ and $\mathcal{F}(\lambda) \to +\infty$ as $\lambda \to 3^-$. Thus, by continuity, there is at least one positive real root to $\zeta(\lambda) = 0$ on $0 < \lambda < 3$ for each $j = 1, \ldots, K-1$ and for any $\hat{\tau}_u \geq 0$. Next, for $\mathcal{D}_0 < \mathcal{D}_{0,c}$, we show that $N = 0$ by using the winding number criterion (4.5) and calculating $[\arg\zeta]_{\Gamma_I^+}$ explicitly. From (4.4a), we decompose $\mathcal{C}(i\lambda_I) = \mathcal{C}_R(\lambda_I) + i\mathcal{C}_I(\lambda_I)$, and for $\hat{\tau}_u = 0$ calculate that

$$\mathcal{C}_I(\lambda_I) = -\frac{ab\lambda_I}{9 + \lambda_I^2} < 0 \qquad \text{for} \quad \lambda_I > 0\,.$$

Since $\mathcal{F}_I(\lambda_I) > 0$ for $\lambda_I > 0$ for $q = 2, 3, 4$ from property (v) of Proposition 4.3, we conclude that $\mathrm{Im}\,[\zeta(i\lambda_I)] < 0$ for $\lambda_I > 0$. Then, since $\mathcal{C}(0) > 1/2$ when $\mathcal{D}_0 < \mathcal{D}_{0,c}$, and $\mathcal{F}(0) = 1/2$ from (i) of Proposition 4.1, we have $\zeta(0) > 0$ for each $j = 1, \ldots, K-1$, and $\zeta(i\lambda_I) \to \omega/(qU_0\chi_{0,j}) > 0$ as $\lambda_I \to +\infty$. It follows that $[\arg\zeta]_{\Gamma_I^+} = -\pi$, and consequently $N = 0$ from the second statement in (4.5) for $\hat{\tau}_u = 0$. ■

We remark that if Conjecture 4.4 holds, then a K-hotspot steady-state is linearly stable when $\mathcal{D}_0 < \mathcal{D}_{0,c}$ and $\hat{\tau}_u = 0$ for any $q > 1$. Moreover, by continuity of eigenvalue paths in $\hat{\tau}_u$, the stability result in Proposition 4.6 should hold for all $\hat{\tau}_u > 0$ but sufficiently small. The possibility of Hopf bifurcations values of $\hat{\tau}_u$ for the range $\mathcal{D}_0 < \mathcal{D}_{0,c}$ is examined for $q = 3$ in §5 and for general $q > 1$ in §6.

4.4 Qualitative Interpretation of the Competition Instability Threshold

Next, we discuss the qualitative behavior of the competition instability threshold $\mathcal{D}_{0,c}$ with respect to the degree q of patrol focus and the total level U_0 of police patrol deployment.

We recall from (2.12) that the maximum $A_{\max}$ of the steady-state attractiveness field is $A_{\max} \sim \epsilon^{-1}\omega/(K\pi)$, which decreases as either ω decreases or K increases. However, from Corollary 2.2, the amplitude of the steady-state criminal density ρ at the hotspot locations is $\rho_{\max} = [w(0)]^2 = 2$, which is independent of all model parameters, while away from the maxima of A the criminal density is $\mathcal{O}(\epsilon^2) \ll 1$. Therefore, it is the reduction of the number of stable steady-state hotspots on a given domain length that is the primary factor in reducing the total crime in the domain. As such, we seek to tune the police parameters q and U_0 so that the range of diffusivity $\mathcal{D}_0$ for which a K-hotspot steady-state is unconditionally unstable, i.e. unstable for all $\hat{\tau}_u > 0$, is as large as possible. This corresponds to minimizing the competition stability threshold $\mathcal{D}_{0,c}$ in (4.9).

From (4.9), we observe that $\mathcal{D}_{0,c}$ increases with q in a linear fashion. Within the context of our RD model (1.5), this predicts that if the police become increasingly focused on patrolling the more crime-attractive areas, then paradoxically the range of $\mathcal{D}_0$ where a K-hotspot steady-state is unstable decreases. Therefore, for the goal of reducing the number of stable crime hotspots, a police deployment with intense focus on crime-attractive areas does not offer an advantage over that of a less focused patrol (assuming that $q > 1$ for our analysis to hold). At a fixed level U_0 of police deployment, and for integer values of q with $q > 1$, the best patrol strategy is to take $q = 2$, which corresponds to the "cops-on-the-dots" strategy (cf. [12], [26], [38]) where the police mimic the movement of the criminals.

For a fixed $q > 1$, we next examine how the competition stability threshold for a K-hotspot steady-state changes with the total police deployment U_0. To this end, we substitute $U_0 = S(\gamma - \alpha) - \omega$ into (4.9), and write $\mathcal{D}_{0,c}$ as

$$\mathcal{D}_{0,c} = \frac{S}{8\pi^2\alpha^2K^4\,(1+\cos(\pi/K))}\,g(U_0)\,, \qquad g(U_0) \equiv \omega^3(1-q) + qS(\gamma-\alpha)\omega^2\,; \qquad \omega \equiv S(\gamma-\alpha) - U_0\,. \tag{4.10}$$

To analyze the critical points of $g(U_0)$, we first observe that $d\omega/dU_0 = -1$ and that $U_0 \to U_{0,\max} = S(\gamma-\alpha)$ as $\omega \to 0$. We then calculate that

$$\frac{dg}{dU_0} = -3(1-q)\omega\,(\omega - \omega_c)\,, \qquad \text{where} \qquad \omega_c \equiv \frac{2qS(\gamma-\alpha)}{3(q-1)}\,.$$

We conclude that $\omega_c < S(\gamma-\alpha)$, so that $0 < U_0 < U_{0,\max}$, iff $q > 3$. Therefore, $g(U_0)$ has a unique maximum point on $0 < U_0 < U_{0,\max}$ iff $q > 3$. Alternatively, for $q \le 3$ we have $dg/dU_0 < 0$ for $0 < U_0 < U_{0,\max}$.

This shows that if the degree of patrol focus q satisfies $q \le 3$, then $\mathcal{D}_{0,c}$ is monotonically decreasing in U_0. Therefore, for this range of q, increasing the level U_0 of police deployment leads to a larger range of $\mathcal{D}_0$ where the K-hotspot steady-state is unconditionally unstable. However, if $q > 3$, then initially as the level of police deployment is increased from zero, the

range of $\mathcal{D}_0$ where the steady-state hotspot pattern is unstable is decreased, until the critical value

$$U_{0,c} \equiv S(\gamma - \alpha) - \omega_c = S(\gamma - \alpha)\frac{(q-3)}{3(q-1)}\,, \qquad q > 3\,, \tag{4.11}$$

is reached. For $U_0 > U_{0,c}$, the hotspot pattern becomes less stable when the policing level is increased. These qualitative results are displayed graphically in Fig. 6.

Finally, we can interpret our competition stability threshold in terms of a critical threshold K_c for which a steady-state pattern of $K \geq 2$ hotspots is unconditionally unstable when $K > K_c$. This instability, which develops on an $\mathcal{O}(1)$ time scale as $\varepsilon \to 0$, is due to a real positive eigenvalue of the NLEP, and as we show from full numerical simulations in §5.2 and in §6.3 it triggers the collapse of some of the hotspots in the pattern. By writing (4.10) in terms of K, this critical threshold $K_c > 0$ when $D = \mathcal{D}_0/\epsilon^2$, and where $g(U_0)$ is defined in (4.10), is the unique root of

$$K\left[1 + \cos\left(\pi/K\right)\right]^{1/4} = \frac{(S/D)^{1/4}}{2^{3/4}\sqrt{\pi\epsilon\alpha}}\left[g(U_0)\right]^{1/4}\,. \tag{4.12}$$

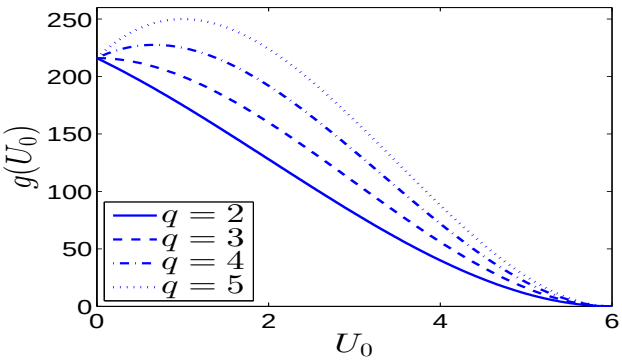

Figure 6: Competition instability threshold nonlinearity $g(U_0)$, as defined in (4.10), versus total police deployment U_0 for patrol focus parameters $q = 2, 3, 4, 5$. Other model parameters are $S = 6$, $\gamma = 2$, $\alpha = 1$, so that $U_{0,\max} = 6$ as shown in the right-most tick of the figure. The competition instability threshold $\mathcal{D}_{0,c}$ is simply a positive scaling of $g(U_0)$ according to (4.10).

5 Explicitly Solvable Case $q = 3$: Asynchronous Hotspot Oscillations

For each $j = 1, \ldots, K-1$, we now analyze the quadratic equation (3.35) in the eigenvalue parameter λ characterizing the discrete spectrum of the NLEP (3.37) for the special case where $q = 3$. In terms of the coefficients of the quadratic (3.35a), for each $j = 1, \ldots, K$ the eigenvalues λ_1 and λ_2 satisfy

$$\lambda_1\lambda_2 = \frac{c_0}{c_2}\,, \qquad \lambda_1 + \lambda_2 = -\frac{c_1}{c_2}\,, \tag{5.1}$$

where c_0, c_1, and $c_2 > 0$, are given in (3.35b). For the j-th mode, we conclude that $\mathrm{Re}(\lambda) < 0$ when $c_0 > 0$ and $c_1 > 0$. We have instability of the j-th mode if either $c_0 < 0$, or if $c_0 > 0$ and $c_1 < 0$. We have purely complex eigenvalues, corresponding to a Hopf bifurcation point, when $c_0 > 0$ and $c_1 = 0$.

We first determine the signs of c_0 and c_1 in terms of D_j and $\hat{\tau}_u$. From (3.35b) we observe that $c_0 = 0$ when the zero-eigenvalue crossing condition (4.6) holds, which yields (4.7) for D_j, which we relabel as

$$D_j = D^{\star}_{\mathrm{up}} \equiv \frac{\omega^3}{4\pi^2 K^3\alpha^2}\left(1 + \frac{3U_0}{\omega}\right)\,. \tag{5.2}$$

Next, we set $c_1 = 0$ in (3.35b) to get, using (3.30) for $\chi_{0,j}^{-1}$, that

$$\frac{\hat{\tau}_u}{D_j \kappa_3} = \frac{2\chi_{0,j}^{-1}}{3\left(2\chi_{0,j}^{-1} - 3\right)} = \frac{1}{3}\frac{(D_j + \alpha/\kappa_3)}{(D_j - \alpha/(2\kappa_3))}\,. \tag{5.3}$$

The denominator of this expression motivates introducing $D_{\rm low}^\star$, defined by

$$D_{\rm low}^\star \equiv \frac{\alpha}{2\kappa_3} = \frac{\omega^3}{4\pi^2 K^3 \alpha^2}\,, \tag{5.4}$$

where we have used the expression (3.29) for κ_3. Upon using (5.4) in (5.3), we obtain that $c_1 = 0$ when $\hat{\tau}_u$ satisfies

$$\hat{\tau}_u = \hat{\tau}_{uH,j} \equiv \mathcal{H}\left(D_j/D_{\rm low}^\star\right)\,, \qquad j = 1, \ldots, K-1\,, \tag{5.5a}$$

where the function $\mathcal{H}(\beta)$ is defined by

$$\mathcal{H}(\beta) \equiv \frac{\alpha\beta}{2}\left(\frac{1}{3} + \frac{1}{\beta - 1}\right)\,. \tag{5.5b}$$

Notice that $\hat{\tau}_{uH,j} > 0$ only when $D_j > D_{\rm low}^\star$. Some simple algebra then shows that we can write c_1 in (3.35b) as

$$c_1 = \frac{1}{\alpha}\left(\frac{D_{\rm low}^\star}{D_j} - 1\right)\left(\hat{\tau}_u - \hat{\tau}_{uH,j}\right)\,. \tag{5.6}$$

For the j-th mode, we have $c_1 < 0$ if $D_j > D_{\rm low}^\star$ and $\hat{\tau}_u > \hat{\tau}_{uH,j}$, while $c_1 > 0$ if either $D_j < D_{\rm low}^\star$, or $D_j > D_{\rm low}^\star$ and $\hat{\tau}_u < \hat{\tau}_{uH,j}$. With these signs for c_0 and c_1, we summarize our stability result for the j-th mode so far as follows:

- For $D_j > D_{\rm up}^\star$ ($c_0 < 0$), we have $\mathrm{Re}(\lambda) > 0$, and instability is due to a positive real eigenvalue.
- For $D_j < D_{\rm low}^\star$ ($c_0 > 0$ and $c_1 > 0$), we have stability $\mathrm{Re}(\lambda) < 0$.
- On the range $D_{\rm low}^\star < D_j < D_{\rm up}^\star$ ($c_0 > 0$), we have instability if $\hat{\tau}_u > \hat{\tau}_{uH,j}$ ($c_1 < 0$) and stability if $\hat{\tau}_u < \hat{\tau}_{uH,j}$ ($c_1 > 0$). On this range of D_j, the Hopf bifurcation threshold, $\hat{\tau}_{uH,j} > 0$, is given in (5.5).

Next, we must reformulate this result in terms of $\mathcal{D}_0$ rather than D_j, by using $D_j = \mathcal{D}_0\,(2K/S)\,(1 - \cos(\pi j/K))$. The interval $D_{\rm low}^\star < D_1 < D_{\rm up}^\star$, where a Hopf bifurcation value of $\hat{\tau}_u$ exists, becomes

$$\frac{S D_{\rm low}^\star}{2K\,(1 - \cos(\pi j/K))} \le \mathcal{D}_0 \le \frac{S D_{\rm up}^\star}{2K\,(1 - \cos(\pi j/K))}\,, \tag{5.7}$$

where $D_{\rm up}^\star/D_{\rm low}^\star = 1 + 3U_0/\omega$ from (5.2) and (5.4). It is convenient to write (5.7) in terms of the competition stability threshold $\mathcal{D}_{0,c}$ defined by setting $q = 3$ in (4.9). In this way, the interval in (5.7) becomes

$$D_{0,j}^- < \mathcal{D}_0 < D_{0,j}^+\,; \qquad D_{0,j}^+ \equiv \mathcal{D}_{0,c}\left(\frac{1 + \cos(\pi/K)}{1 - \cos(\pi j/K)}\right)\,, \qquad D_{0,j}^- \equiv \frac{\mathcal{D}_{0,c}}{(1 + 3U_0/\omega)}\left(\frac{1 + \cos(\pi/K)}{1 - \cos(\pi j/K)}\right)\,, \tag{5.8a}$$

where $\mathcal{D}_{0,c}$ is given by

$$\mathcal{D}_{0,c} \equiv \frac{\omega^3 S}{8\pi^2\alpha^2 K^4\,(1 + \cos(\pi/K))}\left(1 + \frac{3U_0}{\omega}\right)\,. \tag{5.8b}$$

We observe that when $j = K - 1$, we have $D_{0,K-1}^+ = \mathcal{D}_{0,c}$. Now since $D_j/D_{\rm low}^\star = \mathcal{D}_0/D_{0,j}^-$, the Hopf bifurcation threshold in (5.5) becomes

$$\hat{\tau}_{uH,j} = \mathcal{H}\left(\mathcal{D}_0/D_{0,j}^-\right)\,, \qquad \text{on} \quad D_{0,j}^- < \mathcal{D}_0 < D_{0,j}^+\,. \tag{5.9}$$

From this expression, we readily derive the following limiting behavior for $\hat{\tau}_{uH,j}$ at the two ends of the interval:

$$\hat{\tau}_{uH,j} \sim \frac{\alpha}{2}\left[\frac{\mathcal{D}_0}{D_{0,j}^-} - 1\right]^{-1}\,, \quad \text{as} \quad \mathcal{D}_0 \to D_{0,j}^-\,; \qquad \hat{\tau}_{uH_j} \sim \frac{\omega\alpha}{6U_0}\left(\frac{U_0}{\omega} + 1\right)\left(\frac{3U_0}{\omega} + 1\right)\,, \quad \text{as} \quad \mathcal{D}_0 \to D_{0,j}^+\,. \tag{5.10}$$

For each fixed $j = 1, \ldots, K-1$, we summarize the behavior of the roots of the quadratic (3.35), corresponding to the discrete eigenvalues of the NLEP (3.37) as follows:

Proposition 5.1 *For each fixed $j = 1, \ldots, K-1$, let λ_+ and λ_-, with $Re(\lambda_+) \geq Re(\lambda_-)$, denote the two solutions of the quadratic equation (3.35). Then, their location in the complex plane depends on $\mathcal{D}_0$ and $\hat{\tau}_u$ as follows:*

- *For $\mathcal{D}_0 > D^+_{0,j}$, we have $\lambda_+ > 0$ and $\lambda_- < 0$ for all $\hat{\tau}_u \geq 0$.*
- *For $\mathcal{D}_0 < D^-_{0,j}$, we have $Re(\lambda_\pm) < 0$ for all $\hat{\tau}_u \geq 0$.*
- *For $D^-_{0,j} < \mathcal{D}_0 < D^+_{0,j}$ we have $Re(\lambda_\pm) > 0$ when $\hat{\tau}_u > \hat{\tau}_{uH,j}$ and $Re(\lambda_\pm) < 0$ when $0 \leq \hat{\tau}_{uH,j} < \hat{\tau}_u$.*

Here $D^-_{0,j}$ and $D^+_{0,j}$ are defined in (5.8a). The Hopf bifurcation threshold $\hat{\tau}_{uH,j}$, which is defined on the interval $D^-_{0,j} < \mathcal{D}_0 < D^+_{0,j}$, is given in (5.9).

Since $D^+_{0,j}/D^-_{0,j} = 1 + 3U_0/\omega$, we observe that the width of the interval $D^-_{0,j} < \mathcal{D}_0 < D^+_{0,j}$ where an asynchronous oscillatory instability in the hotspot amplitudes occurs is nonzero only as a result of the simple coupling term $-U$ in our three-component RD system (1.1). In the absence of police, this interval disappears and the basic crime model does not support oscillatory instabilities in this parameter regime.

Next, we examine the monotonicity properties of the universal function $\mathcal{H}(\beta)$ characterizing Hopf bifurcations, as defined in (5.5b), on the interval $1 < \beta < D^+_{0,j}/D^-_{0,j} = 1 + 3U_0/\omega$. We calculate $\mathcal{H}'(\beta)$ to get

$$\mathcal{H}'(\beta) = \frac{\alpha}{6(\beta-1)^2}\left[(\beta-1)^2 - 3\right],$$

so that $\mathcal{H}'(\beta) < 0$ if $1 < \beta < 1 + \sqrt{3}$ and $\mathcal{H}'(\beta) > 0$ if $\beta > 1 + \sqrt{3}$. We conclude that $\mathcal{H}'(\beta) < 0$ on $1 < \beta < 1 + 3U_0/\omega$ only when $\omega > \sqrt{3}U_0$. Since $\omega = S(\gamma - \alpha) - U_0$ we conclude that

$$\mathcal{H}'(\beta) < 0 \quad \text{on} \quad 1 < \beta < 3U_0/\omega\,, \quad \text{iff} \quad U_0 < \frac{S(\gamma-\alpha)}{1+\sqrt{3}}\,. \tag{5.11}$$

If $\frac{S(\gamma-\alpha)}{1+\sqrt{3}} < U_0 < U_{0,\max}$, then $\mathcal{H}(\beta)$ increases on $1 + \sqrt{3} < \beta < 1 + 3U_0/\omega$.

Next, we rewrite the coefficients c_0, c_1, and c_2, in the quadratic (3.35) so as to readily calculate the Hopf bifurcation eigenvalue $\lambda = i\lambda_{IH}$. After some algebra we obtain that

$$c_0 = -\frac{1}{2}\left(1 + \frac{3U_0}{\omega}\right)\left(\frac{\mathcal{D}_0}{D^+_{0,j}} - 1\right), \qquad c_1 = \frac{\hat{\tau}_{uH,j}}{\alpha}\left(\frac{D^-_{0,j}}{\mathcal{D}_0} - 1\right)\left(\frac{\hat{\tau}_u}{\hat{\tau}_{uH,j}} - 1\right), \qquad c_2 = \frac{\hat{\tau}_{uH,j}}{3\alpha}\left(\frac{2D^-_{0,j}}{\mathcal{D}_0} + 1\right), \tag{5.12}$$

where $\hat{\tau}_{uH,j}$ is defined in (5.9). The Hopf bifurcation eigenvalue $\lambda = i\lambda_{IH}$ with $\lambda_{IH} > 0$ is $\lambda_{IH} = \sqrt{c_0/c_2}$, which yields

$$\lambda_{IH} = \frac{3}{(2 + \mathcal{D}_0/D^-_{0,j})}\sqrt{\left(1 + \frac{3U_0}{\omega}\right)\left(1 - \frac{\mathcal{D}_0}{D^+_{0,j}}\right)\left(\frac{\mathcal{D}_0}{D^-_{0,j}} - 1\right)}, \quad \text{on} \quad D^-_{0,j} < \mathcal{D}_0 < D^+_{0,j}\,. \tag{5.13}$$

This shows that λ_{IH} vanishes at both endpoints. We use the asymptotic behaviors $\mathcal{D}_0/D^+_{0,j} \to (1 + 3U_0/\omega)^{-1}$ as $\mathcal{D}_0 \to D^-_{0,j}$ and $\mathcal{D}_0/D^-_{0,j} \to (1 + 3U_0/\omega)$ as $\mathcal{D}_0 \to D^+_{0,j}$, so that from (5.13) we obtain the limiting asymptotic behavior

$$\lambda_{IH} \sim \frac{1}{(1+U_0/\omega)}\sqrt{\frac{3U_0}{\omega}\left(1 + \frac{3U_0}{\omega}\right)\left(1 - \frac{\mathcal{D}_0}{D^+_{0,j}}\right)} \quad \text{as} \quad \mathcal{D}_0 \to D^+_{0,j}\,; \qquad \lambda_{IH} \sim \sqrt{\frac{3U_0}{\omega}\left(\frac{\mathcal{D}_0}{D^-_{0,j}} - 1\right)} \quad \text{as} \quad \mathcal{D}_0 \to D^-_{0,j}\,. \tag{5.14}$$

For the special case $K = 2$, we now state our main result stability result related to Hopf bifurcations.

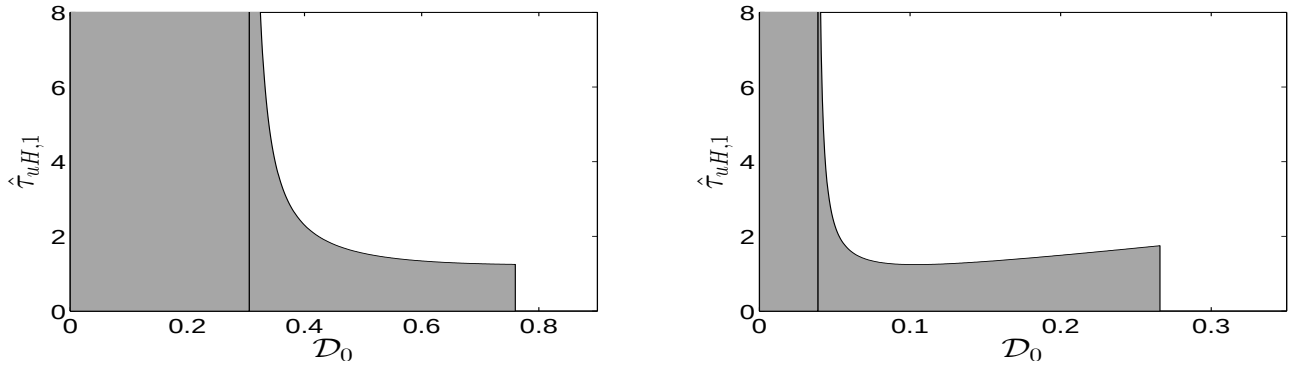

Figure 7: Plot of the Hopf bifurcation threshold $\hat{\tau}_{uH_1}$ versus $\mathcal{D}_0$ on the range $\mathcal{D}_{0,c}/(1+3U_0/\omega) < \mathcal{D}_0 < \mathcal{D}_{0c}$ for $K=2$, $q=3$, $S=6$, $\gamma=2$, $\alpha=1$, and with $U_0=2$ (left panel) and $U_0=4$ (right panel). The shaded region is where the steady-state two-hotspot pattern is linearly stable. The thin vertical line in each figure is the lower boundary $\mathcal{D}_{0,c}/(1+3U_0/\omega)$, while the right edge of the shaded region is the competition stability threshold. The Hopf bifurcation curve in the right panel is not monotonic since $U_0 > S(\gamma-\alpha)/(1+\sqrt{3})$ when $U_0=4$.

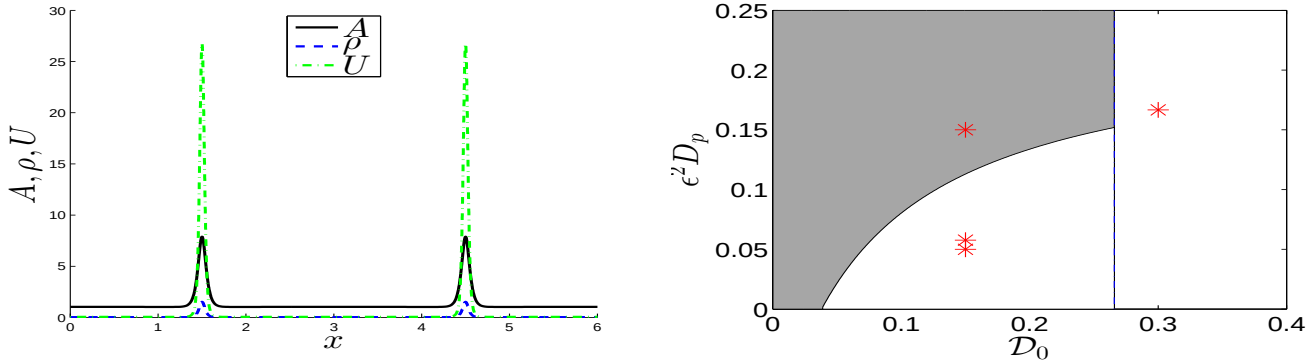

Figure 8: Left panel: the steady-state two-hotspot solution for $S=6$, $\gamma=2$, $\alpha=1$, $U_0=4$, $\mathcal{D}_0=0.15$, $\epsilon=0.035$, and $q=3$. Right panel: Plot of the Hopf bifurcation threshold for the scaled police diffusivity $\epsilon^2 D_p \equiv \mathcal{D}_0/\hat{\tau}_{uH_1}$ versus $\mathcal{D}_0$ on the range $\mathcal{D}_{0,c}/(1+3U_0/\omega) < \mathcal{D}_0 < \mathcal{D}_{0c}$. The thin vertical line is the competition stability threshold $\mathcal{D}_{0,c}$ given in Proposition 5.2. The shaded region is where the steady-state two-hotspot pattern is linearly stable. For $\mathcal{D}_0 > \mathcal{D}_{0c}$ the hotspot solution is unstable due to a competition instability, whereas in the small unshaded region for $\mathcal{D}_0 < \mathcal{D}_{0c}$, the hotspot steady-state is unstable to an asynchronous oscillatory instability of the hotspot amplitudes. The full PDE simulations in Fig. 14 and in Fig. 15 are done at the marked points.

Proposition 5.2 *For $\epsilon \to 0$, $q = 3$, $0 < U_0 < U_{0,max}$, $\hat{\tau}_u \ll \mathcal{O}(\epsilon^{-2})$, and $\mathcal{D}_0 = \epsilon^2 D = \mathcal{O}(1)$, the linear stability properties of a two-hotspot steady-state solution of (1.5) are as follows:*

- *For $\mathcal{D}_0 > D^+_{0,1} \equiv \mathcal{D}_{0,c}$, the NLEP (3.37) has a positive real eigenvalue for all $\hat{\tau}_u \geq 0$ and so the two-hotspot steady-state is unstable. Here $\mathcal{D}_{0,c} = S\omega^3 \left(1 + 3U_0/\omega\right)/[128\pi^2\alpha^2]$ is the competition stability threshold with $\omega \equiv S(\gamma - \alpha) - U_0$.*

- *On the range $D^-_{0,1} \equiv \mathcal{D}_{0,c}/\left(1 + 3U_0/\omega\right) < \mathcal{D}_0 < \mathcal{D}_{0,c}$, there is a Hopf bifurcation corresponding to an asynchronous oscillatory instability of the hotspot amplitudes when*

$$\hat{\tau}_u \equiv \hat{\tau}_{uH,1} = \mathcal{H}\left(\mathcal{D}_0/D^-_{0,1}\right), \quad \text{on} \quad D^-_{0,1} < \mathcal{D}_0 < \mathcal{D}_{0,c}\,, \tag{5.15}$$

  where $\mathcal{H}(\beta)$ is defined in (5.5b). When $\hat{\tau}_u > \hat{\tau}_{uH,1}$, the two-hotspot steady-state is unstable, while if $\hat{\tau}_u < \hat{\tau}_{uH,1}$ the two-hotspot pattern is linearly stable.

- *On the range $0 < \mathcal{D}_0 < D^-_{0,1} \equiv \mathcal{D}_{0,c}/\left(1 + 3U_0/\omega\right)$, the two-hotspot steady-state is linearly stable for all $\hat{\tau}_u \geq 0$.*

In terms of a scaled police diffusivity defined by $\epsilon^2 D_p \equiv \mathcal{D}_0/\hat{\tau}_u$, Proposition 5.2 implies the following:

Corollary 5.3 *Under the conditions of Proposition 5.2 we have the following:*

- *For $\mathcal{D}_0 > \mathcal{D}_{0,c} \equiv S\omega^3 \left(1 + 3U_0/\omega\right)/[128\pi^2\alpha^2]$, the two-hotspot steady-state is unstable for all scaled police diffusivities $\epsilon^2 D_p > 0$.*

- *On the range $\mathcal{D}_{0,c}/\left(1 + 3U_0/\omega\right) < \mathcal{D}_0 < \mathcal{D}_{0,c}$, the two hotspot steady-state is unstable to an asynchronous oscillatory instability of the hotspot amplitudes if $\epsilon^2 D_p < \mathcal{D}_0/\hat{\tau}_{uH,1}$, while the steady-state is linearly stable when $\epsilon^2 D_p > \mathcal{D}_0/\hat{\tau}_{uH,1}$. Here $\hat{\tau}_{uH,1}$ is the Hopf bifurcation threshold in (5.15).*

- *On the range $0 < \mathcal{D}_0 < \mathcal{D}_{0,c}/\left(1 + 3U_0/\omega\right)$, the two-hotspot steady-state is linearly stable for all $\epsilon^2 D_p \geq 0$.*

We now illustrate our main stability results for $K = 2$, $S = 6$, $\gamma = 2$, and $\alpha = 1$. In Fig. 7 we plot the region of linear stability in the $\hat{\tau}_u$ versus $\mathcal{D}_0$ parameter plane for $U_0 = 2$ (left panel) and $U_0 = 4$ (right panel). For $U_0 = 4$, we have $\omega < \sqrt{3}U_0$, and so the Hopf bifurcation threshold $\hat{\tau}_{uH,1}$ is not monotone in $\mathcal{D}_0$, as seen in the right panel of Fig. 7. From this figure, we observe that as U_0 increases the region where the two-hotspot steady-state is linearly stable is smaller, as expected. With regards to the scaled police diffusivity $\epsilon^2 D_p \equiv \mathcal{D}_0/\hat{\tau}_u$, in the right panels of Fig. 1 and Fig. 8 we plot the corresponding region of linear stability in the $\epsilon^2 D_p$ versus $\mathcal{D}_0$ plane for $U_0 = 2$ and $U_0 = 4$, respectively. For $U_0 = 2$ and $U_0 = 4$, the corresponding steady-state two-hotspot solution is shown in the left panels of Fig. 1 and Fig. 8. For $U_0 = 2$, the predicted linear stability results were validated in Fig. 2 by performing full numerical solutions of the PDE system (1.5). A similar validation for the linear stability phase diagram in the right panel of Fig. 8 for $U_0 = 4$ is given by the full PDE simulations reported in Fig. 14 and Fig. 15 below in §5.2.

5.1 The Stability Phase Diagram for $q = 3$: $K \geq 3$ Hotspots

Next, we determine the parameter range of $\mathcal{D}_0$ and $\hat{\tau}_u$ for which a K-hotspot steady-state solution, with $K \geq 3$, is linearly stable. To do so, we need to guarantee that $\mathrm{Re}(\lambda) < 0$ for each of the quadratics in (3.35), i.e. for each $j = 1, \ldots, K-1$. In this way, we will ensure that any discrete eigenvalue of the NLEP (3.37) satisfies $\mathrm{Re}(\lambda) \leq 0$.

By using (5.8a), we readily obtain the ordering principle that

$$D^{\pm}_{0,j+1} < D^{\pm}_{0,j}\,, \quad \text{and} \quad D^-_{0,j} < D^+_{0,j}\,, \qquad \text{for} \quad j = 1, \ldots, K-2\,. \tag{5.16}$$

We conclude that

$$D^+_{0,K-1} = \min_{j=1,\ldots,K-1}\{D^+_{0,j}\}\,, \qquad D^-_{0,K-1} = \min_{j=1,\ldots,K-1}\{D^-_{0,j}\}\,. \tag{5.17}$$

From Proposition 5.1, we conclude for each of the quadratics (3.35), i.e. for each $j = 1,\ldots,K-1$, that $\mathrm{Re}(\lambda) < 0$ for any $\hat{\tau}_u \geq 0$ when $\mathcal{D}_0 < D^-_{0,K-1}$. Therefore, a K-hotspot steady-state pattern is linearly stable for all $\hat{\tau}_u \geq 0$ on the range $0 < \mathcal{D}_0 < D^-_{0,K-1}$. For the range $\mathcal{D}_0 > D^+_{0,K-1}$, we conclude from Proposition 5.1 that the $K-1$ mode must be unstable due to a positive real eigenvalue for any $\hat{\tau}_u \geq 0$. Therefore, for $\mathcal{D}_0 > D^+_{0,K-1}$, a K-hotspot steady-state solution is unstable for all $\hat{\tau}_u \geq 0$. Additional unstable eigenvalues due to Hopf bifurcations associated with the remaining modes $j = 1,\ldots,K-2$ are possible depending on the value of $\hat{\tau}_u$.

To complete the stability phase diagram in the $\hat{\tau}_u$ versus $\mathcal{D}_0$ parameter plane, we need only focus on the interval $D^-_{0,K-1} < \mathcal{D}_0 < D^+_{0,K-1}$. On this interval, the sign-alternating $K-1$ mode undergoes a Hopf bifurcation at $\hat{\tau}_u = \hat{\tau}_{uH,K-1}$, as given from (5.9) by

$$\hat{\tau}_{uH,K-1} \equiv \mathcal{H}(\beta)\,, \qquad \text{on} \quad 1 \leq \beta \leq \frac{D^+_{0,K-1}}{D^-_{0,K-1}} = 1 + \frac{3U_0}{\omega}\,, \qquad \text{where} \quad \beta \equiv \frac{\mathcal{D}_0}{D^-_{0,K-1}}\,. \tag{5.18}$$

Here $\mathcal{H}(\beta)$ is defined in (5.5b). When $\hat{\tau}_u > \hat{\tau}_{uH,K-1}$ the $K-1$ mode is unstable, whereas if $\hat{\tau}_u < \hat{\tau}_{uH,K-1}$ the $K-1$ mode is linearly stable.

We now seek to determine conditions for which the Hopf bifurcation threshold for the $K-1$ mode is smaller than any of the other $K-2$ possible Hopf bifurcation values $\hat{\tau}_{uH,j}$ for $j = 1,\ldots,K-2$ when restricted to the interval $D^-_{0,K-1} < \mathcal{D}_0 < D^+_{0,K-1}$. From (5.9), these other Hopf bifurcation thresholds, for $j = 1,\ldots,K-2$, can be written in terms of β, as defined in (5.18), by

$$\hat{\tau}_{uH,j} = \mathcal{H}(\xi_j\beta)\,, \qquad \text{on} \quad \frac{1}{\xi_j} \leq \beta \leq \frac{1}{\xi_j}\left(1 + \frac{3U_0}{\omega}\right)\,, \tag{5.19a}$$

where, from (5.8), we define

$$\xi_j \equiv \frac{D^-_{0,K-1}}{D^-_{0,j}} = \frac{1-\cos(\pi j/K)}{1+\cos(\pi/K)}\,, \qquad j = 1,\ldots,K-2\,. \tag{5.19b}$$

We observe from (5.19b) that the following ordering principle holds:

$$\xi_j < \xi_{j+1} < 1\,, \qquad j = 1,\ldots,K-3\,, \qquad \xi_{K-2} = \max_{j=1,\ldots,K-2}\{\xi_j\}\,. \tag{5.19c}$$

Comparing the intervals in (5.19a) and (5.18), we want to determine a specific parameter range of the total police deployment U_0 for which, for any $j = 1,\ldots,K-2$, we have that $\hat{\tau}_{uH,K-1} < \hat{\tau}_{uH,j}$ on the overlap domain $\xi_j^{-1} \leq \beta \leq 1+3U_0/\omega$. If the overlap domain is the null-set for the j-th mode, i.e. if $\xi_j < 1/(1+3U_0/\omega)$, then we can simply ignore the j-th mode on $D^-_{0,K-1} < \mathcal{D}_0 < D^+_{0,K-1}$. As such, we need only consider values of j (if any) for which $\xi_j^{-1} < 1 + 3U_0/\omega$, so that an overlap domain exists. Since $\mathcal{H}(\beta)$ is monotone decreasing on $1 < \beta < 1+\sqrt{3}$, we readily obtain that $\mathcal{H}(\beta) - \mathcal{H}(\xi_j\beta) \equiv \int_{\xi_j\beta}^{\beta} \mathcal{H}'(y)\,dy < 0$ on the interval $\xi_j^{-1} < \beta < 1+\sqrt{3}$. In this way, we conclude that

$$\mathcal{H}(\xi_j\beta) < \mathcal{H}(\beta)\,, \qquad \text{on} \quad \xi_j^{-1} \leq \beta \leq 1 + \frac{3U_0}{\omega}\,, \qquad \text{when} \quad \omega > \sqrt{3}U_0\,. \tag{5.20}$$

Therefore, on the range for which $\mathcal{H}(\beta)$ is monotonically decreasing, it follows that the Hopf bifurcation threshold of $\hat{\tau}_u$ for any mode $j = 1,\ldots,K-2$ cannot be smaller than that for the $K-1$ mode. Although the monotonicity of $\mathcal{H}(\beta)$ on $\xi_j^{-1} \leq \beta \leq 1+3U_0/\omega$ for $\omega > \sqrt{3}U_0$ provides a sufficient condition for the ordering principle $\hat{\tau}_{uH,K-1} < \hat{\tau}_{uH,j}$ for $j = 1,\ldots,K-2$ to hold, we now show explicitly that the monotonicity of $\mathcal{H}(\beta)$ is not strictly necessary.

We now determine a precise condition that ensures that $\hat{\tau}_{uH,K-1} < \hat{\tau}_{uH,K-2}$ on an assumed overlap domain $\xi_{K-2}^{-1} \leq \beta \leq 1 + 3U_0/\omega$. Owing to the ordering principle $\xi_j < \xi_{j+1}$ for $j = 1, \ldots, K-3$ from (5.19c), the first Hopf threshold to potentially decrease below that of the $K-1$ mode must be the $K-2$ mode, and so we focus only on a comparison with the $K-2$ mode. From (5.18) and (5.19a), and by using the explicit expression for $\mathcal{H}(\beta)$ in (5.5b), we calculate after some algebra that $\mathcal{H}(\xi_{K-2}\beta) \geq \mathcal{H}(\beta)$ on $\xi_{K-2}^{-1} \leq \beta \leq 1 + 3U_0/\omega$, if and only if

$$\mathcal{K}(\beta) \equiv (\xi_{K-2}\beta - 1)(\beta - 1) < 3\,, \qquad \text{on} \quad 1 < \xi_{K-2}^{-1} \leq \beta \leq 1 + 3U_0/\omega\,. \tag{5.21}$$

Since $\mathcal{K}'(\beta) > 0$ on this interval, this inequality holds if and only if $1 + 3U_0/\omega < \beta_{\max}$, where $\mathcal{K}(\beta_{\max}) = 3$. By setting $\mathcal{K}(\beta) = 3$, and solving the quadratic for $\beta = \beta_{\max}$, we obtain that (5.21) holds if and only if

$$\frac{\sqrt{3}U_0}{\omega} < \mathcal{Z}(\xi_{K-2})\,, \qquad \text{where} \quad \mathcal{Z}(\xi_{K-2}) \equiv \frac{1}{\sqrt{3}}\left(-\frac{1}{2} + \frac{1}{2\xi_{K-2}}\left[1 + \sqrt{\xi_{K-2}^2 + 10\xi_{K-2} + 1}\right]\right)\,. \tag{5.22}$$

Here $\omega = S(\gamma - \alpha) - U_0$ and ξ_{K-2} can be found from (5.19b). On $0 < \xi < 1$, we have that $\mathcal{Z}(\xi)$ satisfies

$$\mathcal{Z}(\xi) \to +\infty \quad \text{as} \quad \xi \to 0^+\,, \qquad \mathcal{Z}(1) = 1\,, \qquad \mathcal{Z}'(\xi) < 0\,, \quad \text{on} \quad 0 < \xi < 1\,. \tag{5.23}$$

It follows that $\mathcal{Z}(\xi) > 1$ on $0 < \xi < 1$. The key inequality (5.22) implies that $\omega > \sqrt{3}U_0/\mathcal{Z}(\xi_{K-2})$, which yields a larger range of ω than the range $\omega > \sqrt{3}U_0$ where $\mathcal{H}(\beta)$ is monotonic. This inequality (5.22) can also be used to give a precise upper bound on U_0 for which the $K-1$ mode determines the Hopf bifurcation threshold for $\hat{\tau}_u$ on the entire range $D_{0,K-1}^- < \mathcal{D}_0 < D_{0,K-1}^+$. In this way, for $K \geq 3$, we summarize our main stability result for a K-hotspot steady-state solution as follows:

Proposition 5.4 *For $\epsilon \to 0$, $q = 3$, $K \geq 3$, $0 < U_0 < U_{0,max}$, $\hat{\tau}_u \ll \mathcal{O}(\epsilon^{-2})$, and $\mathcal{D}_0 = \epsilon^2 D = \mathcal{O}(1)$, the linear stability properties of a K-hotspot steady-state solution of (1.5) are as follows:*

- *For $\mathcal{D}_0 > D_{0,K-1}^+ \equiv \mathcal{D}_{0,c}$, the NLEP (3.37) has at least one positive real eigenvalue for all $\hat{\tau}_u \geq 0$. Additional unstable eigenvalues as a result of Hopf bifurcations associated with the other modes $j = 1, \ldots, K-2$ are possible depending on the value of $\hat{\tau}_u$. Here $\mathcal{D}_{0,c}$ is the competition stability threshold given in (4.9) with $q = 3$.*

- *On the range $D_{0,K-1}^- \equiv \mathcal{D}_{0,c}/(1 + 3U_0/\omega) < \mathcal{D}_0 < \mathcal{D}_{0,c}$, and when U_0 satisfies*

$$U_0 < U_{0,swit} \equiv \left(\frac{\mathcal{Z}(\xi_{K-2})}{\sqrt{3} + \mathcal{Z}(\xi_{K-2})}\right) S(\gamma - \alpha)\,, \qquad \textit{where} \quad \xi_{K-2} \equiv \frac{1 - \cos(\pi(K-2)/K)}{1 + \cos(\pi/K)}\,, \tag{5.24}$$

  and where $\mathcal{Z}(\xi)$ is defined in (5.22), the $K-1$ sign-alternating mode sets the stability threshold on the entire range. For $\hat{\tau}_u > \hat{\tau}_{uH,K-1}$, the K-hotspot pattern is unstable, while if $\hat{\tau}_u < \hat{\tau}_{uH,K-1}$ the K-hotspot pattern is linearly stable. With $\mathcal{H}(\beta)$, as defined in (5.5b), the minimal Hopf bifurcation value of $\hat{\tau}_u$ is

$$\hat{\tau}_{uH,K-1} \equiv \mathcal{H}\left(\mathcal{D}_0/D_{0,K-1}^-\right)\,, \quad \textit{on} \quad D_{0,K-1}^- \equiv \frac{\mathcal{D}_{0c}}{1 + 3U_0/\omega} < \mathcal{D}_0 < \mathcal{D}_{0,c}\,, \tag{5.25}$$

  where

- *On the range $0 < \mathcal{D}_0 < D_{0,K-1}^- \equiv \mathcal{D}_{0,c}/(1 + 3U_0/\omega)$, the K-hotspot steady-state is linearly stable for all $\hat{\tau}_u \geq 0$.*

In terms of a scaled police diffusivity defined by $\epsilon^2 D_p \equiv \mathcal{D}_0/\hat{\tau}_u$, Proposition 5.4 implies the following:

Corollary 5.5 *Under the conditions of Proposition 5.4, we have the following:*

- *For $\mathcal{D}_0 > \mathcal{D}_{0,c}$, the K-hotspot steady-state is unstable for all scaled police diffusivities $\epsilon^2 D_p > 0$. Here $\mathcal{D}_{0,c}$ is defined in (4.9) with $q = 3$.*

- *On the range $\mathcal{D}_{0,c}/\left(1 + 3U_0/\omega\right) < \mathcal{D}_0 < \mathcal{D}_{0,c}$, and when $U_0 < U_{0,swit}$, as defined in (5.24), the K-hotspot steady-state is unstable to a sign-alternating asynchronous oscillatory instability of the hotspot amplitudes if $\epsilon^2 D_p < \mathcal{D}_0/\hat{\tau}_{uH,K-1}$ where $\hat{\tau}_{uH,K-1}$ is defined in (5.25). Alternatively, this steady-state is linearly stable when $\epsilon^2 D_p > \mathcal{D}_0/\hat{\tau}_{uH,K-1}$.*

- *On the range $0 < \mathcal{D}_0 < \mathcal{D}_{0,c}/\left(1 + 3U_0/\omega\right)$, the K-hotspot steady-state is linearly stable for all $\epsilon^2 D_p \geq 0$.*

We remark that the upper bound $U_{0,\text{swit}}$ in (5.24) can be calculated explicitly when $K = 3$ and $K = 4$. When $K = 3$, we calculate $\xi_1 = 1/3$ and $\mathcal{Z}(\xi_1) = \left(1 + \sqrt{10}\right)/\sqrt{3}$. We then obtain from (5.24) that the sign-alternating $K - 1$ mode sets the Hopf bifurcation threshold when

$$U_0 < U_{0,\text{swit}} \equiv \frac{3S(\gamma - \alpha)}{2 + \sqrt{10}} \approx (0.58114)S(\gamma - \alpha)\,, \qquad \text{for} \quad K = 3\,. \tag{5.26}$$

Similarly, for $K = 4$, we calculate $\xi_2 = 2 - \sqrt{2}$, and

$$\mathcal{Z}(\xi_2) = \frac{1}{\sqrt{3}}\left[\frac{\sqrt{2}}{4} + \left(\frac{1}{2} + \frac{\sqrt{2}}{4}\right)\sqrt{27 - 14\sqrt{2}}\right] \approx 1.5265\,.$$

From (5.24), the $K - 1$ mode sets the Hopf bifurcation threshold when

$$U_0 < U_{0,\text{swit}} \approx (0.46847)S(\gamma - \alpha)\,, \qquad \text{for} \quad K = 4\,. \tag{5.27}$$

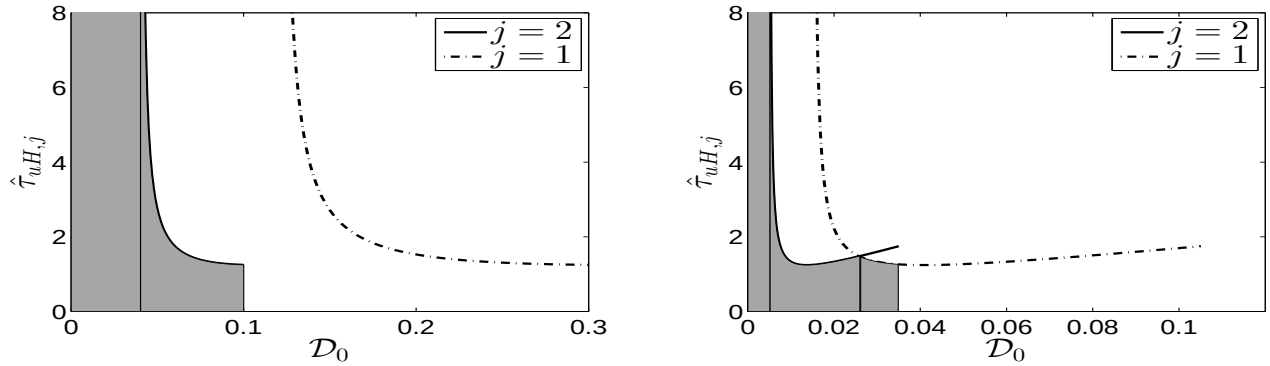

Figure 9: Linear stability (shaded) region in the $\hat{\tau}_u$ versus $\mathcal{D}_0$ plane for $K = 3$ when $S = 6$, $\gamma = 2$, and $\alpha = 1$, and for $U_0 = 2$ (left panel) and $U_0 = 4$ (right panel), as characterized by Proposition 5.4. To the left of the thin vertical line the steady-state is unconditionally stable. The solid and dot-dashed curves are the Hopf bifurcation boundaries for the (sign-alternating) $j = 2$ mode and the $j = 1$ mode, respectively. For $U_0 = 2$ (left panel) the Hopf boundary is determined by the $j = 2$ mode. For $U_0 = 4 > U_{0,swit} \approx 3.478$ (right panel) the Hopf boundary consists of both the $j = 2$ and $j = 1$ mode. The three-hotspot steady-state is unstable to an oscillatory instability above the solid or dotted curves. At the ends of the Hopf bifurcation curves the Hopf eigenvalue tends to zero.

We now illustrate our main stability results in Proposition 5.4 and Corollary 5.5 for $S = 6$, $\gamma = 2$, and $\alpha = 1$. We take $K = 3$ or $K = 4$, and either $U_0 = 2$ and $U_0 = 4$. For these parameters, (5.26) and (5.27) yield that $U_{0,\text{swit}} \approx 3.487$ for $K = 3$ and $U_{0,\text{swit}} \approx 2.811$ for $K = 4$. Therefore, for both $K = 3$ and $K = 4$ it is only for the smaller value $U_0 = 2$ that the sign-alternating mode sets the Hopf bifurcation threshold.

For $K = 3$, the shaded region in Fig. 9 is the theoretically predicted region of linear stability in the $\hat{\tau}_u$ versus $\mathcal{D}_0$ parameter plane for $U_0 = 2$ (left panel) and for $U_0 = 4$ (right panel). In this figure the dotted curve and solid curves are

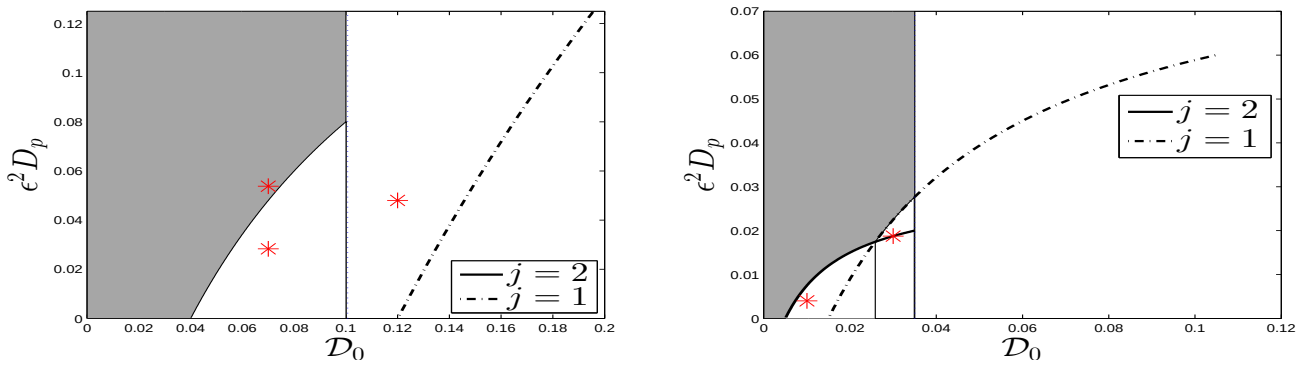

Figure 10: Same plot as Fig. 9 except in the scaled police diffusivity $\epsilon^2 D_p = \mathcal{D}_0/\hat{\tau}_u$ versus $\mathcal{D}_0$ plane for $K = 3$, $S = 6$, $\gamma = 2$, and $\alpha = 1$, with $U_0 = 2$ (left panel) and $U_0 = 4$ (right panel) (see Corollary 5.5). The three-hotspot steady-state is linearly stable in the shaded region. This steady-state undergoes an oscillatory instability below the solid or dot-dashed curves. In the left panel the thin vertical line is the competition threshold $\mathcal{D}_{0,c}$. The additional thin vertical line in the right panel is where the Hopf boundary switches from $j = 2$ to $j = 1$. This switch occurs since $U_0 = 4 > U_{0,swit} \approx 3.478$ (see (5.26) and the second statement of Corollary 5.5). The full PDE simulations in Fig. 16 and in Fig. 17 are done at the marked points in the left and right panels, respectively.

the Hopf bifurcation thresholds for the $j = 1$ mode and the sign-alternating $j = 2$ mode. When $U_0 = 2$ (left panel), the sign-alternating mode sets the boundary of the region of stability, whereas for $U_0 = 4$ (right panel) both the $j = 1$ and $j = 2$ Hopf bifurcation thresholds form the boundary of the region of stability. The corresponding region of stability in the scaled police diffusivity $\epsilon^2 D_p$ versus $\mathcal{D}_0$ parameter plane is shown in Fig. 10.

Similar results for $K = 4$ and for $U_0 = 2$ and $U_0 = 4$ are shown in Fig. 11 in the $\hat{\tau}_u$ versus $\mathcal{D}_0$ plane and in Fig. 12 in the $\epsilon^2 D_p$ versus $\mathcal{D}_0$ plane. From the left panels of Fig. 11 and Fig. 12, the $j = K - 1 = 3$ sign-alternating mode always sets the Hopf bifurcation boundary. However, as seen in the right panels of Fig. 11 and Fig. 12, where $U_0 = 4 > U_{0,\text{swit}} \approx 2.811$, we observe that both the $j = 3$ and $j = 2$ modes determine the Hopf bifurcation boundary when $\mathcal{D}_0 < \mathcal{D}_{0,c}$.

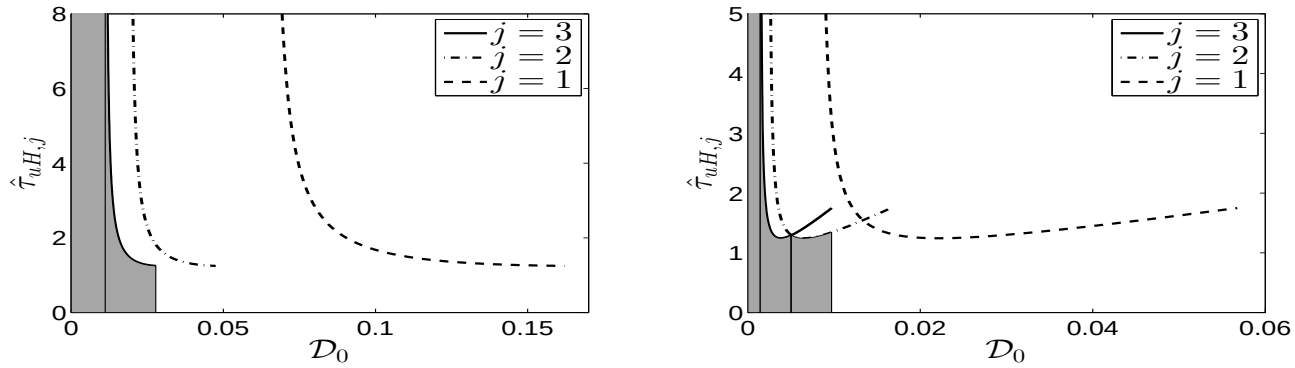

Figure 11: Linear stability (shaded) region in the $\hat{\tau}_u$ versus $\mathcal{D}_0$ plane for $K = 4$ when $S = 6$, $\gamma = 2$, and $\alpha = 1$, and for $U_0 = 2$ (left panel) and $U_0 = 4$ (right panel). The solid, dot-dashed, and dashed curves are the Hopf bifurcation boundaries for the (sign-alternating) $j = 3$ mode and the other $j = 2$ and $j = 1$ modes. For $U_0 = 2$ (left panel) the Hopf boundary is determined by the sign-alternating $j = 3$ mode. For $U_0 = 4 > U_{0,swit} \approx 2.811$ (see (5.27)), the Hopf boundary consists of both the $j = 3$ and $j = 2$ mode. Asynchronous oscillatory instabilities of the hotspot amplitudes occur above any of the Hopf bifurcation curves.

Remark 5.6 *More generally, for $K \geq 3$ there can be $K-2$ distinct mode switches for the minimal Hopf bifurcation threshold on the interval $D^-_{0,K-1} < \mathcal{D}_0 < D^+_{0,K-1}$ when U_0 increases beyond $U_{0,swit}$ towards $U_{0,\max}$. Although we do not work out precise conditions for this* cascading behavior *of the minimal Hopf bifurcation value here, we illustrate this phenomena in*

Fig. 13 for $K = 4$, $S = 6$, $\gamma = 2$, $\alpha = 1$, and $U_0 = 5$. From this figure, we observe two mode switches of the minimal Hopf bifurcation threshold. This suggests that as U_0 approaches the existence threshold $U_{0,\max}$, there is a window of $\mathcal{D}_0$ where $K-2$ distinct modes of oscillatory instability of the hotspot amplitudes can occur if $\hat{\tau}_u$ is large enough, suggesting the possibility of intricate spatio-temporal dynamics in this parameter regime.

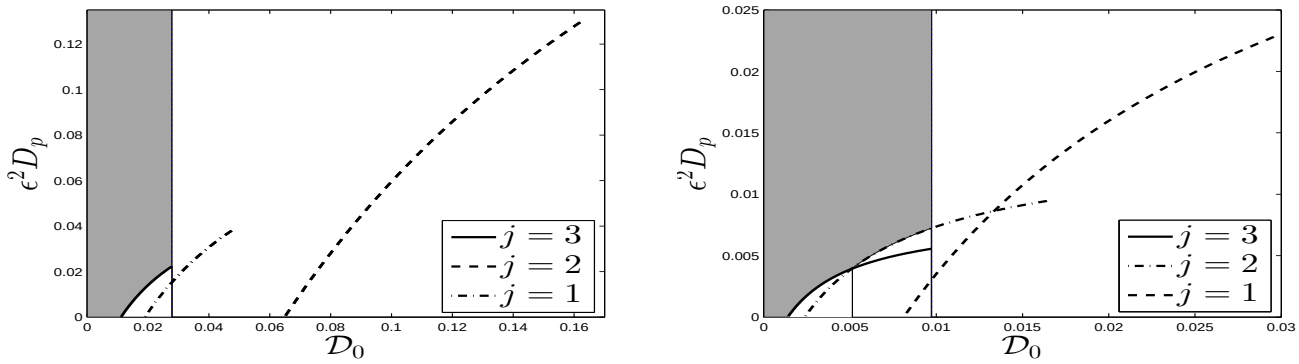

Figure 12: Plot corresponding to Fig. 11 in the scaled police diffusivity $\epsilon^2 D_p = \mathcal{D}_0/\hat{\tau}_u$ versus $\mathcal{D}_0$ plane for $K = 4$, $S = 6$, $\gamma = 2$, and $\alpha = 1$, with $U_0 = 2$ (left panel) and $U_0 = 4$ (right panel). The four-hotspot steady-state is linearly stable in the shaded region. This steady-state undergoes an asynchronous oscillatory instability below either of the three Hopf bifurcation curves. In the left panel the thin vertical line is the competition threshold $\mathcal{D}_{0,c}$. The additional thin vertical line in the right panel is where the Hopf boundary switches from $j = 3$ to $j = 2$. The Hopf eigenvalue tends to zero at the ends of each of the two curves.

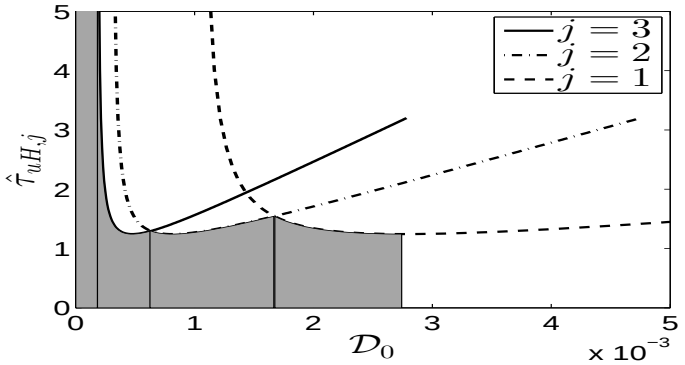

Figure 13: Linear stability (shaded) region in the $\hat{\tau}_u$ versus $\mathcal{D}_0$ plane for $K = 4$ when $S = 6$, $\gamma = 2$, and $\alpha = 1$, and for $U_0 = 5$. The solid, dot-dashed, and dashed curves are the Hopf bifurcation boundaries for the (sign-alternating) $j = 3$ mode, the $j = 2$ mode, and the $j = 1$ mode, respectively. Notice that the minimal Hopf bifurcation threshold on $D^-_{0,K-1} < \mathcal{D}_0 < D^+_{0,K-1}$ now consists of all three modes. Asynchronous oscillatory instabilities of the hotspot amplitudes occur above either of the three Hopf bifurcation curves.

5.2 Comparison of Linear Stability Theory with PDE Simulations: $q = 3$

6 Oscillatory Instabilities of the Hotspot Amplitudes: $q \neq 3$ and $q > 1$

In this section we analyze the NLEP (3.37) for the general case where $q \neq 3$, by determining the roots of $\zeta(\lambda) = 0$ in $\mathrm{Re}(\lambda) > 0$. In (4.4a) we re-write $\mathcal{C}(\lambda)$ as

$$\mathcal{C}(\lambda) = \frac{\eta}{b}\left(1 + \tilde{\tau}_j \lambda\right)\left(1 - \frac{b}{3-\lambda}\right), \qquad \text{where} \qquad \eta \equiv \frac{9\omega}{2qU_0}, \quad b \equiv \frac{9\chi_{0,j}}{2}, \quad \tilde{\tau}_j \equiv \frac{\hat{\tau}_u}{D_j \kappa_q}, \quad \frac{1}{\chi_{0,j}} = 1 + \frac{\kappa_3 D_j}{\alpha}. \tag{6.1}$$

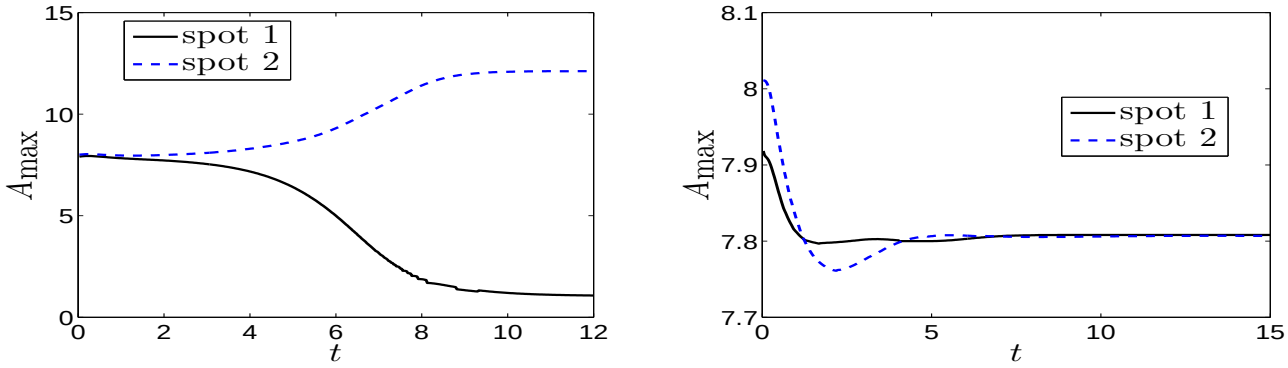

Figure 14: Plot of the spot amplitudes computed numerically from the full PDE system (1.5) for a two-spot pattern with $S = 6$, $\gamma = 2$, $\alpha = 1$, $U_0 = 4$, $\epsilon = 0.035$, and $q = 3$, at two of the marked points in the right panel of Fig. 8. Left panel: $\hat{\tau}_u = 1.8$ and $\mathcal{D}_0 = 0.3$, so that $\epsilon^2 D_p \approx 0.1667$. Spot amplitudes are unstable to a competition instability. Right panel: $\hat{\tau}_u = 1.0$ and $\mathcal{D}_0 = 0.15$, so that $\epsilon^2 D_p = 0.15$. Spot amplitude asynchronous oscillations decay in time and there is no competition instability. These results are consistent with the linear stability predictions in the right panel of Fig. 8 (see also the right panel of Fig. 7).

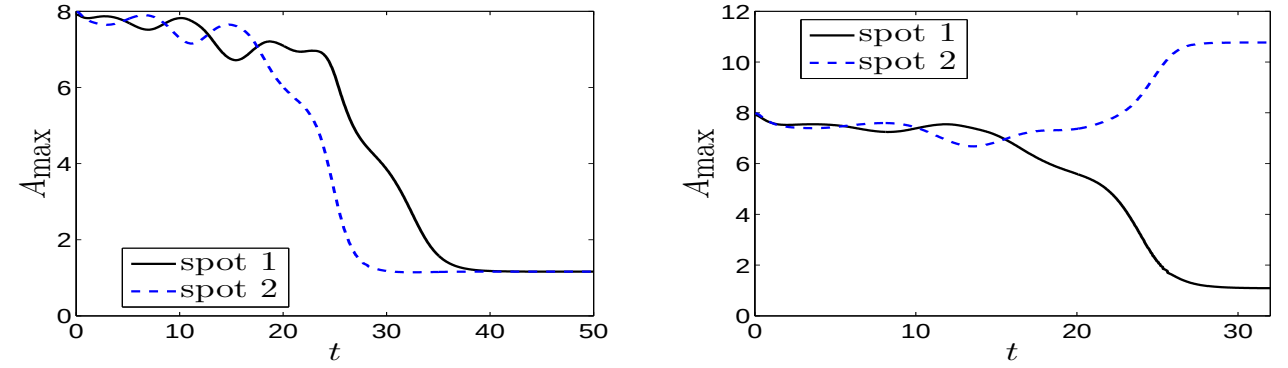

Figure 15: Plot of oscillatory instabilities of the spot amplitudes computed numerically from the full PDE system (1.5) for a two-spot pattern with $S = 6$, $\gamma = 2$, $\alpha = 1$, $U_0 = 4$, $\epsilon = 0.035$, and $q = 3$, at the marked points in the right panel of Fig. 8 where an oscillatory instability occurs. Left panel: $\hat{\tau}_u = 2.6$ and $\mathcal{D}_0 = 0.15$, so that $\epsilon^2 D_p \approx 0.0577$. Spot amplitudes are unstable to asynchronous oscillations, which leads to the collapse of both hotspots. Right panel: $\hat{\tau}_u = 3.0$ and $\mathcal{D}_0 = 0.15$, so that $\epsilon^2 D_p = 0.05$. Spot amplitudes are unstable to asynchronous oscillations, but now only one of the two hotspots collapses.

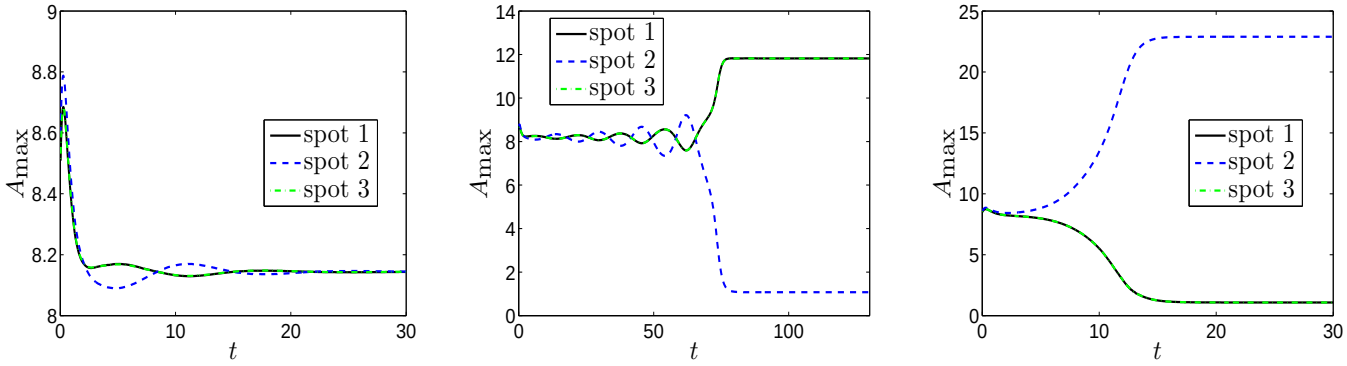

Figure 16: Plot of the spot amplitudes computed numerically from the full PDE system (1.5) for a three-spot pattern with $S = 6$, $\gamma = 2$, $\alpha = 1$, $U_0 = 2$, $\epsilon = 0.05$, and $q = 3$. Left panel: $\hat{\tau}_u = 1.3$ and $\mathcal{D}_0 = 0.07$, so that $\epsilon^2 D_p \approx 0.0538$. Spot amplitudes are stable to asynchronous oscillations and to the competition instability. Middle panel: $\hat{\tau}_u = 2.5$ and $\mathcal{D}_0 = 0.07$, so that $\epsilon^2 D_p = 0.028$. Spot amplitudes are unstable to asynchronous oscillations due to the sign-altering mode, which leads to the collapse of middle hotspot. Right panel: $\hat{\tau}_u = 2.5$ and $\mathcal{D}_0 = 0.12$, so that $\epsilon^2 D_p = 0.048$. Spot amplitudes are unstable to a competition instability due to the sign-altering mode, which leads to the collapse of the first and third hotspots. These results are consistent with the linear stability predictions in the left panels of Fig. 9 and Fig. 10. The results correspond to the marked points in the left panel of Fig. 10.

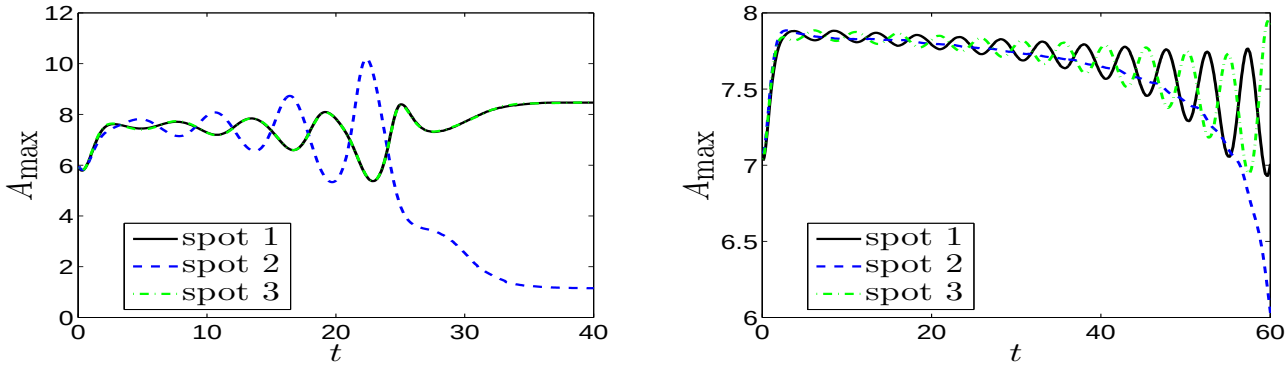

Figure 17: Plot of the spot amplitudes computed numerically from the full PDE system (1.5) for a three-spot pattern with $S = 6$, $\gamma = 2$, $\alpha = 1$, $U_0 = 2$, $\epsilon = 0.025$, and $q = 3$, for the marked points in the right panel of Fig. 10. Left panel: $\hat{\tau}_u = 2.5$ and $\mathcal{D}_0 = 0.01$, so that $\epsilon^2 D_p \approx 0.004$. Unstable asynchronous spot amplitude oscillations are of sign-altering type as predicted by the theory. Right panel: $\hat{\tau}_u = 1.6$ and $\mathcal{D}_0 = 0.03$, so that $\epsilon^2 D_p = 0.01875$. The unstable spot amplitude oscillations are no longer sign-altering. Here the first and third spots exhibit anti-phase oscillations as predicted by the right panel of Fig. 10.

To relate our key parameter b (which depends on j) to the diffusivity $\mathcal{D}_0$, we first use the expression for $\chi_{0,j}$ to write D_j in terms of b as $D_j = [\alpha/(2\kappa_3)]\,(9/b-2)$. Then, upon using (5.4) for $\alpha/(2\kappa_3)$ and (3.21) to relate D_j to $\mathcal{D}_0$, we obtain that

$$\frac{\mathcal{D}_0}{D_{0,j}^-} = \frac{9}{b} - 2\,, \qquad \text{or} \qquad b = \frac{9}{2+\mathcal{D}_0/D_{0,j}^-}\,. \tag{6.2}$$

Thus, $\mathcal{D}_0 > 0$ only when $b < 9/2$. Here $D_{0,j}^-$ is defined in terms of the competition threshold $\mathcal{D}_{0c}$ of (4.9) by

$$D_{0,j}^- \equiv \frac{\mathcal{D}_{0,c}}{(1+qU_0/\omega)}\left(\frac{1+\cos(\pi/K)}{1-\cos(\pi j/K)}\right), \qquad D_{0,j}^+ \equiv \mathcal{D}_{0,c}\left(\frac{1+\cos(\pi/K)}{1-\cos(\pi j/K)}\right), \qquad \frac{D_{0,j}^+}{D_{0,j}^-} = 1+\frac{qU_0}{\omega}\,, \tag{6.3}$$

where $D_{0,K-1}^+ = \mathcal{D}_{0,c}$. In our analysis below, the following ranges of b will play a prominent role:

$$(I): \quad 3 < b < 9/2 \quad \Longrightarrow \quad D_{0,j}^- > \mathcal{D}_0 > 0 \quad \Longrightarrow \quad \mathcal{C}(0) < 0\,, \tag{6.4a}$$

$$(II): \quad b_c \equiv 3\eta/(\eta+3/2) < b < 3 \quad \Longrightarrow \quad D_{0,j}^+ > \mathcal{D}_0 > D_{0,j}^- \quad \Longrightarrow \quad 1/2 > \mathcal{C}(0) > 0\,, \tag{6.4b}$$

$$(III): \quad b < b_c \quad \Longrightarrow \quad \mathcal{D}_0 > D_{0,j}^+ \quad \Longrightarrow \quad \mathcal{C}(0) > 1/2\,. \tag{6.4c}$$

Since $\mathcal{F}(0) = 1/2$, and $\mathcal{C}(0) = 1/2$ when $b = b_c$, we conclude that $b = b_c$ corresponds to a zero-eigenvalue crossing.

6.1 Analytical Results Based on the Winding Number Criterion

Here we use the winding number criterion of §4.2 to determine some rigorous results for the number N of unstable eigenvalues in $\mathrm{Re}(\lambda) > 0$ for the ranges of b listed in (6.4). In our analysis we will assume that Conjecture 4.4 on $\mathcal{F}_R(\lambda_I)$ and $\mathcal{F}_I(\lambda_I)$ holds for $q > 1$. With $\zeta(\lambda)$ as defined in (3.42), (4.5) when $\hat{\tau}_u > 0$ yields that

$$N = \frac{3}{2} + \frac{1}{\pi}\left[\arg\zeta\right]_{\Gamma_I^+}\,. \tag{6.5}$$

To calculate $[\arg\zeta]_{\Gamma_I^+}$ we need the following properties of the real and imaginary parts of $\mathcal{C}(i\lambda_I)$:

Lemma 6.1 *Let $\mathcal{C}(i\lambda_I) = \mathcal{C}_R(\lambda_I) + i\mathcal{C}_I(\lambda_I)$. Then, from (6.1) we have*

$$\mathcal{C}_R(\lambda_I) = \frac{\eta}{b}\left(1+\tilde{\tau}_j b - \frac{3b}{9+\lambda_I^2}\,(1+3\tilde{\tau}_j)\right), \qquad \mathcal{C}_I(\lambda_I) = \frac{\eta\lambda_I}{b}\left[\tilde{\tau}_j - \frac{b(1+3\tilde{\tau}_j)}{(9+\lambda_I^2)}\right]. \tag{6.6}$$

For the imaginary part we have:

(i) $\mathcal{C}_I(\lambda_I) \sim (9b)^{-1}\,\eta\lambda_I\,[3\tilde{\tau}_j(3-b)-b]$ *as* $\lambda_I \to 0^+$,

(ii) $\mathcal{C}_I(\lambda_I) \sim b^{-1}\eta\tilde{\tau}_j\lambda_I$ *as* $\lambda_I \to +\infty$.

(iii) If $b < 3/(1+\frac{1}{3\tilde{\tau}_j})$, *then* $\mathcal{C}_I(\lambda_I) > 0$ *for all* $\lambda_I > 0$.

(iv) If $b > 3/(1+\frac{1}{3\tilde{\tau}_j})$, *then* $\mathcal{C}_I(\lambda_I) < 0$ *on* $0 < \lambda_I < \sqrt{3(b-3)+\frac{b}{\tilde{\tau}_j}} \equiv \lambda_{I_1}$ *and* $\mathcal{C}_I(\lambda_I) > 0$ *on* $\lambda_I > \lambda_{I_1}$.

Alternatively, for the real part we have:

(v) $\mathcal{C}_R'(\lambda_I) > 0$ *for* $\lambda_I > 0$.

(vi) $\mathcal{C}_R(\lambda_I) \sim b^{-1}\eta(1+\tilde{\tau}_j b)$ *as* $\lambda_I \to \infty$.

(vii) $\mathcal{C}_R(0) > 0$ *if* $b < 3$ *and* $\mathcal{C}_R(0) < 0$ *if* $b > 3$. *When* $b > 3$, *then* $\mathcal{C}_R(\lambda_I) < 0$ *on* $0 < \lambda_I < \sqrt{\frac{3(b-3)}{1+\tilde{\tau}_j b}} \equiv \lambda_{IR}$, *and* $\mathcal{C}_R(\lambda_I) > 0$ *on* $\lambda_I > \lambda_{IR}$.

(viii) $\mathcal{C}_R(0) > 1/2$ *iff* $b < b_c \equiv 3\eta/(\eta + 3/2)$*, where* b_c *is the zero-eigenvalue crossing.*

With properties (ii) and (vi) of Lemma 6.1, together with the decay of $\mathcal{F}_R(\lambda_I)$ and $\mathcal{F}_I(\lambda_I)$ as $\lambda_I \to +\infty$ (see Proposition 4.3), we conclude that

$$\zeta(i\lambda_I) \sim b^{-1}\eta\,(1 + \tilde{\tau}_j b) + ib^{-1}\eta\tilde{\tau}_j\lambda_I \quad \text{as} \quad \lambda_I \to +\infty\,.$$

Therefore, with respect to the origin, the path $\zeta(i\lambda_I) = \zeta_R(\lambda_I) + i\zeta_I(\lambda_I)$ begins (as $\lambda_I \to \infty$) asymptotically close to the positive infinity of the imaginary axis in the complex ζ plane.

Moreover, from property (v) of Lemma 6.1, and under Conjecture 4.4 that $\mathcal{F}_R'(\lambda_I) < 0$ for all $\lambda_I > 0$, we conclude that

$$\zeta_R'(\lambda_I) > 0 \quad \text{for all} \quad \lambda_I > 0\,. \tag{6.7}$$

With this key result, the path $\zeta(i\lambda_I)$ in the ζ-plane for $\lambda_I > 0$ can only intersect the imaginary ζ_I axis exactly one or zero times. In particular if $\zeta(0) \equiv \zeta_R(0) > 0$, then $\zeta_R(\lambda_I) > 0$ for all $\lambda_I > 0$ so that $[\arg\zeta]_{\Gamma_I^+} = -\pi/2$ and $N = 1$ from (6.5). In contrast, if $\zeta(0) \equiv \zeta_R(0) < 0$, then there is a unique $\lambda_I^\star > 0$ for which $\zeta_R(\lambda_I^\star) = 0$. In this case, (6.5) yields that

$$(I): \quad \zeta_I(\lambda_I^\star) > 0 \quad \Longrightarrow \quad [\arg\zeta]_{\Gamma_I^+} = \pi/2 \quad \Longrightarrow \quad N = 2 \tag{6.8a}$$

$$(II): \quad \zeta_I(\lambda_I^\star) < 0 \quad \Longrightarrow \quad [\arg\zeta]_{\Gamma_I^+} = -3\pi/2 \quad \Longrightarrow \quad N = 0\,. \tag{6.8b}$$

With these preliminary observations, we obtain the following instability result for the j-th mode on the range $\mathcal{D}_0 > D_{0,j}^+$.

Proposition 6.2 *Suppose that* $\mathcal{D}_0 > D_{0,j}^+$ *and that Conjecture 4.4 holds. Then, for the* j*-th mode with* $j = 1, \ldots, K-1$*, we have* $N = 1$ *for all* $\tilde{\tau}_j \geq 0$*.*

Proof: When $\mathcal{D}_0 > D_{0,j}^+$, we have $b < b_c \equiv 3\eta/(\eta + 3/2)$ and consequently $\mathcal{C}_R(0) > 1/2$ from (III) of (6.4). This yields $\zeta_R(0) > 0$, and thus $\zeta_R(\lambda_I) > 0$ for all $\lambda_I > 0$ using the monotonicity result (6.7), which holds when $\mathcal{F}_R'(\lambda_I) < 0$ for all $\lambda_I > 0$. Therefore $[\arg\zeta]_{\Gamma_I^+} = -\pi/2$ and (6.5) yields $N = 1$ for all $\tilde{\tau}_j > 0$. ■

Together with the ordering principle $D_{0,j+1}^+ < D_{0,j}^+$ for $j = 1, \ldots, K-2$ from (5.16), this instability result proves, for any $\hat{\tau}_u > 0$, that there are exactly $K-1$ positive real eigenvalues of the NLEP (3.37) when $\mathcal{D}_0 > D_{0,1}^+$.

Proposition 6.3 *Suppose that* $\mathcal{D}_0 < D_{0,j}^+$ *and that Conjecture 4.4 holds. Then, for the* j*-th mode with* $j = 1, \ldots, K-1$*, we have either* $N = 0$ *or* $N = 2$ *for all* $\tilde{\tau}_j > 0$*. Moreover, if* $\tilde{\tau}_j \ll 1$ *we have* $N = 0$*.*

Proof: If $\mathcal{D}_0 < D_{0,j}^+$, then $b > 3\eta/(\eta + 3/2)$, and so $\mathcal{C}_R(0) < 1/2$ by (II) of (6.4). Therefore, since $\zeta_R(0) < 0$, $\zeta_R(\infty) > 0$, and $\zeta_R'(\lambda_I) > 0$, which holds when $\mathcal{F}_R'(\lambda_I) < 0$ for all $\lambda_I > 0$, it follows that there is a unique root $\lambda_I^\star$ for which $\zeta_R(\lambda_I^\star) = 0$. From (6.8), we have for all $\hat{\tau}_j > 0$ that either $N = 0$ or $N = 2$ depending on the sign of $\zeta_I(\lambda_I^\star)$.

Next, we prove that $N = 0$ if $\tilde{\tau}_j \ll 1$. For $\tilde{\tau}_j \ll 1$, (6.6) yields that

$$\mathcal{C}_R(\lambda_I) \sim \frac{\eta}{b}\left(1 - \frac{3b}{9 + \lambda_I^2}\right)\,,$$

uniformly in λ_I. It follows that $\zeta_R(\lambda_I^\star) = 0$ at some $\lambda_I^\star = \mathcal{O}(1)$ when $\tilde{\tau}_j \ll 1$. However, for $\tilde{\tau}_j \ll 1$, we have from (6.6) that $\mathcal{C}_I(\lambda_I^\star) \sim -\eta\lambda_I/\left(9 + \lambda_I^2\right) < 0$. Under Conjecture 4.4 that $\mathcal{F}_I(\lambda_I) > 0$, we conclude that $\zeta_I(\lambda_I^\star) = \mathcal{C}_I(\lambda_I^\star) - \mathcal{F}_I(\lambda_I^\star) < 0$. Therefore, from (6.8b) we conclude that $N = 0$. ■

This result proves that the j-th mode is linearly stable on the range $\mathcal{D}_0 < D_{0,j}^+$ whenever $\tilde{\tau}_j \ll 1$. The next result determines N for $\tilde{\tau}_j \gg 1$ on the entire range $\mathcal{D}_0 < D_{0,j}^+$.

Proposition 6.4 *Suppose that $D_{0,j}^- < \mathcal{D}_0 < D_{0,j}^+$ and that Conjecture 4.4 holds. Then, for the j-th mode with $j = 1, \ldots, K-1$, we have $N = 2$ when $\tilde{\tau}_j \gg 1$. In contrast, if $\mathcal{D}_0 < D_{0,j}^-$, then $N = 0$ when $\tilde{\tau}_j \gg 1$.*

Proof: We first observe from (6.4) that $D_{0,j}^- < \mathcal{D}_0 < D_{0,j}^+$ when $b_c < b < 3$ and $\mathcal{D}_0 < D_{0,j}^-$ when $b > 3$. For $\mathcal{D}_0 < D_{0,j}^+$, we have $\zeta_R(0) < 0$ and so there is a unique root $\lambda_I^\star$ to $\zeta_R(\lambda_I^\star) = 0$. For $\tilde{\tau}_j \gg 1$, and for $b > b_c \equiv 3\eta/(\eta + 3/2)$, this unique root of $\zeta_R(\lambda_I)$ occurs for $\lambda_I = \mathcal{O}(\tilde{\tau}_j^{-1/2}) \ll 1$. By setting $\mathcal{C}_R(\lambda_I) = \mathcal{F}_R(\lambda_I)$, and using $\lambda_I = \mathcal{O}(\tilde{\tau}_j^{-1/2}) \ll 1$ together with (6.6) for $\mathcal{C}_R$, we get that

$$\frac{\eta}{b}\left(1 + \frac{b}{9}(\tilde{\tau}_j \lambda_I^2 - 3)\right) \sim \mathcal{F}_R(0) = \frac{1}{2}\,.$$

In this way, we obtain for $\tilde{\tau}_j \gg 1$ that the unique root $\lambda_I^\star$ of $\zeta_R(\lambda_I) = 0$ occurs when

$$\lambda_I^\star \sim \beta/\tilde{\tau}_j^{1/2}\,, \qquad \beta \equiv \sqrt{3\left(1 - \frac{3}{b}\right) + \frac{9}{2\eta}}\,. \tag{6.9}$$

From (6.6) for $\mathcal{C}_I$, we then calculate for $\tilde{\tau}_j \gg 1$ that

$$\mathcal{C}_I(\lambda_I^\star) \sim \frac{\eta\beta}{3b}(3-b)\tilde{\tau}_j^{1/2} = \mathcal{O}(\tilde{\tau}_j^{1/2})\,. \tag{6.10}$$

When $b > 3$, corresponding to $\mathcal{D}_0 < D_{0,j}^-$, we have $\mathcal{C}_I(\lambda_I^\star) < 0$. Therefore, with $\mathcal{F}_I(\lambda_I) > 0$ from Conjecture 4.4, we conclude that $\zeta_I(\lambda_I^\star) < 0$. This yields that $N = 0$ from (6.8b). Now suppose that $b_c < b < 3$, corresponding to $D_{0,j}^- < \mathcal{D}_0 < D_{0,j}^+$. Then, since $\mathcal{C}_I(\lambda_I^\star) > 0$, with $\mathcal{C}_I(\lambda_I^\star) = \tilde{\tau}_j^{1/2} \gg 1$ for $\tilde{\tau}_j \gg 1$, while $\mathcal{F}_I(\lambda_I^\star) = \mathcal{O}(1)$, we conclude that $\zeta_I(\lambda_I^\star) > 0$. This yields that $N = 2$ from (6.8a). ■

On the range $D_{0,j}^- < \mathcal{D}_0 < D_{0,j}^+$, Propositions 6.4 and 6.3 show for the j-th mode that $N = 2$ for $\tilde{\tau}_j \gg 1$ and $N = 0$ for $\tilde{\tau}_j \ll 1$. Therefore, by continuity, there is a Hopf bifurcation value of $\tilde{\tau}_j$ on this range of $\mathcal{D}_0$. Although this proves the existence of a Hopf bifurcation threshold for $\hat{\tau}_u$ on the range $D_{0,j}^- < \mathcal{D}_0 < D_{0,j}^+$ for any mode $j = 1, \ldots, K-1$, it does not establish uniqueness of this threshold or provide any its qualitative properties. This is done numerically in §6.2.

The remaining issue relates to the range $\mathcal{D}_0 < D_{0,j}^-$, where we have proved that $N = 0$ when either $\tilde{\tau}_j \ll 1$ or $\tilde{\tau}_j \gg 1$. Next, we study for this range of $\mathcal{D}_0$ whether $N = 0$ *for all* $\tilde{\tau}_j > 0$.

To examine this question we will proceed as follows: Suppose that $\mathcal{C}_R(0) < 1/2$ and that $\mathcal{C}_R(\infty) > 1/2$. Then, with Conjecture 4.4 that $\mathcal{F}_R'(\lambda_I) < 0$ for all $\lambda_I > 0$, and with $\mathcal{F}_R(0) = 1/2$, it follows that the unique root $\lambda_I^\star$ to $\zeta_R(\lambda_I) = 0$ satisfies $\lambda_I^\star < \lambda_{Im}$ where λ_{Im} is defined by $C_R(\lambda_{Im}) = 1/2$. If we can then show that $C_I(\lambda_{Im}) < 0$, it follows that $C_I(\lambda_I^\star) < 0$. Then, by Conjecture 4.4 that $\mathcal{F}_I(\lambda_I) > 0$ for all $\lambda_I > 0$, we obtain that $\zeta_I(\lambda_I^\star) < 0$, and consequently $N = 0$ from (6.8b). Therefore, our goal is to determine the range of b, with $b > 3$, for which

$$\mathcal{C}_R(0) < 1/2\,, \qquad \mathcal{C}_R(\infty) > 1/2\,, \qquad \text{and} \quad \mathcal{C}_I(\lambda_{Im}) < 0 \quad \text{where} \quad \mathcal{C}_R(\lambda_{Im}) = 1/2\,. \tag{6.11}$$

When $b > b_c$ we have $\mathcal{C}_R(0) < 1/2$, and from property (vi) of Lemma 6.1 we have $\mathcal{C}_R(\infty) > 1/2$ provided that

$$\frac{\eta}{b}\,(1 + \tilde{\tau}_j b) > \frac{1}{2}\,. \tag{6.12}$$

Now by using (6.6) for $\mathcal{C}_R$, we obtain that $\mathcal{C}_R(\lambda_{Im}) = 1/2$ when

$$\frac{1 + 3\tilde{\tau}_j}{9 + \lambda_{Im}^2} = \frac{1}{3\eta}\left[\frac{\eta}{b}(1 + \tilde{\tau}_j b) - \frac{1}{2}\right]\,.$$

By using this expression in (6.6) for $\mathcal{C}_I(\lambda_I)$ we get, after some algebra, that

$$\mathcal{C}_I(\lambda_{Im}) = \frac{\eta\lambda_{Im}}{b}\left(\tilde{\tau}_j - \frac{b(1+3\tilde{\tau}_j)}{9 + \lambda_{Im}^2}\right) = -\frac{\eta\lambda_{Im}}{3b}\left[\tilde{\tau}_j(b-3) + 1 - \frac{b}{2\eta}\right]\,.$$

We conclude that $\mathcal{C}_I(\lambda_{Im}) < 0$ when $1+\tilde{\tau}_j b - b/(2\eta) > 3\tilde{\tau}_j$. Since, from (6.12), we have $\mathcal{C}_R(\infty) > 1/2$ when $1+\tilde{\tau}_j b - b/(2\eta) > 0$, we conclude that the inequalities in (6.11) hold when

$$b > b_c \equiv \frac{3\eta}{\eta + 3/2} \qquad \text{and} \qquad 1 + \tilde{\tau}_j b - b/(2\eta) > 3\tilde{\tau}_j \,. \tag{6.13}$$

We now determine a range of b, independent of $\tilde{\tau}_j$, for which the inequalities (6.13) hold. A sufficient condition for (6.13) to hold is that $b > 3$ and $b < 2\eta$. If $\eta < 3/2$, there is no such range of b. If $\eta > 9/2$, these inequalities hold on the full range $3 < b < 9/2$ where $\mathcal{D}_0 < D^-_{0,j}$, as given in (I) in (6.4). However, when $3/2 < \eta < 9/2$, the interval $3 < b < 2\eta$ is only a subset of the full range in (I) of (6.4) where $\mathcal{D}_0 < D^-_{0,j}$. By using (6.1) for η, together with (6.2) to relate b to $\mathcal{D}_0$, we summarize our result as follows:

Proposition 6.5 *Suppose that Conjecture 4.4 holds. Then, for the j-th mode with $j = 1, \ldots, K-1$ we have the following:*

$$(I) \quad \textit{Suppose } U_0 < 2\omega/q \textit{ and } \mathcal{D}_0 < D^-_{0,j} \,. \textit{ Then } N = 0 \textit{ for all } \hat{\tau}_u > 0 \,. \tag{6.14a}$$

$$(II) \quad \textit{Suppose } 2\omega/q < U_0 < 3\omega/q \textit{ and } \left(\frac{qU_0}{\omega} - 2\right) D^-_{0,j} < \mathcal{D}_0 < D^-_{0,j} \,. \textit{ Then } N = 0 \textit{ for all } \hat{\tau}_u > 0 \,. \tag{6.14b}$$

This result provides no stability information for the range $\mathcal{D}_0 < D^-_{0,j}$ when $U_0 > 3\omega/q$.

As a result of the ordering principle $D^-_{0,K-1} < D^-_{0,j}$ for $j = 1, \ldots, K-2$ and $K \geq 3$, we conclude from (I) of Proposition 6.5, upon recalling $\omega = S(\gamma - \alpha) - U_0$, that a K-hotspot pattern is linearly stable for all $\hat{\tau}_u > 0$ on the range $\mathcal{D}_0 < D^-_{0,K-1}$ when $U_0 < 2S(\gamma - \alpha)/(q+2)$. This result is weaker than that obtained for the explicitly solvable case $q = 3$, In fact, since $\omega = S(\gamma - \alpha) - U_0$, it provides no stability information on $\mathcal{D}_0 < D^-_{0,j}$ when $U_0 > 3(S - \gamma)/(q+3)$. For $q = 3$, we recall from Proposition 5.1 that for the j-th mode we have $N = 0$ for $\mathcal{D}_0 < D^-_{0,j}$ for all $\hat{\tau}_u > 0$ without any restriction on U_0.

In §6.2 we will investigate numerically the possibility of a Hopf bifurcation for the range $0 < \mathcal{D}_0 < D^-_{0,j}$ when $U_0 > 3\omega/q$, for which Proposition 6.5 does not apply. Our numerical procedure in §6.2 suggests that no Hopf bifurcation exists on the range $0 < \mathcal{D}_0 < D^-_{0,j}$ for any $U_0 < U_{0,\max}$, as qualitatively identical to the second statement proved in Proposition 5.1 for the explicitly solvable case $q = 3$.

To gain some insight into the behavior of the Hopf bifurcation threshold $\tilde{\tau}_j$ for the j-th mode, we now derive a scaling law for it to show that $\tilde{\tau}_j \to \infty$ and $\lambda_I \to 0^+$ as $\mathcal{D}_0 \to D^-_{0,j}$ from above, or equivalently as $b \to 3$ from below. For $b \to 3^-$, we look for a solution to $\zeta(i\lambda_I) = 0$ with $\lambda_I \to 0$, $\tilde{\tau}_j \to \infty$, with the distinguished balance $\lambda_I = \mathcal{O}(\tilde{\tau}_j^{-1/2})$. By setting $\mathcal{C}_R(\lambda_I) = \mathcal{F}_R(\lambda_I)$, and using $\mathcal{F}_R(\lambda_I) \sim 1/2$ together with (6.6) for $\mathcal{C}_R$, we get that

$$\frac{\eta}{b}\left(1 - \frac{b}{9}\left(3 - \tilde{\tau}_j \lambda_I^2\right)\right) \sim \frac{1}{2} \,.$$

By solving for $\tilde{\tau}_j \lambda_I^2$ and letting $b \to 3$, we obtain that $\tilde{\tau}_j \lambda_I^2 = 9/(2\eta) + 3(b-3)/b$. By letting $b \to 3$, we conclude that

$$\lambda_I \sim \sqrt{\frac{9}{2\eta\tilde{\tau}_j}} \,, \qquad \text{as} \quad \tilde{\tau}_j \to \infty \,. \tag{6.15}$$

Then, we set $\mathcal{C}_I(\lambda_I) = \mathcal{F}_I(\lambda_I)$, and use (6.6) for $\mathcal{C}_I$, together with the local behavior for $\mathcal{F}_I(\lambda_I)$ as $\lambda_I \to 0$ from (iv) of Proposition 4.3. This yields that

$$\frac{\eta\lambda_I}{b(9+\lambda_I^2)}\left(3\tilde{\tau}_j(3-b) - b + \tilde{\tau}_j\lambda_I^2\right) \sim \frac{\lambda_I}{4}\left(1 - \frac{1}{q}\right) \,.$$

Upon cancelling the factor of λ_I and using $\tilde{\tau}_j \lambda_I^2 \sim 9/(2\eta)$, we solve for $\tilde{\tau}_j$ in the expression above to get

$$\tilde{\tau}_j \sim \frac{1}{3(3-b)} \left[b - \frac{9}{2\eta} + \frac{9b}{4\eta} \left(1 - \frac{1}{q} \right) \right] \sim \frac{1}{3-b} \left[1 + \frac{3}{4\eta} \left(1 - \frac{3}{q} \right) \right], \quad \text{as} \quad b \to 3\,. \tag{6.16}$$

In terms of the original variables $\mathcal{D}_0$, U_0 and $\hat{\tau}_u$ we use (6.1) and (6.2) to get

$$\frac{3}{4\eta} = \frac{qU_0}{6\omega}\,, \qquad \hat{\tau}_u = \frac{\alpha}{2} \left(\frac{\kappa_q}{\kappa_3} \right) \frac{\mathcal{D}_0}{D_{0,j}^-} \tilde{\tau}_j\,, \qquad b - 3 \sim 1 - \frac{\mathcal{D}_0}{\mathcal{D}_{0,j}^-} \quad \text{as} \quad \mathcal{D}_0 \to D_{0,j}^-\,. \tag{6.17}$$

Upon substituting (6.17) into (6.16) and (6.15) we get the limiting Hopf bifurcation threshold

$$\hat{\tau}_{u,H} \sim \frac{\alpha}{2} \left(\frac{\kappa_q}{\kappa_3} \right) \frac{1}{\left(\mathcal{D}_0/D_{0.j}^- - 1 \right)} \left(1 + \frac{qU_0}{6\omega} \left(1 - \frac{3}{q} \right) \right)^{1/2}, \qquad \lambda_{IH} \sim \sqrt{\frac{\mathcal{D}_0}{D_{0,j}^-} - 1} \left(\frac{qU_0}{\omega} \right)^{1/2} \left[1 + \frac{qU_0}{6\omega} \left(1 - \frac{3}{q} \right) \right]^{-1/2}, \tag{6.18}$$

as $\mathcal{D}_0 \to D_{0,j}^-$. For the special case where $q = 3$, this limiting result for λ_{IH} and $\hat{\tau}_{u,H}$ agrees with that in (5.14) and (5.10), respectively.

Finally, for the j-th mode we will calculate an additional scaling law for the Hopf bifurcation threshold and the Hopf eigenvalue as $b \to b_c \equiv 3\eta/(\eta + 3/2)$ from above, corresponding to the limit $\mathcal{D}_0 \to D_{0,j}^+$ from below. We look for a root $\lambda_I \ll 1$ to $\mathcal{C}_R(\lambda_I) = \mathcal{F}_R(\lambda_I)$ and use

$$\mathcal{F}_R \sim \frac{1}{2} - k_R \lambda_I^2 + \cdots, \quad \text{as} \quad \lambda_I \to 0\,, \tag{6.19}$$

for some $k_R > 0$, together with (6.6) for $\mathcal{C}_R(\lambda_I)$, to obtain that

$$\frac{\eta}{b(9 + \lambda_I^2)} \left[9 - 3b + \lambda_I^2 (1 + \tilde{\tau}_j b) \right] \sim \frac{1}{2} - k_R \lambda_I^2\,.$$

Upon isolating λ_I, we get

$$\frac{\eta}{b}(9 - 3b) - \frac{9}{2} = \lambda_I^2 \left(\frac{1}{2} - 9\kappa_R - \frac{\eta}{b_c} \left(1 + \tilde{\tau}_j b_c \right) \right). \tag{6.20}$$

We then set $\mathcal{C}_I(\lambda_I) = \mathcal{F}_I(\lambda_I)$ as $\lambda_I \to 0$ using the local behavior (i) of Lemma 6.1 for $\mathcal{C}_I(\lambda_I)$ and that in (iv) of Proposition 4.3 for $\mathcal{F}_I(\lambda_I)$. This yields that

$$\frac{\eta}{9b_c} \left(3\tilde{\tau}_j (3 - b_c) - b_c \right) \sim \frac{1}{4} \left(1 - \frac{1}{q} \right).$$

Upon using $b_c = 3\eta/(\eta + 3/2)$, we solve for $\tilde{\tau}_j$ in this expression to obtain

$$\tilde{\tau}_j \sim \frac{2\eta}{9} \left[1 + \frac{9}{4\eta} \left(1 - \frac{1}{q} \right) \right], \quad \text{as} \quad b \to b_c\,. \tag{6.21}$$

Upon substituting (6.21) into (6.20) and solving for λ_I we obtain, after some algebra, that $\lambda_I \equiv \lambda_{IH}$ satisfies

$$\lambda_{IH} \sim \sqrt{\frac{27}{2}} \left(\frac{1 - b_c/b}{3 - b_c} \right)^{1/2} \left(9\kappa_R + \frac{\eta}{3} + \frac{2\eta^2}{9} + \frac{\eta}{2} \left(1 - \frac{1}{q} \right) \right)^{-1/2}, \quad \text{as} \quad b \to b_c\,. \tag{6.22}$$

To write $\tilde{\tau}_j$ in (6.21) in terms of the original variables, we use (6.17), together with $D_{0,j}^+/D_{0,j}^- = 1 + qU_0/\omega$, to obtain

$$\hat{\tau}_{u,H} \sim \frac{\alpha\omega}{2qU_0} \left(\frac{\kappa_q}{\kappa_3} \right) \left(1 + \frac{qU_0}{\omega} \right) \left(1 + \frac{U_0}{2\omega}(q - 1) \right), \qquad \text{as} \quad \mathcal{D}_0 \to D_{0,j}^+\,. \tag{6.23}$$

When $q = 3$, the expression in (6.23) agrees with that obtained in (5.10) for the explicitly solvable case. To determine if (6.22) yields the limiting Hopf eigenvalue given in (5.14) when $q = 3$, we use $\mathcal{F}(i\lambda_I) = 3/\left[2(3 - i\lambda_I)\right]$, from (4.1). This

yields $\mathcal{F}_R(\lambda_I) \sim 1/2 - \lambda_I^2/18$, which identifies $k_R = 1/18$ in (6.19). With this value for k_R and $q = 3$, the expression in the brackets in (6.22) is a perfect square, and simplifies to

$$\lambda_{IH} \sim \sqrt{\frac{27}{2}} \left(1 - \frac{b_c}{b}\right)^{1/2} \frac{(9/2)^{1/2}}{(3-b_c)^{1/2}(\eta + 3/2)} \,.$$

We then use $b_c = 3\eta/(\eta + 3/2)$ together with $\eta = 3\omega/(2U_0)$ when $q = 3$ from (6.1), to get

$$\lambda_{IH} \sim \sqrt{\frac{27}{2}} \sqrt{1 - \frac{b_c}{b}} \left(1 + \frac{\omega}{U_0}\right)^{-1/2} \,. \tag{6.24}$$

Finally, we use (6.2) for b, $D_{0,j}^+/D_{0,j}^- = 1 + 3U_0/\omega$, and $\eta = 3\omega/(2U_0)$ to calculate

$$\frac{b_c}{b} - 1 = \frac{\eta}{3(\eta + 3/2)} \left(\frac{\mathcal{D}_0}{\mathcal{D}_{0,j}^-} + 2\right) = \left(\frac{\mathcal{D}_0}{D_{0,j}^+} - 1\right) \left(\frac{1 + 3U_0/\omega}{3\,(1 + U_0/\omega)}\right) \,. \tag{6.25}$$

Upon substituting this expression into (6.24), we recover the result for λ_{IH} given in (5.14) for $\mathcal{D}_0 \to D_{0,j}^+$ from below.

6.2 Parameterization of the Hopf Bifurcation Curve

To compute the Hopf bifurcation threshold numerically for the j-th mode on the range $D_{0,j}^- < \mathcal{D}_0 < D_{0,j}^+$, and to explore the range $\mathcal{D}_0 < D_{0,j}^-$ where Proposition 6.5 only gives partial stability information, we now formulate a convenient parameterization of any Hopf bifurcation curve in the $\hat{\tau}_u$ versus $\mathcal{D}_0$ parameter plane.

We set $\zeta(i\lambda_I) = 0$ in (3.42) to get $\mathcal{C}(i\lambda_I) = \mathcal{F}(i\lambda_I)$, where $\mathcal{C}(i\lambda_I)$ and $\mathcal{F}(i\lambda_I)$ are given in (6.1) and (4.2) respectively. By taking the squared modulus of both sides we get

$$\frac{\eta^2}{b^2} \left(1 + \tilde{\tau}_j^2 \lambda_I^2\right) \left[\frac{(3-b)^2 + \lambda_I^2}{9 + \lambda_I^2}\right] = |\mathcal{F}(i\lambda_I)|^2 \,,$$

which we solve for $\tilde{\tau}_j^2$ to get

$$\tilde{\tau}_j^2 = \frac{1}{\lambda_I^2} \left[-1 + \frac{b^2}{\eta^2} \left(\frac{9 + \lambda_I^2}{(3-b)^2 + \lambda_I^2}\right) |\mathcal{F}(i\lambda_I)|^2\right] \,. \tag{6.26}$$

To derive a second equation for $\tilde{\tau}_j$ we set $\mathrm{Im}\,[\zeta(i\lambda_I)] = 0$ to get, upon using (6.6) for $\mathcal{C}_I(\lambda_I)$, that

$$\frac{\eta\lambda_I}{b(9 + \lambda_I^2)} \left(3\tilde{\tau}_j\,(3-b) - b + \tilde{\tau}_j \lambda_I^2\right) = \mathcal{F}_I(\lambda_I) \,.$$

Upon isolating $\tilde{\tau}_j$ from this expression we obtain that

$$\tilde{\tau}_j = \frac{b}{\eta\lambda_I} \frac{[\eta\lambda_I + \mu\mathcal{F}_I(\lambda_I)]}{\mu - 3b} \,, \qquad \text{where} \quad \mu \equiv 9 + \lambda_I^2 \,. \tag{6.27}$$

Then, by eliminating $\tilde{\tau}_j$ between (6.26) and (6.27) we obtain, after some algebra, that λ_I must satisfy the nonlinear algebraic problem $\mathcal{M}(\lambda_I) = 0$, defined by

$$\mathcal{M}(\lambda_I) \equiv (\mu + b^2 - 6b) \left[(\eta\lambda_I + \mu\mathcal{F}_I)^2 + \frac{\eta^2}{b^2}(\mu - 3b)^2\right] - \mu(\mu - 3b)^2 |\mathcal{F}|^2 \,, \qquad \text{where} \quad \mu \equiv 9 + \lambda_I^2 \,. \tag{6.28a}$$

Here we have labeled $\mathcal{F}_I \equiv \mathcal{F}_I(\lambda_I)$ and $|\mathcal{F}|^2 \equiv |\mathcal{F}(i\lambda_I)|^2 = [\mathcal{F}_R(\lambda_I)]^2 + \left[\mathcal{F}_I^2(\lambda_I)\right]^2$. In terms of the original $\hat{\tau}_u$ variable, we have from (6.17) and $\mathcal{D}_0/D_{0,j}^- = 9/b - 2$ that the Hopf bifurcation threshold is

$$\hat{\tau}_{u,H} = \frac{\alpha}{2\eta\lambda_I} \left(\frac{\kappa_q}{\kappa_3}\right) (9 - 2b) \, \frac{[\eta\lambda_I + \mu\mathcal{F}_I(\lambda_I)]}{\mu - 3b} \,, \qquad \text{where} \quad \mu \equiv 9 + \lambda_I^2 \,. \tag{6.28b}$$

This parameterization (6.28b) and (6.28a) is used numerically as follows: For a given η and q, we will show numerically that (6.28a) has a unique root $\lambda_I = \lambda_{IH}(b)$ on the range $b_c < b < 3$, where $b_c \equiv 3\eta/(\eta + 3/2)$. This corresponds to the range $D^-_{0,j} < \mathcal{D}_0 < D^+_{0,j}$, via the mapping

$$\mathcal{D}_0 = D^-_{0,j}\left(\frac{9}{b} - 2\right). \tag{6.28c}$$

To compute this root $\lambda_{IH}(b)$ by applying a Newton solver to (6.28a), we must compute the functions $\mathcal{F}_R(\lambda_I)$ and $\mathcal{F}_I(\lambda_I)$, as defined in (4.2), using a BVP solver, for any $\lambda_I > 0$. A key simplifying feature of this parameterization is that the root $\lambda_{IH}(b)$ can be used *for all* of the modes $j = 1, \ldots, K-1$, as the range of $\mathcal{D}_0$ for the specific mode is only identified at the last step (6.28c). A similar universality feature of the Hopf bifurcation curve was exploited in (5.9) for the explicitly solvable case $q = 3$. We further remark that for the explicitly solvable case $q = 3$ where $\mathcal{F}(i\lambda_I) = 3/\left[2(3 - i\lambda_I)\right]$, some lengthy but straightforward algebra shows that the root of (6.28a) is given explicitly by (5.13).

On the range $b_c < b < 3$, for which Proposition 6.4 ensures that a Hopf bifurcation exists, the Hopf threshold $\hat{\tau}_{u,Hj}$ for a specific mode $j = 1, \ldots, K-1$ is given uniquely by simply evaluating (6.28b) at the unique root $\lambda_I = \lambda_{IH}(b)$ of $\mathcal{M}(\lambda_I) = 0$. We remark that on the range $b < 3$ we have $\mu - 3b > 0$ for all $\lambda_I > 0$, so that (6.28b) is well-defined. To establish that (6.28a) has a root on $b_c < b < 3$, we set $\lambda_I = 0$ in (6.28a) and use $\mathcal{F}_I(0) = 0$, $|\mathcal{F}(0)|^2 = 1/4$, and $\mu = 9$, to get that

$$\mathcal{M}(0) = (9 - 3b)^2\left[\frac{\eta^2}{b^2}(b-3)^2 - \frac{9}{4}\right].$$

From this expression, we conclude that $\mathcal{M}(0) = 0$ at $b = b_c \equiv 3\eta/(\eta + 3/2)$ and $b = 3$, and that $\mathcal{M}(0) < 0$ on the interval $b_c < b < b$. Since $\mathcal{M}(\lambda_I) \to +\infty$ as $\lambda_I \to +\infty$, we conclude that there exists a $\lambda_{IH} > 0$ for which $\mathcal{M}(\lambda_{IH}) = 0$.

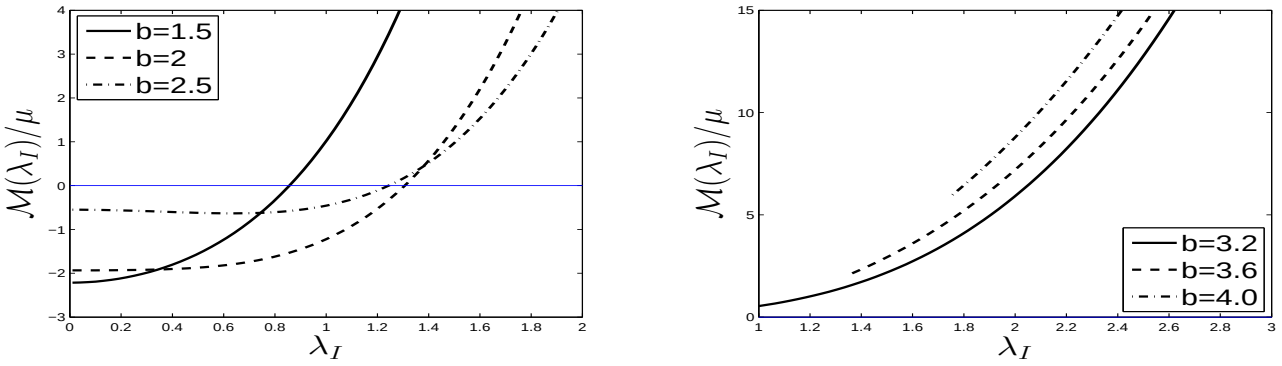

Figure 18: Plots of $\mathcal{M}(\lambda_I)/\mu$, where $\mu \equiv \lambda_I^2 + 9$, versus λ_I for $S = 6$, $\gamma = 2$, $\alpha = 1$, $U_0 = 4$, and $q = 2$. In the left panel, where $b = 1.5, 2.0, 2.5$, which satisfies $b_c < b < 3$, there is a unique root to $\mathcal{M}(\lambda_I) = 0$, yielding the Hopf eigenvalue. In the right panel, where $b = 3.2, 3.6, 4.0$, there is no root to $\mathcal{M}(\lambda_I) = 0$, and hence no Hopf eigenvalue. For our choice $U_0 = 4$, where $U_0 > 3\omega/q$, Proposition 6.5 gives no information regarding Hopf bifurcations on the range $b > 3$.

To examine numerically the uniqueness of the Hopf threshold on the range $b_c < b < 3$, we take the same parameter set $S = 6$, $\gamma = 2$, and $\alpha = 1$, as used in §5 for the $q = 3$ case. We choose $q = 2$ and $U_0 = 4$ for which $\eta \approx 1.286$. For $b = 1.5$, $b = 2.0$, and $b = 2.5$, in the left panel of Fig. 18 we plot $\mathcal{M}(\lambda_I)/\mu$ versus λ_I for $U_0 = 4$ showing numerically the existence of a unique root to $\mathcal{M}(\lambda_I) = 0$, and consequently a unique Hopf bifurcation value of $\hat{\tau}_{uH,j}$ for the j-th mode.

In contrast, suppose that $b > 3$. To investigate whether a Hopf bifurcation is possible for $3 < b < 9/2$, we must determine whether there is a root of $\mathcal{M}(\lambda_I) = 0$ on the range $\mu \equiv 9 + \lambda_I^2 > 3b$ for which $\hat{\tau}_{u,H} > 0$ (see (6.28b)). From (6.28a), we first observe that $\mathcal{M}(\lambda_I) = (b-3)^2\left(\eta\sqrt{3b-9} + 3b\mathcal{F}_I(3b)\right)^2 > 0$ when $\mu = 3b$ and that $\mathcal{M}(\lambda_I) \to \infty$ as $\lambda_I \to \infty$. Therefore, if such a root exists, $\mathcal{M}(\lambda_I)$ cannot be monotone on $\mu > 3b$. We study this issue numerically in the right panel of Fig. 18

where we plot $\mathcal{M}(\lambda_I)/\mu$ versus λ_I for $b = 3.2$, $b = 3.6$, and $b = 4.0$, on the range $\mu > 3b$, for our parameter set $S = 6$, $\gamma = 2$, $\alpha = 1$, $U_0 = 4$, and $q = 2$. Numerically, we find that there is no root to $\mathcal{M}(\lambda_I) = 0$ when $\mu > 3b$. For $U_0 = 4$ and $q = 2$, we remark that $U_0 > 3\omega/q$, and so Proposition 6.5 gives no information regarding Hopf bifurcations on the range $b > 3$. Further computations (not shown) with $\mathcal{M}(\lambda_I)$ for $b > 3$ suggest that there is never a root to $\mathcal{M}(\lambda_I) = 0$ on $\mu > 3b$ for any $U_0 < U_{0,\max}$. Based on this numerical evidence, we conjecture that no Hopf bifurcations can occur when $\mathcal{D}_0 < D_{0,j}^-$ for any $q > 1$ and $U_0 < U_{0,\max}$.

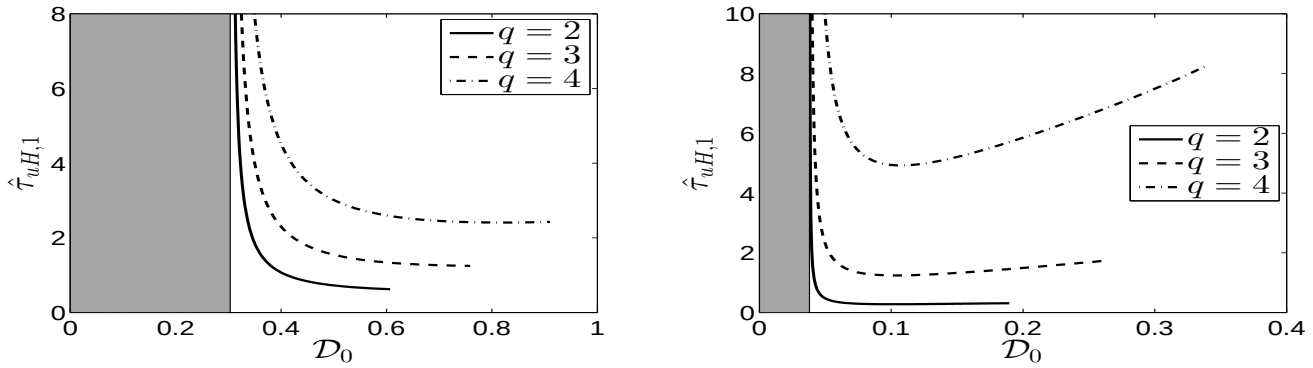

Figure 19: Plot of the Hopf bifurcation threshold $\hat{\tau}_{uH_1}$ versus $\mathcal{D}_0$ for $q = 2$ (solid), $q = 3$ (dashed), and $q = 4$ (dot-dashed) on the range $\mathcal{D}_{0,c}/(1 + qU_0/\omega) < \mathcal{D}_0 < \mathcal{D}_{0c}$ for $K = 2$, $S = 6$, $\gamma = 2$, $\alpha = 1$, and with $U_0 = 2$ (left panel) and $U_0 = 4$ (right panel). Here $\mathcal{D}_{0,c}$ is the competition stability threshold defined in (4.9), which depends on q. The lower bound $\mathcal{D}_{0,c}/(1 + qU_0/\omega)$ is independent of q. The two-hotspot steady-state is linearly stable for $\mathcal{D}_0 < \mathcal{D}_{0,c}/(1 + qU_0/\omega)$ (shaded region) as well as under the Hopf bifurcation curve. For $\mathcal{D}_0 > \mathcal{D}_{0,c}$ the hotspot pattern is unstable for all $\hat{\tau}_u$. We observe that the interval in $\mathcal{D}_0$ where an oscillatory instability of the hotspot amplitudes can occur increases with q. The Hopf bifurcation threshold $\hat{\tau}_{uH,1}$ also increases with q.

Next, we use our parameterization to compute the Hopf bifurcation threshold for $\hat{\tau}_u$ on the range $D_{0,j}^- < \mathcal{D}_0 < D_{0,j}^+$, and plot the region of linear stability for $q = 2$ and $q = 4$ in order to compare with our previous results in §5 for $q = 3$.

For our parameter set, and for a two-hotspot solution, in Fig. 19 we plot the linear stability phase diagram in the $\hat{\tau}_u$ versus $\mathcal{D}_0$ plane when either $U_0 = 2$ (left panel) and for $U_0 = 4$ (right panel). In both panels we compare the linear stability thresholds for $q = 2, 3, 4$. In the left and right panels of Fig. 19, the two-hotspot steady-state is linearly stable in the shaded region, which is the same for each q, and in the region below the Hopf bifurcation threshold for the given q. Since the competition instability threshold $\mathcal{D}_{0,c}$ increases with q, as was shown in §4.4, the interval in $\mathcal{D}_0$ where an oscillatory instability of the hotspot amplitudes can occur increases with q. We further observe from Fig. 19 that the Hopf bifurcation threshold value of $\hat{\tau}_u$ increases with q, and when $U_0 = 4$ the Hopf bifurcation threshold is not monotone in $\mathcal{D}_0$ when either $q = 3$ or $q = 4$ (recall the right panel of Fig. 7 for the $q = 3$ case). These results are discussed qualitatively in §6.3.

For a three-hotspot pattern similar results for the linear stability region in the $\hat{\tau}_u$ versus $\mathcal{D}_0$ plane are shown in Fig. 20 for $U_0 = 2$ and in Fig. 21 for $U_0 = 4$. Results for $q = 2, 3, 4$ are shown in the three subpanels of these figures. We observe that the minimal Hopf threshold value for $\hat{\tau}_u$ increases with q, and this increase is more pronounced for $U_0 = 4$ than for $U_0 = 2$. For $U_0 = 4$, we observe from Fig. 21, as similar to that analyzed for the explicitly solvable case $q = 3$ in §5.1, that when $q = 4$ the minimal Hopf threshold value for $\hat{\tau}_u$ switches between two modes at some critical $\mathcal{D}_0$.

Overall, our numerical results for the linear stability region for $q = 2$ and $q = 4$, as computed from our parameterization (6.28), are qualitatively similar to those obtained from our detailed analysis in §5 for the explicitly solvable case $q = 3$.

6.3 Comparison of Linear Stability Theory with PDE Simulations: $q \neq 3$

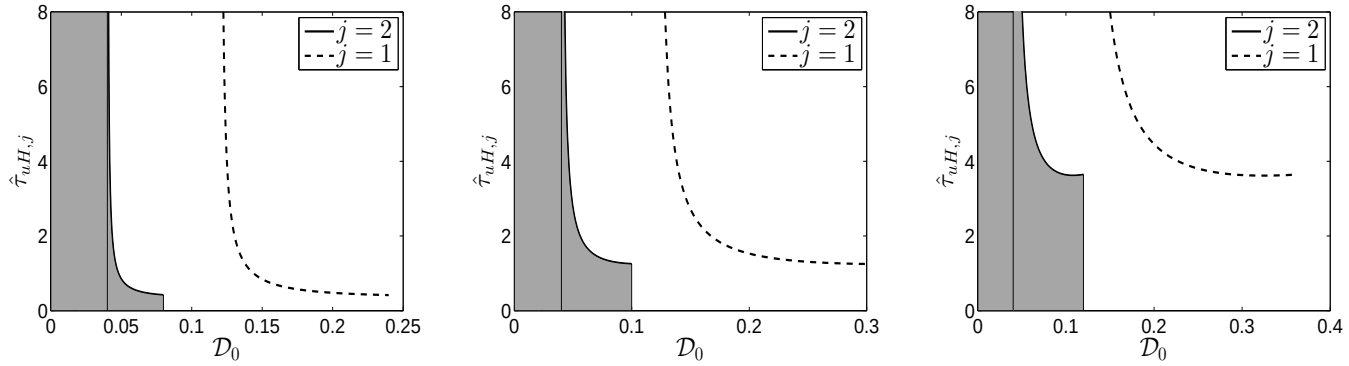

Figure 20: Linear stability (shaded) region in the $\hat{\tau}_u$ versus $\mathcal{D}_0$ plane for $K = 3$, $S = 6$, $U_0 = 2$, $\gamma = 2$ and $\alpha = 1$, and for $q = 2$ (left panel), $q = 3$ (middle panel), $q = 4$ (right panel). The solid and dashed curves are the Hopf bifurcation boundaries for the (sign-alternating) $j = 2$ mode and the $j = 1$ mode, respectively. In each case, the minimal Hopf boundary threshold for $\hat{\tau}_u$ is determined by the sign-alternating $j = 2$ mode. Observe that $\hat{\tau}_{u,H}$ increases as q increases.

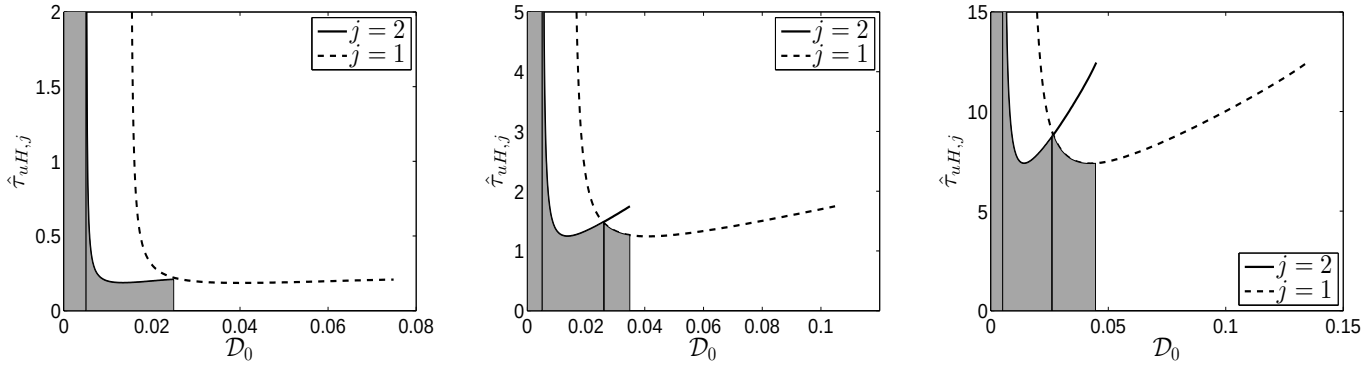

Figure 21: Same plot and parameters as in Fig. 20 except that $U_0 = 4$: $q = 2$ (left panel), $q = 3$ (middle panel), and $q = 4$ (right panel). The shaded region is the region of linear stability. The solid and dashed curves are the Hopf bifurcation boundaries for the (sign-alternating) $j = 2$ mode and the $j = 1$ mode, respectively. The minimal Hopf bifurcation threshold switches between the two modes only for $q = 3$ and $q = 4$. As q increases the Hopf bifurcation threshold increases significantly (see the different vertical scales in the subfigures). The horizontal edge of the stability region is the competition stability threshold $\mathcal{D}_{0,c}$.

To be written once I get the full numerics for the PDE system working.

Here we discuss our main stability result qualitatively and we validate our Hopf bifurcation threshold values with full numerical solutions of the PDE system (1.5).

This section is to be written once I get the full numerics working. I might use some of the blurb below. This analysis reveals a qualitatively novel phenomenon in the context of the study of the stability of spike patterns to reaction-diffusion systems. In particular, for a two-hotspot equilibrium, then $j = 1$ is the only mode of oscillation, and our theory predicts the possibility of an *asynchronous* Hopf bifurcation so that the amplitudes of the two crime hotspots begin to exhibit temporal anti-phase oscillations. In terms of the urban crime model, this means that when police patrols with a certain specific diffusivity relative to the criminals (determined by $\tilde{\tau}_{j,\mathrm{H}opf}$), one observes an interesting picture that the police concentration is drifting to and fro from the hotspots without annihilating any of them. However, if the police patrol diffusivity exceeds such a threshold, then one of the hotspot will dissipate due to an oscillatory instability. Such a qualitative behavior in the possible types of detstabilization of localized spike patterns was not observed in other well-studied reaction-diffusion systems exhibiting similar concentration phenomena, such as the Gray-Scott, Gierer-Meinhardt and Schnakenburg models.

8 Discussion

We have used a combination of matched asymptotic expansions and the analysis of nonlocal eigenvalue problems (NLEP) to study the existence and linear stability of localized hotspot steady-state solutions of the three-component RD system (1.1) in the limit $\epsilon \to 0$ with $D = \mathcal{D}_0/\epsilon^2$ on the 1-D domain $0 \le x \le S$. We have investigated how the multiple hotspot steady-states and their linear stability properties depend on the total police deployment $U_0 > 0$, the patrol focus parameter $q > 1$, and the police diffusivity $D_p \equiv D_0/\varepsilon^2\tau_u$, where $\tau_u = \epsilon^{q-3}\hat{\tau}_u$ with $\hat{\tau}_u = \mathcal{O}(1)$.

In the limit $\epsilon \to 0$, our formal asymptotic construction of hotspot steady-states for (1.1) with a common hotspot amplitude, and with $q > 1$, has shown that they exist only when $U_0 < U_{0,\max} \equiv S(\gamma - \alpha)$ (see Proposition 2.15. The derivation of the nonlocal eigenvalue problem (NLEP) characterizing the the linear stability properties of these localized steady-states was based on combining Floquet theory with the derivation of appropriate jump conditions for the components of the eigenfunction across a hotspot region. Although the NLEP has two nonlocal terms, we have shown how to reduce it to a more traditional form with only one nonlocal term for which some analytical results are available (cf. [36]).

Our NLEP linear stability analysis has revealed that a steady-state with a single hotspot is always linearly stable, and that a steady-state with $K \ge 2$ hotspots is always linearly stable to synchronous perturbations in the amplitudes of the hotspots. This latter conclusion is in marked contrast to previous NLEP analyses of spike amplitude instabilities for two-component RD systems in the large diffusivity ration limit whereby the dominant temporal oscillatory instability in the spike amplitudes resulting froma Hopf bifurcation is always due to the synchronous mode (cf. [34], [16]).

For $K \ge 2$ hotspots, and for a given $U_0 > 0$ and a fixed $q \in \{2, 3, 4\}$, our NLEP analysis has provided phase diagrams in the $\hat{\tau}_u$ versus $\mathcal{D}_0$ characterizing the linear stability of the hotspot steady-state to asynchronous perturbations in the hotspot amplitudes.

For the special case $q = 3$, and for $K \ge 2$, we have shown that the discrete spectrum of the NLEP can be reduced to the study of a family of $K - 1$ quadratic equations in the eigenvalue parameter. Such explicitly solvable NLEP problems also appear in [14, 19, 20]. As a result of this simplification, we have pro

- Special case $q = 3$ (family of quadratics) as compared to general q (argument principle: rigorous) (parameterization: numerics).

- explain three key regimes
- derivation of the NLEP is more challenging; leads to two nonlocal terms, one that can be eliminated self-consistently.

[14, 19, 20]. The general case was then studied using the argument principle to count the number of unstable eigenvalues in the right half plane. This procedure was first developed to study the stability of steady-state spike patterns for the Gierer-Meinhardt model (cf. [34]) and now has a rather large body of literature (see [14] and the references therein). Our conclusions from the explicitly solvable case $q = 3$ are considerably stronger than those for the non-explicitly solvable case $q \neq 3$.

In particular, when $q = 3$, two thresholds $\mathcal{D}_{0,lower}$ and $\mathcal{D}_{0,upper}$ given were determined so that the a multiple-hotspot pattern is stable when $\mathcal{D}_0 < \mathcal{D}_{0,lower}$ and unstable due to a competition instability when $\mathcal{D}_0 > \mathcal{D}_{0,upper}$. Moreover, an explicit formula for the existence of Hopf bifurcation $\tau_u = \tau_{Hopf}$ when $\mathcal{D}_{0,lower} < \mathcal{D}_0 < \mathcal{D}_{0,upper}$ was given in In contrast to the absence of a Hopf bifurcation for the basic crime model with no police intervention, as discovered in [14], the window of existence for a Hopf bifurcation given by $(\mathcal{D}_{0,lower}, \mathcal{D}_{0,upper})$ vanishes exactly when $U_0 = 0$. In other words, the third component of the PDE system (1.5), modeling the police interaction, is essential to inducing the possibility of oscillations. Moreover, unlike the case of the Gray-Scott and Gierer-Meinhardt models studied in [16] and [34], where synchronous oscillatory instabilities of the spike amplitudes robustly occur and are the dominant instability, our three-component system exhibits asynchronous oscillatory instabilities. These asynchronous, anti-phase, oscillations of the spike amplitudes have the qualitative interpretation that, for a range of police diffusivities, the police presence is only able to mitigate the amplitude of certain hotspots at the expense of the growth of other hotspots in different spatial regions.

However, when $q \neq 3$, we had difficulty in analytically proving results as strong as for the case $q = 3$. In particular, we were not able to prove, without assuming further conditions, that a multiple hotspot pattern is stable when the rescaled criminal diffusivity $\mathcal{D}_0$ is below the same lower threshold defined earlier in the $q = 3$ case. One possibility is that the definition of the lower threshold should be revised and should change with q. When $\mathcal{D}_0$ is between the lower and upper thresholds, we were able to prove the existence of a Hopf bifurcation, but we cannot show uniqueness of the critical Hopf bifurcation value in τ_u. These are interesting open problems that warrant further study. Most importantly, we would like to investigate what are the mathematical relationships between the explicitly solvable case $q = 3$ and the non-explicitly solvable case $q \neq 3$, so that the strong results from the explicitly solvable case can potentially carry over to the general case.

A reason for considering integral values of q only in the range $\{2, 3, 4\}$ is that we assumed in the course of deriving the NLEP that $\tau_u \ll \mathcal{O}(\epsilon^{-2})$ (see the calculations leading to 3.15). Then, for the parameter

$$\tilde{\tau}_j = \tau_u \mathcal{O}(\epsilon^{q-3}),$$

to be $\mathcal{O}(1)$, we must have that $\tau_u = \mathcal{O}(\epsilon^{3-q})$. This establishes that $q < 5$ is required to satisfy the assumption that $\tau_u \ll \mathcal{O}(\epsilon^{-2})$. If $q = 1$, then the ODE for the perturbation η at (3.16a) will be changed to

$$\mathcal{D}_0 \alpha^q \eta_{xx} = \hat{\tau}_u \lambda \alpha^q \eta,$$

where $\tau_u = \epsilon^{-2}\hat{\tau}_u$. This will result in a different problem to be solved for $\eta(x)$, and consequently a different value for $\eta(0)$. Ultimately, this leads to a different NLEP that requires a separate analysis.

8.1 Open Problems and Future Directions

With regards to our police model, with simple police interaction, studied in this chapter, it would be interesting to consider the more challenging $D = \mathcal{O}(1)$ regime. One key question would be to investigate whether the police presence can eliminate

the peak insertion behavior that was found for the basic crime model to lead to the nucleation of new spikes of criminal activity. In this direction it would be interesting to determine the influence of the police presence on the global bifurcation of multiple hotspot steady-state solutions.

This suggests that there should also be discrete spectra of the full problem that are near zero as $\epsilon \to 0$. These are the "small" eigenvalues that are related to translational instabilities. Our analysis of the NLEP characterizes only those eigenvalues that are $\mathcal{O}(1)$ as $\epsilon \to 0$, which can lead to $\mathcal{O}(1)$ time-scale instabilities.

A second interesting direction would be to study the effect of police presence on crime patterns when the police interaction is modeled by the predator-prey dynamics case $I(U, \rho) = U\rho$. Preliminary results suggest that the NLEP will now have three nonlocal terms, which makes a detailed stability analysis very challenging. However, the determination of the competition instability threshold, corresponding to the zero-eigenvalue crossing, should be readily amenable to analysis.

A third direction would be to consider spatial patterns in more than a simple 1-D spatial context. In this context, it would be interesting to extend the 2-D stability results in [14] for the basic crime model, to study the existence of stability of crime hotspots in 2-D domains in the presence of police. In particular, we would like to investigate the stability and dynamics of 2-D hotspots, allowing for either of our two different models of police intervention.

A The Continuum Limit of the Agent-Based Model

Acknowledgments

M. J. Ward was supported by the NSERC Discovery Grant 81541. We gratefully acknowledge helpful discussions with Theodore Kolokolnikov and Juncheng Wei on the NLEP analysis.

References

[1] H. Berestycki, J.-P. Nadal, *Self-organised critical hot spots of criminal activity*, Europ. J. Appl. Math., **21**(4-5), (2010), pp. 371–399.

[2] H. Berestycki, J. Wei, M. Winter, *Existence of symmetric and asymmetric spikes for a crime hotspot model*, SIAM J. Math. Anal., **46**(1), (2014), pp. 691–719.

[3] P. L. Brantingham, P. J. Brantingham, *Crime patterns*, McMillan, (1987).

[4] R. Cantrell, C. Cosner, R. Manasevich, *Global bifurcation of solutions for crime modeling equations*, SIAM J. Math. Anal., **44**(3), (2012), pp. 1340–1358.

[5] Discover, Science for the Curious (2010), [Fight Crime with Mathematics ranks in Top 100 Stories in 2010]. Retrieved from http://discovermagazine.com/2011/jan-feb/60.

[6] A. Doelman, R. A. Gardner, T. J. Kaper, *Large stable pulse solutions in reaction-diffusion equations*, Indiana U. Math. J., **50**(1), (2001), pp. 443–507.

[7] A. Doelman, H. van der Ploeg, *Homoclinic stripe patterns*, SIAM J. Appl. Dyn. Systems, **1**(1), (2002), pp. 65-104.

[8] M. R. D'Orsogna, M. Perc, *Statistical physics of crime: A review*, Physics of Life Reviews, **12**, (2015), pp. 1-21

[9] Y. Gu, Q. Wang, G. Yi, *Stationary patterns and their selection mechanism of urban crime models with heterogeneous near-repeat victimization effect*, Europ. J. Appl. Math., **28**(1), (2017), pp. 141–178.

[10] D. Iron, M. J. Ward, J. Wei, *The stability of spike solutions to the one-dimensional Gierer-Meinhardt model*, Physica D, **150**(1-2), (2001), pp. 25–62.

[11] S. Johnson, K. Bower, *Domestic burglary repeats and space-time clusters: The dimensions of risk*, Europ. J. of Criminology, **2**, (2005), pp. 67–92.

[12] P. A. Jones, P. J. Brantingham, L. Chayes, *Statistical models of criminal behavior: The effect of law enforcement actions*, Math. Models. Meth. Appl. Sci., **20**, Suppl., (2010), pp. 1397–1423.

[13] T. Kolokolnikov, M. J. Ward, J. Wei, *The existence and stability of spike equilibria in the one-dimensional Gray-Scott model: The low feed-rate regime*, Studies in Appl. Math., **115**(1), (2005), pp. 21–71.

[14] T. Kolokolnikov, M. J. Ward, J. Wei, *The stability of steady-state hot-spot patterns for a reaction-diffusion model of urban crime*, DCDS-B, **19**(5), (2014), p. 1373–1410.

[15] R. McKay, T. Kolokolnikov, *Stability transitions and dynamics of localized patterns near the shadow limit of reaction-diffusion systems*, DCDS-B, **17**(1), (2012) pp. 191–220.

[16] T. Kolokolnikov, M. J. Ward, J. Wei, *The existence and stability of spike equilibria in the one-dimensional Gray-Scott model: The low feed rate regime*, Studies in Appl. Math, **115**(1), (2005), pp. 21–71.

[17] T. Kolokolnikov, J. Wei, *Stability of spiky solutions in a competition model with cross-diffusion*, SIAM J. Appl. Math., **71**(4), (2011), pp. 1428–1457.

[18] D. J. B. Lloyd, H. O'Farrell, *On localised hotspots of an urban crime model*, Physica D, **253**, (2013), pp. 23–39.

[19] I. Moyles, W.-H. Tse, M. J. Ward, *Explicitly solvable nonlocal eigenvalue problems and the stability of localized stripes in reaction-diffusion systems*, Studies in Appl. Math., **136**(1), (2016), pp. 89–136.

[20] Y. Nec, M. J. Ward, *An explicitly solvable nonlocal eigenvalue problem and the stability of a spike for a class of reaction-diffusion system with sub-diffusion*, Math. Model. of Nat. Phenom., **8**(2), (2013), pp. 55–87.

[21] K. Painter, T. Hillen, *Spatio-temporal chaos in a chemotaxis model*, Physica D, **240**, (2011), pp. 363–375.

[22] H. van der Ploeg, A. Doelman, *Stability of spatially periodic pulse patterns in a class of singularly perturbed reaction-diffusion equations*, Indiana Univ. Math. J., **54**(5), (2005), pp. 1219–1301

[23] A. B. Pitcher, *Adding police to a mathematical model of burglary*, Europ. J. Appl. Math., **21**(4-5), (2010), pp. 401–419.

[24] J. D. M. Rademacher, *First and second order semi-strong interaction in reaction-diffusion systems*, SIAM J. Appl. Dyn. Syst., **12**(1), (2013), pp. 175–203.

[25] RAIDS Online, *Crime density maps for West Vancouver, B.C., Canada and Santa Clara-Sunnyville, California, US*, BAIR Analytics, (2015), Inc. Retrieved from http://raidsonline.com/.

[26] L. Ricketson, *A continuum model of residential burglary incorporating law enforcement*, unpublished, (2011). Retrieved from http://cims.nyu.edu/~lfr224/writeup.pdf.

[27] N. Rodriguez, A. Bertozzi, *Local existence and uniqueness of solutions to a PDE model for criminal behavior*, M3AS (special issue on Mathematics and Complexity in Human and Life Sciences), **20**(1), (2010), pp. 1425–1457.

[28] I. Rozada, S. Ruuth, M. J. Ward, *The stability of localized spot patterns for the Brusselator on the sphere*, SIAM J. Appl. Dyn. Sys., **13**(1), (2014), pp. 564–627.

[29] M. B. Short, M. R. D'Orsogna, V. B. Pasour, G. E. Tita, P. J. Brantingham, A. L. Bertozzi, L. B. Chayes, *A statistical model of criminal behavior*, Math. Models. Meth. Appl. Sci., **18**, Suppl., (2008), pp. 1249–1267.

[30] M. B. Short, A. L. Bertozzi, P. J. Brantingham *Nonlinear patterns in urban crime - hotspots, bifurcations, and suppression*, SIAM J. Appl. Dyn. Sys., **9**(2), (2010), pp. 462–483.

[31] M. B. Short, P. J. Brantingham, A. L. Bertozzi, G. E. Tita (2010), *Dissipation and displacement of hotpsots in reaction-diffusion models of crime*, Proc. Nat. Acad. Sci., **107**(9), pp. 3961-3965.

[32] W. Sun, M. J. Ward, R. Russell, *The slow dynamics of two-spike solutions for the Gray-Scott and Gierer-Meinhardt systems: competition and oscillatory instabilities*, SIAM J. Appl. Dyn. Syst., **4**(4), (2005), pp. 904–953.

[33] W.-H. Tse, M. J. Ward, *Hotspot formation and dynamics for a continuum model of urban crime*, Europ. J. Appl. Math., **27**(3), (2016), pp. 583–624.

[34] M. J. Ward, J. Wei, *Hopf bifurcations and oscillatory instabilities of spike solutions for the one-dimensional Gierer-Meinhardt model*, J. Nonlinear Sci., **13**(2), (2003), pp. 209–264.

[35] J. Wei, *On single interior spike solutions of the Gierer-Meinhardt system: uniqueness and spectrum estimates*, Europ. J. Appl. Math., **10**(4), (1999), pp. 353–378.

[36] J. Wei, *Existence and stability of spikes for the Gierer-Meinhardt system*, book chapter in *Handbook of Differential Equations, Stationary Partial Differential Equations*, Vol. 5 (M. Chipot ed.), Elsevier, (2008), pp. 489–581.

[37] J. Q. Wilson, G. L. Kelling, *Broken windows and police and neighborhood safety*, Atlantic Mon., **249**, (1998), pp. 29–38.

[38] J. R. Zipkin, M. B. Short, A. L. Bertozzi, *Cops on the dots in a mathematical model of urban crime and police response*, DCDS-B, **19**(5), (2014), pp. 1479–1506.